SUPER-ORTHOGONAL SPACE-TIME TURBO CODES IN RAYLEIGH FADING CHANNELS

Jayesh Narayana Pillai

Submitted in fulfilment of the academic requirements for the degree of MScEng in the School of Electrical, Electronic and Computer Engineering at the University of KwaZulu-Natal, Durban, South Africa

November 2005

Dedicated in loving memory of my father

ABSTRACT

The vision of anytime, anywhere communications coupled by the rapid growth of wireless subscribers and increased volumes of internet users, suggests that the widespread demand for always-on access data, is sure to be a major driver for the wireless industry in the years to come. Among many cutting edge wireless technologies, a new class of transmission techniques, known as Multiple-Input Multiple-Output (MIMO) techniques, has emerged as an important technology leading to promising link capacity gains of several fold increase in data rates and spectral efficiency. While the use of MIMO techniques in the third generation (3G) standards is minimal, it is anticipated that these technologies will play an important role in the physical layer of fixed and fourth generation (4G) wireless systems.

Concatenated codes, a class of forward error correction codes, of which Turbo codes are a classical example, have been shown to achieve reliable performance which approach the Shannon limit. An effective and practical way to approach the capacity of MIMO wireless channels is to employ space-time coding (STC). Space-Time coding is based on introducing joint correlation in transmitted signals in both the space and time domains. Space-Time Trellis Codes (STTCs) have been shown to provide the best trade-off in terms of coding gain advantage, improved data rates and computational complexity.

Super-Orthogonal Space-Time Trellis Coding (SOSTTC) is the recently proposed form of space-time trellis coding which outperforms its predecessor. The code has a systematic design method to maximize the coding gain for a given rate, constellation size, and number of states. Simulation and analytical results are provided to justify the improved performance. The main focus of this dissertation is on STTCs, SOSTTCs and their concatenated versions in quasi-static and rapid Rayleigh fading channels.

Turbo codes and space-time codes have made significant impact in terms of the theory and practice by closing the gap on the Shannon limit and the large capacity

gains provided by the MIMO channel, respectively. However, a convincing solution to exploit the capabilities provided by a MIMO channel would be to build the turbo processing principle into the design of MIMO architectures. The field of concatenated STTCs has already received much attention and has shown improved performance over conventional STTCs. Recently simple and double concatenated STTCs structures have shown to provide a further improvement performance. Motivated by this fact, two concatenated SOSTTC structures are proposed called Super-orthogonal space-time turbo codes. The performance of these new concatenated SOSTTC is compared with that of concatenated STTCs and conventional SOSTTCs with simulations in Rayleigh fading channels. It is seen that the SOST-CC system outperforms the ST-CC system in rapid fading channels, whereas it maintains performance similar to that in quasi-static. The SOST-SC system has improved performance for larger frame lengths and overall maintains similar performance with ST-SC systems. A further investigation of these codes with channel estimation errors is also provided.

ACKNOWLEDGEMENTS

I wish to take this opportunity to thank my supervisor, Prof. Stanley H. Mneney, for his invaluable guidance, help and support. His willingness to always set aside his time to assist me in any way has been most appreciated. His valuable input into my research and constant encouragement has been of paramount importance to the completion of this dissertation. Thanks also go to Dr. H. Xu and Dr. G. J. Byers for always having time for me and providing valuable suggestions and help with my work.

Words cannot truly express my deepest gratitude and appreciation to my mother for her loving support and constant encouragement throughout my life. My sincere appreciation also goes to my brother Rajesh and sister-in-law Indu, for their support and keen interest in my work. Their love has provided me the inspiration to overcome some of life's exciting challenges.

Thanks are owed to Telkom SA LTD and Alcatel S.A. for their much appreciated financial support and for providing the equipment necessary for completion of my dissertation.

I would like to thank Mrs. M. Wayne, Miss. Brigette Le Breton, Mrs. Rene Truter, Mrs. B. J. Bennet and Mr. Bruce Harrison for their help in one way or another during my course.

Finally, I would like to thank my post graduate colleagues for their help and friendship and for making the time spent together a most memorable one.

PREFACE

The research work presented in this dissertation was performed by Mr. Jayesh Narayana Pillai under the supervision of Prof. S. H. Mneney at the University of KwaZulu-Natal's School of Electrical, Electronic and Computer Engineering in the Centre of Radio Access and Rural Technologies. This work is partly sponsored by Telkom South Africa Ltd and Alcatel S.A. as part of the Centre of Excellence programme.

Parts of this dissertation have been presented at the SATNAC 2004 conference held in Stellenbosh, South Africa and in the IEEE AFRICON 2004 conference held in Gaborone, Botswana, SATNAC 2005 conference held in Drakensburg, Durban, South Africa, and EUROCON 2005 conference held in Belgrade, Serbia and Montenegro, and to appear in the Transactions of Springer's International Journal on Wireless Personal Communication, Denmark.

The entire dissertation, unless otherwise indicated, is the author's work and has not been submitted in part, or in whole, to any other university for degree purposes.

TABLE OF CONTENTS

INDEX OF FIGURES

INDEX OF TABLES

LIST OF ACRONYMS

1G	First Generation
2G	Second Generation
3G	Third Generation
4G	Fourth Generation
3GPP	3rd Generation Partnership Project
AMPS	Advanced Mobile Phone Service
AWGN	Additive White Gaussian Noise
ARQ	Automatic Repeat Request
AWSTTC	Adaptively Weighted Space-Time Trellis Codes
BER	Bit Error Rate
BLAST	Bell Laboratories Layered Space Time
BPSK	Binary Phase Shift Keying
CDCM	Codeword Difference Covariance Matrix
CDMA	Code Division Multiple Access
CC	Convolutional Codes
CCI	Co-Channel Interference
CGD	Coding Gain Distance
CSI	Channel State Information
DAB	Digital Audio Broadcast
DVB	Digital Video Broadcast
ECC	Error Correcting Codes
FEC	Forward Error Correction
FER	Frame Error Rate
GSM	Global System for Mobile Communication
HSDPA	High Speed Downlink Packet Access
IMT-2000	International Mobile Telecommunication for the 21st Century
IMT-DS	IMT Direct Sequence
IMT-FT	IMT Frequency Time

IMT-MC	IMT Multicarrier
IMT-SC	IMT Single Carrier
IMT-TC	IMT time Code
ITU	International Telecommunication Union
LDPC	Linear Density Parity Check Codes
LST	Layered Space Time
DLST	Diagonal LST
HLST	Horizontal LST
TLST	Threaded LST
VLST	Vertical LST
MIMO	Multiple-Input Multiple-Output
MAP	Maximum a Posteriori
MEA	Multi-element Array
MGF	Moment Generating Function
MLD	Maximum Likelihood Decoding.
MLSE	Maximum Likelihood Sequence Estimator
NMT	Nordic Mobile Telephone
NRC	Non-recursive Convolutional
PDC	Personal Digital cellular
PCCC	Parallel Concatenated Convolutional Code
PWEP	Pairwise Error Probability
RS	Reed-Solomon
RSC	Recursive Systematic Convolutional
SCCC	Serial Concatenated Convolutional Code
SISO	Soft-Input Soft-Output
SiSo	Single Input Single Output
STC	Space-Time Coding
SOSTTC	Super-Orthogonal Space-Time Trellis Codes
STBC	Space-Time Block Code
STTC	Space-Time Trellis Codes
SOVA	Soft Output Viterbi Algorithm

SOSTTuC	Super-Orthogonal Space-Time Turbo Codes
TACS	Total Access Communication System
TCM	Trellis Coded Modulation
TDMA	Time Division Multiple Access
UE	User Equipment
UMTS	Universal Mobile Telecommunication System
UTRA	UMTS Terrestrial Radio Access
UTRA-TDD	UTRA Time Division Duplex
UTRA-FDD	UTRA Frequency Division Duplex
WCDMA	Wideband Code Division Multiple Access
WLAN	Wireless Local Area Network

CHAPTER 1

INTRODUCTION

1.1 Evolution of Mobile Communication

The evolution of the Internet during the last 40 years or so has dramatically changed the way in which both individuals and organizations view their means of communication. With the advent of broadband technology accelerating the use of the Internet as a medium for transmitting data, it was inevitable that there would be a challenge to the telephone as the principal means of voice communication. Emerging wireless communication systems require a combination of data rates, robustness and quality of service of unprecedented levels.

Initially the first generation of mobile cellular telecommunications systems appeared in the 1980's. They used analog transmission techniques for traffic, which was almost entirely voice, were restricted by limited system capacity and support for mobility was weak. At the time there were no dominant standard, as each country developed its own system, limiting usage within national boundaries and avoiding economies of scale. The most successful standards of the time were Nordic Mobile Telephone (NMT), Total Access Communication System (TACS), and Advanced Mobile Phone Service (AMPS) [2].

The second generation (2G) mobile cellular systems use digital radio transmission for traffic. These networks have much higher capacity than first generation (1G) systems. The four main standards for 2G systems are Global system for Mobile (GSM) communications, IS-95 code division multiple access (CDMA), TDMA-time division multiple access or (D-AMPS) and personal digital cellular (PDC). GSM is by far the most successful and widely used 2G system. By September 2002 there were more than 460 GSM operators with approximately 747.5 million users [2]. While the step from the first to second generation mainly brought the transition from analog to digital, the approach to third generation (3G) system is mainly driven by the fast rise of Internet and the ever increasing need for fast data transmission capabilities while on the move.

The idea of 3G became evident with the need for more capacity, new frequencies and higher bit rates. In the same year that GSM was commercially launched, the European Telecommunication Standards Institute had already started the standardization work for the next new system called the Universal Mobile Telecommunication System (UMTS) or 3rd Generation Partnership Project (3GPP). All the significant 3G versions serve to protect their corresponding 2G system investments and UMTS/3GPP is an extension of GSM. In order to coordinate global standardization of 3G systems, the International Telecommunications Union (ITU) formed the International Mobile Telecommunications for the 21st century (IMT-2000) program. The IMT-2000 is the umbrella specification of all 3G systems. The IMT-2000 accepted the following proposals as IMT-2000 compatible. They are IMT Direct Spread (IMT-DS, also known as UTRA FDD), IMT Multicarrier (IMT-MC, also known as CDMA2000), IMT Time Code (IMT-TC, also known as UTRA-TDD/TD-SCDMA), IMT Single Carrier (IMT-SC, also known as UWC-136) and IMT Frequency Time (IMT-FT, also known as DECT). The number of accepted systems indicates that the ITU adopted a policy that no serious candidate should be excluded from the IMT-2000 specification. Thus, IMT-2000 is not actually a single radio interface specification but a family of specifications.

It is often said that it is rather difficult to predict what kind of system will constitute the 4G mobile telecommunication systems. It should be noted that the term 4G is not defined

yet and there will not be a single network branded as 4G in the same way that there is 2G-GSM or 3G-UMTS. Instead 4G will be a collection of networks and a wide variety of smart devices communicating with each other. The future 4G-compatible networks will certainly include the UMTS and enhanced GSM deployments, but these may also include wireless local area network (WLAN) (e.g. 802.11 family), satellite networks, broadcast networks such as digital audio broadcasting (DAB) or even digital video broadcasting (DVB), and many other types of networks. The 4G technology will produce for a collection of different kinds of multiple access networks in which a user can gain a portal to the internet by the most appropriate means. This will be a departure from one-network-can-do-anything approach. These networks must cooperate seamlessly.

It is predicted that there will be more than two billion mobile users worldwide by 2010, and about half of them will use 3G systems. This is only the number of users; there will be even more wireless telecommunication devices around. The devices or modules will be embedded into other equipment, such as cars, laptop computers, and household appliances. Moreover, there will be communication chips in various kinds of vending machines, traffic control systems, payment terminals and so on.

Among many cutting edge wireless technologies, a new class of transmission scheme, known as Multiple-Input Multiple-Output (MIMO) transmission schemes which employ space-time coding techniques has emerged as an important technology, leading to promising link capacity gains of several-fold increase in spectral efficiency. While the use of MIMO techniques in the 3G standard is minimal, it is anticipated that these techniques will play an important role in the physical layer of fixed broadband and 4G wireless systems. Currently the 3GPP standard defines a maximum user data rate of 2.048Mb/s to the user equipment (UE). The high speed downlink packet access (HSDPA) extension to the 3GPP standard defines a new maximum user data rate of 10.8Mb/s to the UE [4]. Furthermore, with the proposed use of multiple antennas (i.e. MIMO extensions to HSDPA), even higher user data rates up to 21.6Mb/s may be defined. These downlink data rates are up to a factor of 10 times higher than the current 3GPP standards and so the

HSDPA UE would require the inclusion of a turbo decoder capable of operating at much higher data rates.

The increasing demand for high data rates in wireless communications due to emerging new technologies makes wireless communications an exciting and challenging field. The spectrum or bandwidth available to the service provider is often limited and the allotment of new spectrum is often not forthcoming. A further requirement is that the decoding operation is simple enough to allow real time processing, low power consumption, compact implementations and low cost. The success of 2G and 3G digital wireless standards provide a concrete demonstration that good ideas from communication theory can have a significant impact in practice. The research thrust in the past decade has led to a much richer set of perspectives and tools on how to communicate over wireless channels, and the future of wireless technology in general is looking bright.

1.2 Digital Communication Systems

This section describes the basic components that make up a digital communication system. Various methods that are used to improve system performance are discussed and lastly the field of space-time coding (STC) is introduced.

1.2.1 An Overview

The goal of a communication system is to transform the information generated by a source into a form that can withstand the effects of noise over the transmission medium and so can be reliably and efficiently recovered at the destination. A basic communication system [3], shown in Fig. 1.1, is essentially composed of the transmitter, the channel and the receiver.

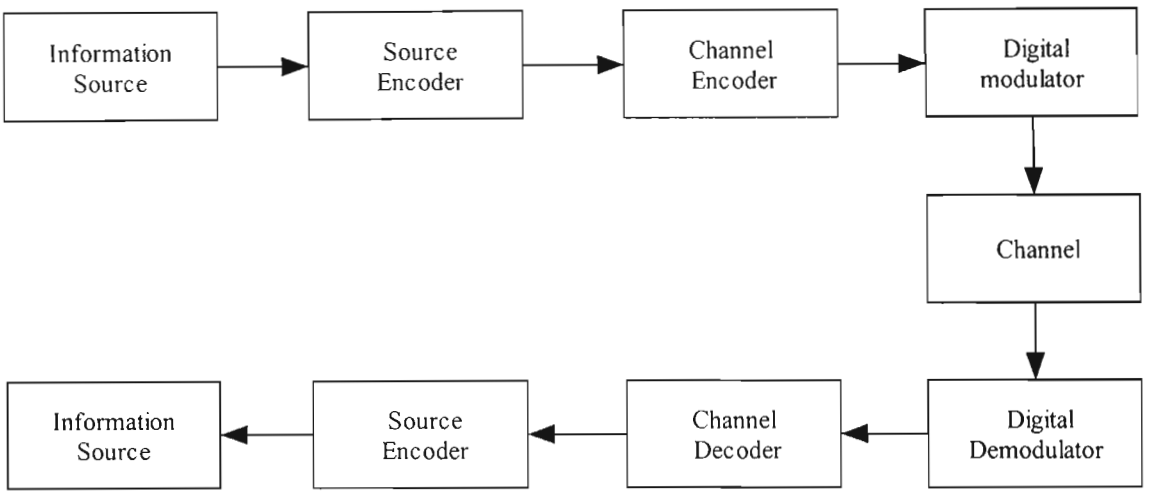

Fig. 1.1: A communications system.

The information source may be analog or digital in nature. An analog signal would be sampled and quantized before transmission through a digital system. The information source usually contains redundancy. These are either dependencies between successive symbols, or the probability of the occurrence of each symbol is not uniform. A source encoder is beneficial in these circumstances and is used to remove the redundancy before transmission so that the fewest number of bits are used to represent the information. This process is often referred to as compression. The channel encoder then adds a controlled amount of redundancy to the compressed data in order to make the transmission of the compressed data more reliable. The redundancy is introduced by means of an error correcting code that enables the receiver to detect and correct a limited number of errors that corrupt the information during transmission through the channel. Since the bits are not suitable for transmission over a physical channel, the digital modulator is used to transform them into a continuous-time waveform for transmission this waveform is then sent over the physical channel.

The channel is the medium that separates the transmitted and received data. The communication channel between the transmitter and receiver corrupts the transmitted signal in a random like manner. The main processes that corrupt the transmitted signal are time-varying multipath fading, additive white Gaussian noise (AWGN) and

cochannel interference. Typical transmission channels include wireline channels, wireless channels, fibre optic channels, underwater acoustic channels, etc.

At the receiver side, the digital demodulator processes the corrupted waveform and produces the estimation of the transmitted data. The output of the demodulator is passed to the channel demodulator is passed to the channel decoder which uses the redundancy and the knowledge of the channel code to detect and correct errors caused by the physical media. Finally, the source decoder accepts the decoded bits and attempts to reconstruct the original information source with knowledge of the source encoding method.

Due to the corruption caused by the channel, the demodulated signals may be in error, and the channel decoder may not be in a position to correct these errors. The rate of errors in the information stream can be expressed in terms of the number of bit errors in a frame which is the bit error rate (BER) or the number of frames in error after the transmission of a number of frames (FER), and can be used as a tool to measure the performance of the channel encoder and modulator. The capacity that can be achieved by the system indicates the bandwidth efficiency of the scheme and can be measured as a ratio of data rate in bits per second to the bandwidth in Hz used. Hence a highly bandwidth efficient system implies a system having high capacity and its units are bps/Hz.

1.2.2 Error Correcting Codes

The transmission system shown in Fig. 1.1 is strictly a one way system as it is in the forward direction. Unlike a two way system which can use automatic repeat request (ARQ) with error detection and retransmission, the error control strategy for a one way system must be forward error correction (FEC), which automatically corrects errors detected at the receiver. FEC includes block codes, convolutional codes, as well as concatenated codes which are built from block and convolutional codes. These FEC codes improve system performance at the cost of increased system bandwidth.

Block codes were developed initially and include the following types of codes: Bose-Chaudhuri-Hocquenghem (BCH) codes [3], Reed-Solomon (RS) codes [5], Low Density Parity Check (LDPC) codes [6] etc. The first practical decoding algorithm for block codes was threshold decoding introduced by Reed [7]. Recently, soft decision decoding of block codes have gained increasing attention by the coding research community [8].

Convolutional codes (CCs) are fundamentally different from block codes as they have memory so that the mapping from the information bits to he code bits is a function of the past information bits. CCs were first invented by Elias [9], who proved that randomly chosen codes of this type were good. Convolutional codes were first decoded using sequential decoding, but the first optimal (maximum likelihood) decoder was proposed by Viterbi in 1967. Another advantage of convolutional codes over block codes is the existence of soft-decision decoding algorithm such as the soft decision Viterbi algorithm, the Maximum-a-posteriori (MAP) [10] or Soft-Input Soft-Output (SISO) algorithm [11]. Forney first introduced concatenation in 1966 [12] where an inner CC code and an outer RS code were in cascade. A symbol interleaver is used between the inner and outer code so that long bursty error from the inner decoder are broken into separate blocks for the outer decoder. In 1993 a major breakthrough was made in concatenated coding with the discovery of turbo codes by Berrou *et al.* [13], [14]. A detailed description and study of these codes are discussed in the next chapter. Turbo codes achieve performance close to Shannon limit with the combination of two or more recursive systematic convolutional (RSC) codes, a pseudorandom interleaver, and a MAP iterative decoding algorithm. The algorithm exchanges extrinsic information between decoders, which allows the decoding process to be iterated several times, decreasing the number of errors per iteration. The design of decoders for 3G systems is heavily dependant on the intended use, either base station or user equipment. Two distinct channel coding methods which form the core of error control coding at the physical layer for 2G and 3G mobile cellular systems (e.g. GSM, GPRS, 3GPP/UMTS, CDMA2000) are convolutional coding and turbo coding.

1.2.3 Diversity

The wireless environment presents a challenging communication problem due to multipath fading caused by destructive addition of multipaths and interference from other users in multiple access systems. For example, a basic wireless multi-antenna system in a fading channel as seen in Fig. 1.2, every signal received at the receiver comprises multiple components of the same signal caused by reflection, refraction and scattering, normally within a certain angular range.

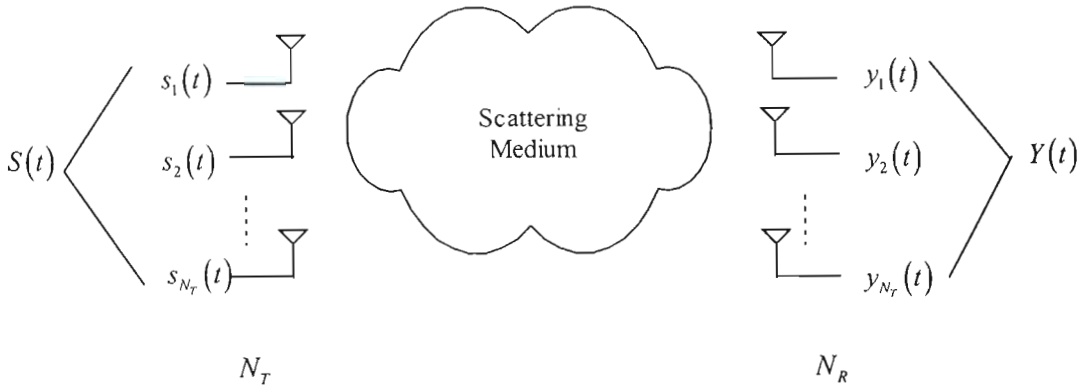

Fig. 1.2: A wireless multi-antenna channel.

Owing to the movement of the mobile users and the change of the surrounding environment, these components vary from in phase to out of phase, and therefore the strength of the resultant signal at any given point, moving or stationary, fluctuates between highs and lows. The fading profiles of such signals depend on many factors, but they tend to become uncorrelated if the points of measurements are distant. If multiple copies of the original signal are transmitted over independently fading sub channels, the probability of each signal undergoing a deep fade is greatly reduced. The idea of obtaining a number of different copies of the same signal is called diversity, such techniques provide a powerful toolset for achieving reliable transmission over fading channels.

Diversity is the technique resorted to in order to combat fading. There are several methods of obtaining more than one version of a signal at the receiver. These are basically divided into three main categories namely time, frequency and space diversity.

In time or temporal diversity, replicas of the transmitted signal are provided across time by a combination of channel coding and time interleaving strategies. The key requirements here for this form of diversity to be effective is that the channel must provide sufficient variation in time, and hence provide little diversity gain in quasi-static fading channels. One of the drawbacks of the scheme is that due to the redundancy introduced in the time domain, there is a loss in bandwidth efficiency.

In frequency diversity, replicas of the original signal in the frequency domain are provided. It is applicable in cases where the frequency separation between sub channels is greater than the coherence bandwidth. Like time diversity, frequency diversity induces a loss in bandwidth efficiency due to a redundancy introduced in the frequency domain.

Space diversity, has been a popular technique in wireless communications and is also called antenna diversity. It is implemented by using multiple replicas of the same transmitted signal which are provided across different antennas. In space diversity, the replicas of the transmitted signals are usually provided to the receiver in the form of redundancy in the space domain. Unlike time and frequency diversity, space diversity does not induce any loss in bandwidth efficiency. This property is very attractive for future high data rate wireless communications. Polarization diversity and angle diversity are two examples of space diversity. In polarization diversity, orthogonal polarization signals are transmitted by two different polarized antennas and received by two different polarized antennas. Different polarizations ensure that the two signals are uncorrelated without having to place the two antennas far apart [15]. Angle diversity resolves and combines signals with different angles of arrival.

Diversity schemes can also be classified according to the type of combining methods employed at the receiver. According to the implementation complexity and the level of

channel state information required by the combining method at the receiver, there are four main types of combining techniques, including selection combining, switched or scanning combining, equal gain combining and maximal ratio combining, of which maximal ratio combining achieves superior performance.

Depending on whether multiple antennas are used for transmission or reception, we can classify space diversity into two categories namely receive diversity and transmit diversity. In receive diversity, multiple antennas are used at the receiver site to pick up independent copies of the transmitted signals. In present cellular mobile communications multiple antennas are used at the base station to create uplink (from mobiles to base stations) receive diversity. This improves the quality and range in the uplink. For the downlink (from base station to mobile), it is difficult to utilize receive diversity at the mobile. This is due to the fact that generally mobile terminals are required to be small, light weight and have low power consumption. The use of receive diversity at the mobile terminal, increases its cost, size and power consumption due to multiple antennas and radio frequency down conversion chains.

Transmit diversity decreases the required processing power of the receivers, resulting in simpler system structure, lower power consumption and lower cost. It is also easier to install multiple transmit antennas in the base station and provide more power for the multiple transmit antennas resulting in extra power for multiple transmissions. Furthermore transmit diversity schemes have shown to increase channel capacity considerably [14], [15]. Transmit diversity is one of the key contributing technologies involved in defining the ITU endorsed 3G systems such as W-CDMA and CDMA2000. Diversity in the mobile terminals exists in Korean and Japanese mobile communication systems, and UMTS is prepared for it.

In order to improve the performance of the multiple antenna transmissions, it is possible to combine error control coding with the transmit diversity design. This can be done by viewing coding, modulation and multiple transmissions as one single processing module.

Coding techniques designed for multiple antenna transmission are called space-time coding [17] and an important form of that scheme is briefly discussed in the next section.

1.2.4 Super-Orthogonal Space-Time Trellis Codes

With the increasing demand on high data rate services and advances in DSP chips, the development of technology related to MIMO systems that rely on the use of multiple antennas at both the base stations and mobile terminals is emerging. The use of these systems relates to increase in capacity of wireless channel which is expressed as the maximum achievable data rate for an arbitrarily low probability of error. Space-time coding schemes combine the channel code design and the use of multiple transmit and receive antennas. In general the construction of space-time coding schemes is to a large extent a trade-off between the three conflicting goals of maintaining a simple decoding (i.e. limit the complexity of the receiver), maximizing the error performance, and maximizing the information rate. A number of different approaches have been proposed. These are layered space-time codes [18], [19] space-time block codes (STBC) [20], space-time trellis codes (STTC) [17] and recently super-orthogonal space-time trellis codes (SOSTTC) [21]. These schemes are discussed in more detail in section 3.4 and section 4.2. These schemes generalize the classical concept of coding on the temporal domain to coding on both spatial and temporal domain.

Space-time trellis codes constitute one of the first proposed and studied classes of space-time codes. It is well known that the STTCs achieve higher coding gains than STBCs [22] and both achieve maximum diversity gain. STTCs have also shown to outperform layered STCs. A new class of STCs called SOSTTC codes provides a new structure STTC that guarantees full diversity and provides opportunity to maximize the coding gain. They have shown to have a systematic design method for a given diversity, rate and state size. A number of concatenated STTC schemes have been proposed in the literature. But there have not been any such schemes proposed for the SOSTTC case in the literature. As these codes are relatively new not much work has been published in this area.

1.3 Motivation

With the integration of the internet and multimedia applications in next generation wireless communications, the demand for reliable high data rate services has grown in a literally explosive manner during the last couple of years. An issue with current wireless systems is the conflict between the increasing demand for wireless services and scarce electromagnetic spectrum. With limitations on spectrum, size, cost and power consumption of the mobile terminal, these systems must be power and bandwidth efficient. Unlike the Gaussian channel, the wireless channel introduces a variety of impairments to the transmitted signal, of which time-varying multipath fading can be considered to be one of the most significant. The main goal of the systems to be designed would be to overcome this problem without increasing system bandwidth or transmission power.

The best remedy for these imperfections would be to apply diversity techniques. Antenna diversity is a suitable choice as it successfully mitigates the effects of multipath fading at no increase in system power or bandwidth, unlike time and frequency diversity techniques. Receive diversity techniques have been employed in a number of systems especially in the uplink in cellular systems. However, due to the receive terminal for example where the mobile terminal being restricted in terms of cost, size, and power constraints, receive diversity is not very efficient. In such a situation, transmit diversity has shown to deliver the required tasks of overcoming multiple fading at no increase in system power or bandwidth and without sacrificing the limitations placed on the mobile terminal.

Space-time coding (STC) schemes combine the channel code design and the use of multiple transmit antennas. Space-time trellis codes are a form of STCs and have received much attention in their singular forms and various concatenated forms for a variety of channel realizations. Super-orthogonal space-time trellis codes are a relatively new form of STTC codes which have recently shown improved performance and

systematic design principles. An in depth study and variations of this code in either conventional or concatenated forms are yet to be investigated in the current literature.

The research focuses on the use of coded diversity techniques in multiple-input multiple-output (MIMO) systems. Two concatenated forms of SOSTTCs referred to as super-orthogonal space-time turbo codes are proposed to further improve the performance in terms of coding gain of conventional SOSTTCs.

1.4 Dissertation Overview

This dissertation is divided into six chapters. The outline of each of the chapters is as follows. Chapter 1 gave a brief overview of the evolution of the different generations and discussed 3G cellular systems and shed light on future necessities and requirements for 4G systems. A basic communication system model was described, various error correcting codes and diversity techniques used to improve system performance were outlined. Space-time coding and SOSTTCs which merge spatial and temporal diversity with channel coding techniques were discussed. The general motivation for the work done in this dissertation was then given.

In Chapter 2 a review on error correcting coding techniques using convolutional and concatenated codes, turbo coding in particular is carried out. The iterative decoding scheme and explanation of the MAP algorithm is presented. Simulation of the turbo codes and analytical results using union bounds are also provided.

In chapter 3, a generalized system model employing multiple transmit and receive antennas is presented. Next a literature survey on multi-antenna transmission systems employing error control coding is provided. The prospects of achievable channel capacity for these systems are described and some results are given. The various types of space-time coding schemes capable of approaching these theoretical limits are reviewed. We look at adaptively weighted space-time trellis codes (AWSTTC) which employ channel

state information (CSI) at the transmitter. Space-time trellis codes provide a good trade-off in terms of constellation size, trellis complexity and system performance are discussed in a broader detail in this chapter. Recent work in the field is reviewed, the STTC system architecture is described and performance results are presented.

A relatively new form of space-time trellis coding called super-orthogonal space-time trellis codes which provide improved performance over its predecessors, and also employs systematic code design is discussed in detail in chapter 4. The performance of these codes in both quasi-static and rapid fading channels is discussed. A specific design method for improvement of the codes performance is also provided. Analytical results using coding gain distance (CGD) and moment generating function (MGF) methods are also presented.

Chapter 5 focuses on the concatenation of convolutional codes with super-orthogonal space-time trellis codes as constituent codes. A brief review on previous concatenated convolutional codes and space-time trellis codes is given. Two concatenated SOSTTC structures are proposed where the encoding and decoding of each system is described in detail. A look at the codes performance in the presence of channel state information estimation through pilot symbol estimation method is also investigated. Simulation results for the codes are presented for both quasi-static and rapid fading channels, and are compared with the performance of similar concatenated STTC codes.

The results presented in chapter 2 through 5, were generated using custom built software simulation environments which were developed by the author using the C++ programming language.

Lastly, conclusions are drawn and possible topics for future work are discussed in chapter 6.

1.5 Original Contributions in this Dissertation

The original contributions of this dissertation include:

1. A mathematical analysis of coding gain for AWSTTC in quasi-static fading channel is performed.
2. A look into the computational complexity of implementing turbo codes, space-time trellis codes and their concatenated versions in hardware.
3. Two new concatenated SOSTTC structures are proposed and their performance investigated for Rayleigh fading channels..
4. The effect of imperfect channel estimation is incorporated into the concatenated SOSSTC code for quasi-static channels.

Parts of the work in this dissertation have been presented, or submitted by the author to the following local and international conferences and journals:

1. J. N. Pillai and S. H. Mneney, "Adaptively weighted space-time trellis codes," *Proceedings of South African Telecommunications Networks and Applications Conference (SATNAC 2004),* Spier, Stellenbosch, South Africa, Sep. 2004.
2. J. N. Pillai and S. H. Mneney, "A review on issues related to the implementation of Turbo codes and space-time trellis codes," *Proceedings of IEEE Africon 2004,* Gabarone, Botswana, Sep. 2004.
3. J. N. Pillai and S. H. Mneney, "Super-orthogonal space-time trellis codes for rapid Rayleigh fading channels," *Proceedings of South African Telecommunications Networks and Applications Conference (SATNAC 2005),* Central Drakensburg, Durban, South Africa, Sep. 2005.
4. J. N. Pillai and S. H. Mneney, "Concatenated super-orthogonal space-time trellis codes in Rayleigh fading channels," *Accepted IEEE EUROCON 2005, Conference on Computer as a Tool, Belgrade, Serbia and Montenegro, Nov. 21-24 2005.*

5. J. N. Pillai and S.H. Mneney, "Turbo decoding of super-orthogonal space-time trellis codes in Rayleigh fading channels," *to appear in Transactions on Springer's International Journal on Wireless Personal Communication in June 2006.*

CHAPTER 2

TURBO CODES

2.1 Introduction

Novel communication and information services are being introduced almost on a daily basis and the demands for higher data rates and communication capacity continue to grow. This spectacular progress of communication is to a great extent due to consistent performance increase and cost reduction of devices and circuit technology. Such advancements have also been fostered by major theoretical developments [23].

Shannon's 1948 paper entitled "A Mathematical Theory of Communication" [1] launched the twin fields of Information Theory and Error Control Coding. Shannon's noisy channel coding theorem implies that arbitrarily low decoding error probabilities can be achieved at any transmission rate R less than the channel capacity C by using sufficiently long block (or constraint) lengths. In particular, Shannon showed that randomly chosen codes, along with maximum likelihood decoding (MLD), can provide capacity achieving performances. However, he gave no guidance about how to actually construct good codes which perform close to capacity, or to implement MLD for such codes.

In the ensuing years after the publication of Shannon's paper, a large amount of research was conducted into the construction of specific codes with good error-correcting

capabilities and the development of efficient decoding algorithms for these codes [24]. The structure is a key component of the code design, since it can be used to guarantee good minimum distance properties. However, structure does not always result in the best distance properties for a code, and most highly structured code designs usually fall far short of achieving the performance promised by Shannon. Primarily because of the need to provide structure to develop easily implementable decoding algorithms, little attention was paid to the design of codes with randomlike properties, as originally envisaged by Shannon. Random code designs were thought to be too difficult to decode because they lacked structure. It was with the discovery of a relatively new coding technique, dubbed *turbo coding* by its inventors that succeeded in achieving randomlike code design with just enough structure to allow for an efficient iterative decoding method. It was due to this feature that these codes have exceptionally good performance, particularly at moderate BERs and for large block lengths and these codes with iterative decoding could achieve BERs as low as 10^{-5} at SNRs within 1 dB of the Shannon limit. In this chapter, turbo codes are described in greater detail, giving insights into their development and regarding their performance capabilities.

In this chapter we introduce the field of channel coding using convolutional codes. The introduction of various fundamental concepts of convolutional coding followed by concatenated coding will also be discussed. In section 2.5 we discuss in detail the principles of iterative decoding using the MAP algorithm. Analytical results using the method of the union bounds are also provided. Lastly some results on the performance of these codes obtained through simulation and analysis are provided.

2.2 Current Literature

The history of error correcting codes (ECC) started with the introduction of Hamming codes [25], at about the same time as the seminal work of Shannon [1]. Since that time many researchers have extended their knowledge and have invented detailed techniques

for communicating efficiently. The entire field of error control is devoted to the development of techniques to achieve the performance that Shannon proved possible.

Convolutional codes were first introduced by Elias [9] in 1955 as an alternative to block codes. Shortly thereafter, Wozencroft and Reiffen [26] proposed sequential decoding as an efficient decoding method for convolutional codes with large constraint lengths. In 1963 Massey [27] proposed a less efficient but simpler to implement decoding method called threshold decoding. This advance spawned a number of practical applications of convolutional codes to digital transmission over telephone, satellite, and radio channels [24]. Then in 1967 Viterbi [28], proposed a MLD algorithm that was relatively easy to implement for soft-decision decoding of convolutional codes of small constraint lengths. In 1974, Bahl, Cocke, Jelinek, and Raviv (BCJR) [10] introduced a maximum a posteriori probability MAP decoding algorithm for convolutional codes with unequal a priori probabilities for the information bits. The BCJR algorithm has been applied in recent years to soft-decision iterative decoding schemes in which the a priori probabilities of the information bits change from iteration to iteration. Applications using feedback systematic convolutional encoders which will be discussed in detail in the next section, called *turbo coding,* were introduced by Berrou, Glavieux and Thitimajshima [14], in an IEEE conference on communications in 1993, which had amazing performance for large block lengths and approached very close to Shannon's limit. Much of the research community was originally skeptical of the performance claims, but by the end of 1994 the basic results had been confirmed by several other research groups [29]. Two papers by Benedetto and Montorsi [30], [31] produced the first theoretical justification for the exceptional performance of the codes, and further insights were presented in [32], [33]. The research group of Haganaur was primarily responsible for illuminating the benefits of iterative decoding [32, 34]. The progress reports of Divsalar, Pollara, Dolinar and colleagues at the Jet Propulsion Laboratory provided a detailed look at many aspects of turbo coding [35, 36]. Numerous variations of turbo coding have also appeared in the literature, such as serial concatenation, hybrid parallel and serial concatenation, and self concatenation [31, 37]. A book by B.Vucetic and J.Yuan [23], and a very comprehensive study of the aspects of turbo coding, with an emphasis on iterative decoding was

published by W.E.Ryan [33]. Tutorials on turbo codes have also been published in [38] and [29].

2.3 Convolutional Codes

Convolutional codes have been widely used in various applications such as space and satellite communications, cellular mobile, digital video broadcasting etc. The reason for the widespread use of CCs is because of their simple structure and availability of easily implementable maximum likelihood decoding procedures. Convolutional codes were first introduced by Elias [9] in 1955 and later it was Forney [12] who performed the major ground work on the algebraic theory of CCs.

A convolutional code can be defined as a linear code with memory. It encodes a stream of data symbols, taking 'k' simultaneous input symbols and producing 'n' simultaneous output symbols at each time instant. The memory 'm' of a convolutional encoder is the number of consecutive k-symbol blocks that the encoder can store. Hence the set of all possible code sequences produced by the encoder is called the code rate. An optional puncturing scheme can be employed in order to increase the rate of the CC provided that the puncturing pattern is available at the receiver. Unfortunately increasing the rate degrades the performance of CCs. Consider a simple rate ½ convolutional code generated by the encoder [23] shown in Fig.2.1.

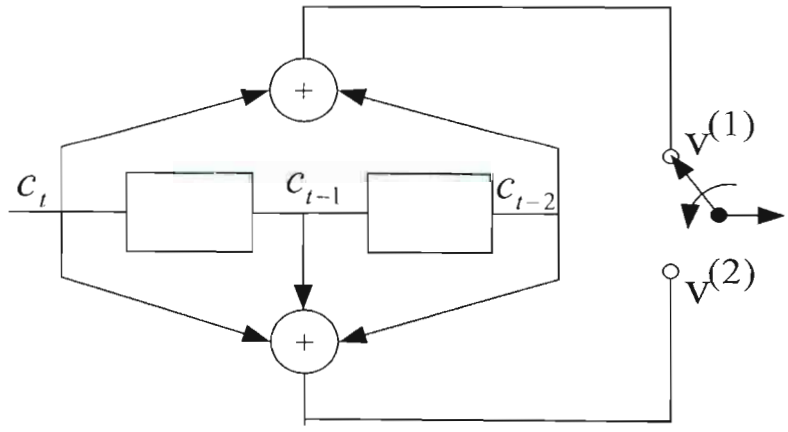

Fig.2.1: A rate ½ convolutional encoder

The encoder is a linear feedforward shift register. At time 't' the input to the encoder is c_t and the output is a code block v_t.

$$v_t = \left(v_t^{(1)}, v_t^{(2)}\right). \tag{2.1}$$

The elements of the output code block are computed as,

$$\begin{aligned} v_t^{(1)} &= c_t + c_{t-2} \\ v_t^{(2)} &= c_t + c_{t-1} + c_{t-2}, \end{aligned} \tag{2.2}$$

where ' $+$ ' denotes modulo-2 addition. The memory of the encoder is $m = 2$. The connections between the shift register's elements and the modulo-2 adders can be conveniently described by the following two generator sequences,

$$\begin{aligned} g^{(1)} &= (g_0^{(1)} g_1^{(1)} g_2^{(1)}) = (101)_8 \\ g^{(2)} &= (g_0^{(2)} g_1^{(2)} g_2^{(2)}) = (111)_8, \end{aligned} \tag{2.3}$$

where $g^{(1)}$ represents the upper and $g^{(2)}$ the lower connections. The term convolutional code originates from the observation that the i^{th} output sequence, i=1,2 represents the convolution of the input sequence and the i^{th} generator sequence.

$$v^{(i)} = c * g^{(i)}, \quad i = 1,2 \tag{2.4}$$

where $*$ denotes the convolution operator. CCs may be divided as systematic or non-systematic depending on whether or not the information sequence appears directly within the code sequence. CCs may be further classified as either non-recursive CCs or recursive CCs which is shown in the next section.

2.3.1 Non-Recursive and Recursive Convolutional Codes

The recursive CC has an IIR and non-recursive CC has a FIR. The generator set for non-recursive CCs G_{nrc} and recursive CCs G_{src} are defined as

$$G_{nrc} = \{g^i, 1 \le i \le k\}, \quad g^i = \sum_{k=0}^{m} g_k^i D^k, \tag{2.5}$$

and

$$G_{src} = \{1, \frac{g^i}{g^j}, 2 \le i \le k\} \quad g^i = \sum_{k=0}^{m} g_k^i D^k, \quad g^l = \sum_{k=1}^{m} g_k^l D^k, \quad g_0^1 = 1, \tag{2.6}$$

where, D can be interpreted as the unit delay operator. Fig.2.2 and Fig.2.3 show the diagrams of non-recursive and recursive CCs for $n = 1$ and $k = 2$.

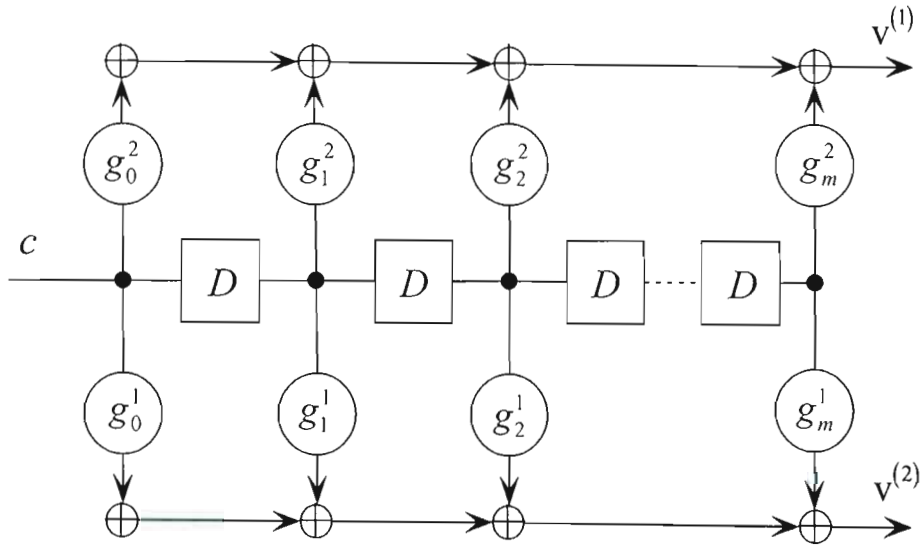

Fig.2.2: Diagram of non-recursive CC

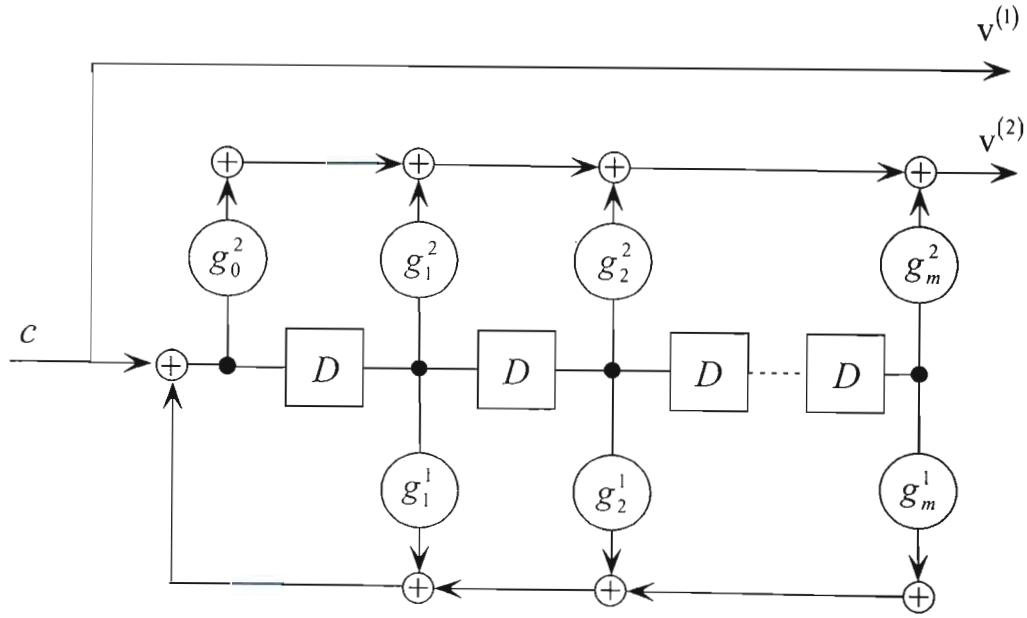

Fig.2.3: Diagram of a recursive CC

There are three equivalent ways of describing a convolutional code, namely

i.) the block diagram (shift register)

ii.) state diagram

iii.) trellis diagram

As a finite state linear circuit, a convolutional encoder can be described by a state diagram. The state diagram is a graph that consists of nodes, representing the encoder states, and directed lines, representing state transitions. Each directed line is labeled with the input/output pair. Given a current encoder state, the information sequence at the input determines the path through the state diagram and the output sequence. For example, consider the nonsystematic encoder shown in Fig.2.1. The state diagram and trellis representation for this encoder is shown in Fig.2.4. The encoder has four states labeled S_0, S_1, S_2 and S_3, where the subscripts correspond to the integer representations of the contents of the shift register elements. There are two paths leaving each state, corresponding to two possible values of the input message bit.

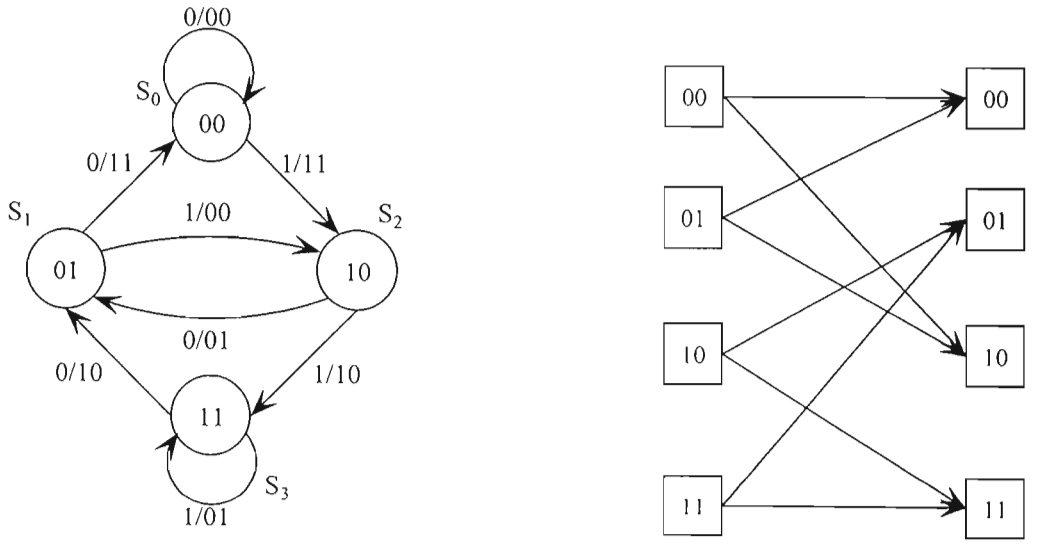

Fig.2.4: State and trellis diagram representations

2.3.2 Decoding

The decoder has knowledge of the code structure (i.e. it has a copy of the code trellis), the received sequence, and a statistical characterization (e.g. the transition probabilities) of the channel. The optimum decoding rule for the convolutional codes involves the decoder to estimate the transmitted code sequence to be the sequence which was most likely to have been transmitted, given the known code structure, channel characteristics and received sequence with minimum possible number of errors. Thus, the job of the decoder may be viewed as estimating the path through the trellis which was followed by the coder.

2.3.3 Trellis Termination

The decoding capability of a CC can be improved if the initial and final states are the same. Trellis termination involves driving the encoder to the all-zero state using additional bits that are required at the end of the frame to make sure that the initial state for the next frame of bits is in the all-zero state. It would require adding redundant bits at the end of the block equal to the memory order m of an encoder.

2.4 Concatenated Convolutional Codes

In a bid to find a class of codes whose probability of error decreased exponentially at rates less than channel capacity, while the decoding complexity increased only algebraically, Forney [12] arrived at a solution consisting of multilevel coding structure known as a concatenated code. His approach used a relatively shorter inner convolutional code admitting simple ML decoding, and a long high rate algebraic non-binary RS outer code equipped with a powerful algebraic error-correction algorithm which uses reliability information from the inner decoder. Initially motivated by theoretical research interests,

concatenated codes have since then evolved as a standard for those applications where very high coding gains are needed, such as deep space applications and many others.

As mentioned above a concatenated code is composed of two separate codes that are combined to form a large code [3]. In effect the use of two convolutional encoders in conjunction with the interleaver produces a code that contains very few code words of low weight. However this does not imply that the free distance of the concatenated code is especially large, but maintains that the use of the interleaver in conjunction with the two encoders results in code words that have relatively few nearest neighbors. Hence the codewords are relatively sparse. The interleaver was also proposed between the two encoders to separate bursts of errors produced by the inner decoder and also increase the randomness of the code. Concatenated codes are mainly divided into two types, the parallel and serial concatenation schemes. Fig. 2.5 shows the parallel concatenation transmission scheme.

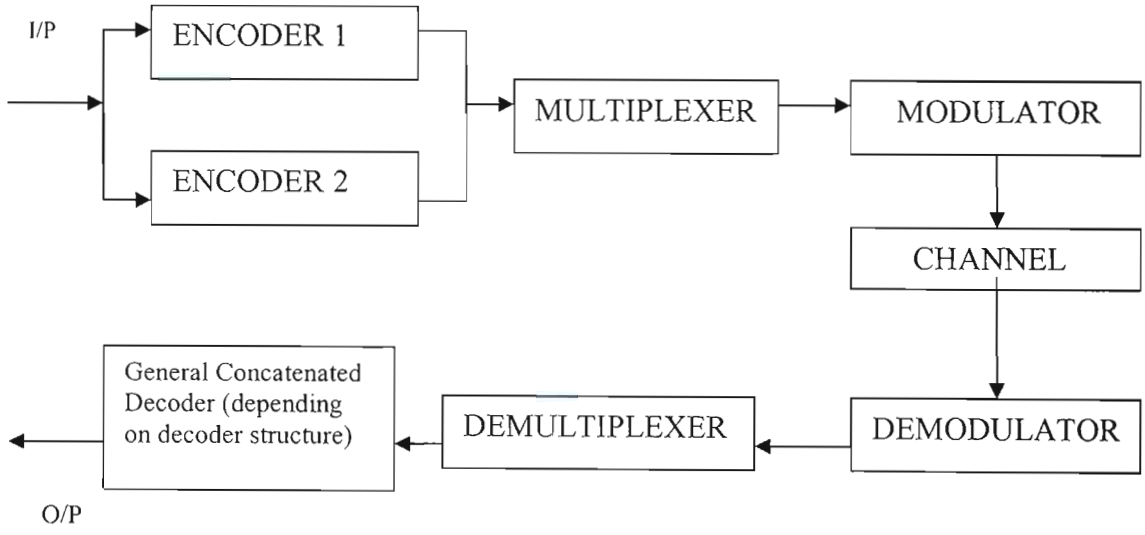

Fig. 2.5: Parallel concatenation scheme

The total code rate for the parallel concatenation scheme is $r_{TOT} = \frac{k}{n_1 + n_2}$

The serial concatenation of CCs with an interleaver is shown in Fig. 2.6. The code rate is given by $r_{TOT} = \frac{k_1 k_2}{n_1 n_2}$.

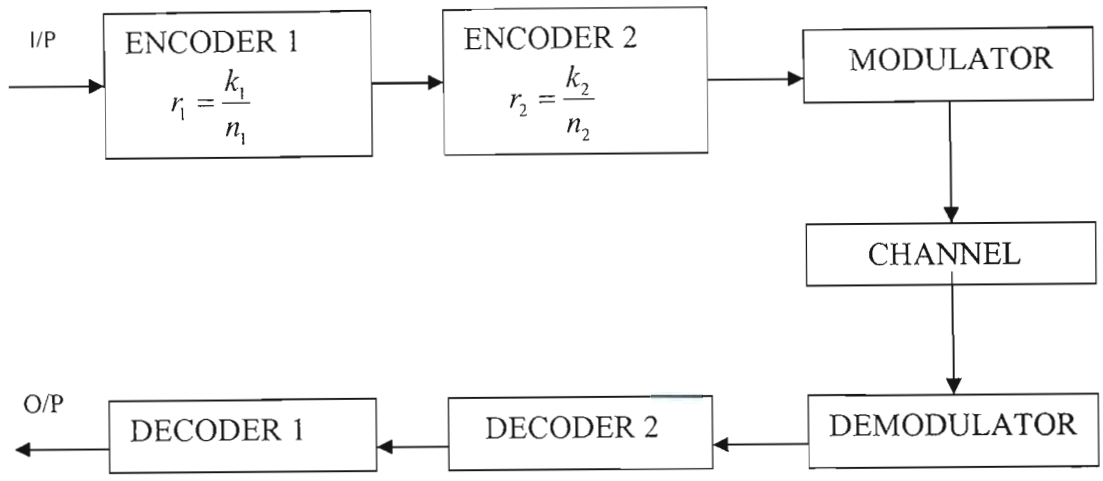

Fig. 2.6: Serial concatenation scheme

It should be noted that in the case of serial concatenation, the information is included only once in the concatenated codeword, whereas in the parallel concatenation there are two codewords that encode identical information. In comparing the error rate performance of serially concatenated convolutional code (SCCC) with the parallel concatenated convolutional code (PCCC), Benedetto et al [31] found that SCCC generally exhibits better performance than PCCC for error rates below 10^{-2}.

Concatenated codes can be decoded using maximum likelihood decoding algorithms based on the entire code trellis. Although it gets too complex to implement for medium to large interleaver sizes, their decoders can be implemented with realizable complexity using suboptimal yet powerful, iterative decoding algorithm whereby the constituent codes are decoded separately and soft information is exchanged between decoders in an iterative fashion. This method of soft-decision decoding for both the inner and outer decoders significantly improves the error performance of the system. The type, constraint length and generator polynomials of the constituent encoders have a large influence on the overall code's performance. Increasing the constraint length of the constituent codes improves the overall code's performance at high signal to noise ratios (SNRs) but

generally degrades its performance at low SNRs [23]. The joint effect of the interleaver and constituent codes must be considered when designing the required concatenated code.

The parallel concatenation of two convolutional codes using a pseudorandom interleaving and iterative decoding produced a powerful class of codes commonly called Turbo Codes which is discussed in detail in the next section.

2.5 Turbo Codes

The original concept of Turbo coding was introduced in a paper by C.Berrou, A.Glavieux and P.Thitimajshima [14] delivered at the IEEE International Conference on Communications held in Geneva, Switzerland in May 1993. This parallel concatenated convolutional code or more commonly called Turbo Codes, succeeded in achieving randomlike code design with just enough structure to allow for an efficient iterative decoding method. The importance of turbo codes is that they enable reliable communications with power efficiencies close to the theoretical limit predicted by Shannon in [13]. The announced performances of these codes was so good that the initial reaction of the coding establishment was deep skepticism, but later as time progressed researchers around the world have been able to reproduce those results [13, 14]. The introduction of turbo codes has opened a whole new way of looking at the methods of constructing good codes and decoding them with low complexity.

In a nutshell, turbo coding consists of two fundamental ideas: a code design that produces a code with randomlike properties, and a decoder design that makes use of soft-output values and iterative decoding. However, the great performance of these codes is affected by a large decoding delay. This is owing to large block lengths and many iterations of decoding required for near capacity performance and significantly weakened performance at BER below 10^{-5}. This is due to the fact that the codes have a relatively poor minimum distance which manifests itself at very low BERs in the form of error floors. Since its recent invention, turbo coding has evolved at an unprecedented rate and

has reached a state of maturity within just a few years due to the intensive efforts of the turbo coding community. As a result turbo codes have been proposed for power limited applications such as deep-space and satellite communications, as well as interference limited applications such as third generation cellular and personal communication services.

2.5.1 Turbo Encoder

Turbo coding can be accomplished by the parallel concatenation of two recursive systematic convolutional (RSC) encoders separated by an N-bit random interleaver or permuter together with an optional puncturing mechanism [23]. The encoder structure is called a parallel concatenation because the two encoders operate on the same set of input bits, rather than one encoding the output of the other. Thus they are also sometimes referred to as parallel concatenated convolutional codes. A block diagram of a turbo encoder is shown in Fig. 2.7. The overall code rate of a turbo code composed from the parallel concatenation of two rate $1/2$ systematic codes is $R = 1/3$, and so the encoder maps N data bits to 3N code bits. Since both encoders are systematic and receive the same set of data (although in permuted order), only one of the systematic outputs needs to be sent. By convention, the systematic output of the first encoder is sent and the parity outputs of both the encoders are sent. The code rate can be improved by incorporating a puncturing mechanism.

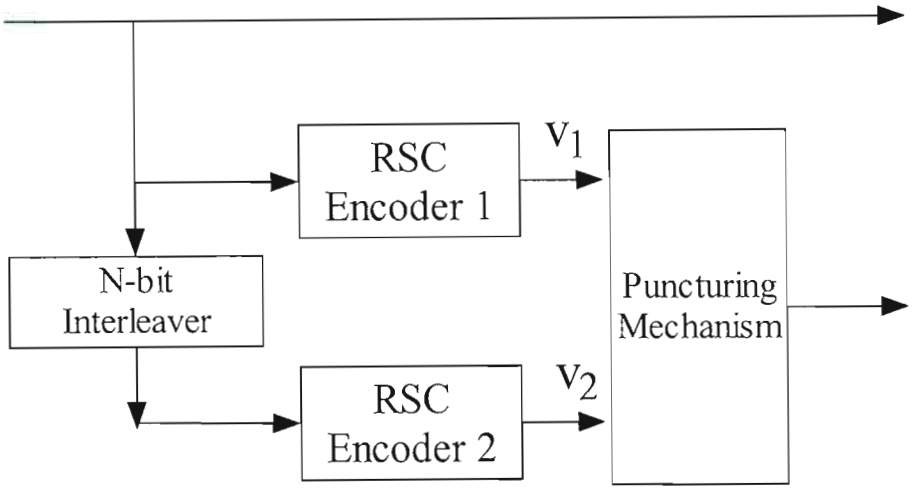

Fig. 2.7: A Turbo Encoder

The generator matrix of a rate $1/2$ component RSC code can be represented as,

$$G(D)=\left[1,\frac{g_1(D)}{g_0(D)}\right] \tag{2.7}$$

where, $g_0(D)$ and $g_1(D)$ are feedback and feedforward polynomials with degree v, respectively. It is observed that a codeword containing a single 1 (0000100), will propagate through any interleaver as a single 1. So, the conclusion is that if we use the codes in the feedforward form in the turbo scheme, the resulting code will have a large number of codewords with low weights. Hence, by using the recursive systematic form, we do not change the set of encoded sequences, but change the mapping of input sequences to the output. This ensures that there is a chance to find an interleaver where the information patterns giving low weight words from the first encoder are interleaved to patterns giving words with high weight from the second encoder [13].

2.5.2 Interleaver Design

The interleaver in turbo codes plays a very vital role in the performance of the code. Turbo codes use a pseudorandom interleaver defined by a permutation of N elements

with no repetitions. The first role of the interleaver is to generate a long block code from small memory convolutional codes, as long codes can approach the Shannon capacity limit. Secondly, it decorelates the inputs to the two decoders so that an iterative sub-optimum decoding algorithm based on the information exchange between the two component decoders can be applied. If the input sequence to the two component decoders is decorelated there is a high probability that after correction of some errors in one decoder, some of the remaining errors should become correctable in the second decoder. The final role of the interleaver is to break low weight input sequences, and hence increase the code's free Hamming distance or reduce the number of codewords with small distances in the code distance spectrum. This in turn reduces the probability that the decoder will mistake one codeword for another.

Unlike the classical interleaver (e.g. block or convolutional), which rearranges the bits in some systematic fashion, it is important that the interleaver sorts the bits in a manner that lacks apparent order, although it might be tailored in a certain way for weight-two and weight-three inputs. The BER curves of many turbo codes flatten at low BER. This occurs because although the effect of the pseudorandom interleaver means that the code sequences at small Hamming distances are rare, they may nevertheless occur somewhere in the code. These then result in as small residual BER term which does not decrease so rapidly with SNR. The probability of such sequences, and hence the level of this 'floor', decreases rapidly with increasing interleaver length. A number of interleaving structures are discussed in [23], which are block, convolutional, random, circular-shifting, semi-random and odd-even interleavers to name a few.

2.5.3 Turbo Decoder

If we were to assume as an example, a ML decoder for a rate $1/2$ convolutional code (recursive or not), and assume a data word of length N, $N \geq 1000$, ideally the decoder would have to compare (correlate) 2^N code sequences to the noisy received sequence, choosing in favour of the codeword with the best correlation metric. Clearly the

complexity of such an algorithm is exorbitant. Fortunately, as we know, such a brute force approach is simplified greatly by Viterbi's algorithm which permits a systematic elimination of candidate code sequences (in the first step, 2^{N-1} are eliminated then another 2^{N-2} are eliminated on the second step and so on). Unfortunately in the case of turbo codes the presence of the interleaver immensely complicates the structure of a turbo code trellis.

Prior to the discovery of turbo codes, there was much interest in the coding community in suboptimal decoding strategies for concatenated codes involving multiple (usually two) decoders, operating cooperatively in an iterative manner. Most of the focus was spent on a type of Viterbi decoder which provides soft-output information to a companion soft-output Viterbi decoder for use in a subsequent decoding [33]. Also receiving some attention was the symbol-by-symbol MAP algorithm often called the BCJR algorithm, which Berrou et al [14] utilized in the iterative decoding of turbo codes. The block diagram of the turbo decoder is shown below in Fig. 2.8.

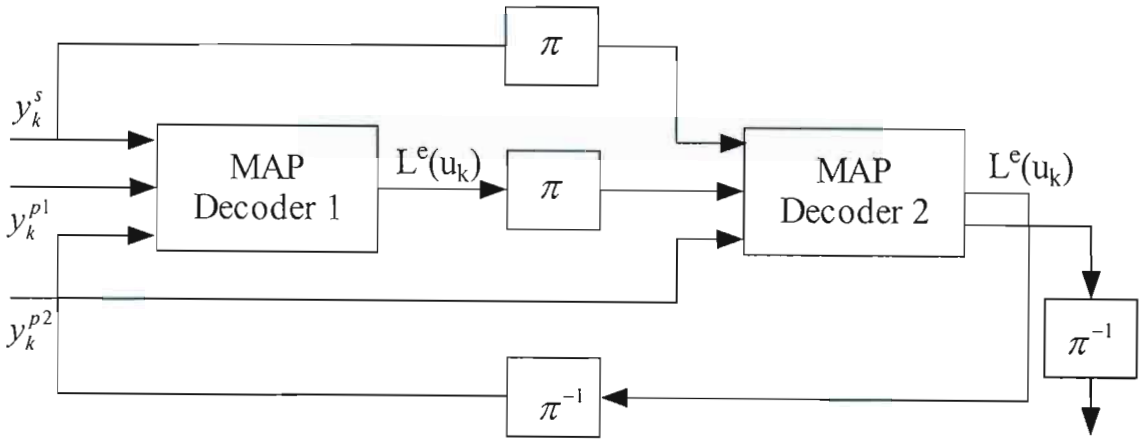

Fig. 2.8: Turbo Decoder

As seen in Fig. 2.8, each decoder takes three inputs: 1) the systematically encoded channel output bits; 2) the parity bits transmitted from the associated component encoder; and 3) the information from the other component decoder about the likely values of the bits concerned. This information from the other decoder is referred to as *a-priori* information. The component decoders have to exploit both the inputs from the channel and this *a-priori* information and provide soft outputs for the decoded bits. So, in addition

to proving the decoded output bit sequence, the component decoders must also give the associated probabilities for each bit that it has been correctly decoded.

The soft outputs from the component decoders are typically represented in terms of the so called Log Likelihood Ratios (LLR), the magnitude of which gives the sign of the bit, and the amplitude the gives probability of a correct decision. The LLRs are the logarithmic ratio of two probabilities. For example, the LLR $L(u_k)$ for the value of a decoded bit u_k is given by,

$$L(u_k) = \ln\left(\frac{P(u_k = +1)}{P(u_k = -1)}\right), \tag{2.8}$$

where, $P(u_k = +1)$ is the probability that the bit $u_k = +1$, and similarly for $P(u_k = -1)$. The two possible values of the bit u_k are taken to be +1 and -1, rather than 1 and 0, as this simplifies the algorithms involved to avoid overflow errors that may occur in the recursive calculation of the various metric updates.

2.5.4 Iterative Decoding

Iterative decoding may be defined as technique employing a soft-output decoding algorithm that is iterated several times to improve the error performance of a coding scheme, with the aim of approaching true maximum likelihood decoding (MLD) with less complexity. Hence the error correcting capability of a code is improved by the increase of the number of iterations. Iterative techniques date back to 1954 with the work of Elias [9] on iterated codes. It was later, in the 1960s that Gallagar [114] and Massay [27] made important contributions in this field. Iterative decoding was then referred to as probabilistic decoding and the main concept was to maximize the a-posteriori probability of a symbol being sent, given a noisy version of the coded sequence.

The decoder in Fig. 2.8 operates iteratively, and in the first iteration the first component decoder takes channel outputs, (which is the received information sequence r_0 and the

received parity sequence r_1 generated by the first encoder) and produces a soft output estimate of the data bits. The soft outputs from the first decoder are then used as additional information for the second decoder, which uses this information along with the channel outputs, (which is the interleaved received information sequence $\tilde{r}_0$ and the received parity sequence r_2 produced by the second encoder) to calculate its estimate of the data bits. Now during the next iteration, the first decoder decodes the channel outputs again, but now with additional information about the value of the input bits provided by the output of the second decoder in the first iteration. This additional information allows the first decoder to obtain a more accurate set of soft outputs, which are then used by the second decoder as a-priori information. This cycle is repeated and with every increase in the number of iterations, the BER of the decoded bits tends to fall. However, the improvement in performance obtained with increasing numbers of iterations decreases as the number of iterations increases. Hence, for complexity reasons, usually only about seven or eight iterations are used.

2.6 Map Algorithm

In this section we describe the theory behind the Maximum A-Posteriori algorithm as used for soft output decoding of the component convolutional codes of turbo codes. It is assumed that binary codes are used. The derivation of this algorithm has been well documented in previous papers [10, 14, 33, 39] and so for notational purposes, the algorithm is briefly reviewed here [40].

The MAP algorithm gives, for each decoded bit u_k, the probability that this bit was +1 or -1, given the received symbol sequence $\mathbf{y}$. Hence the decision $\tilde{u}_k$ is given by,

$$\tilde{u}_k = \text{sign}[L(u_k)], \tag{2.9}$$

where, $L(u_k)$ is the a-posteriori LLR or sometimes called log a-posteriori probability (LAPP) ratio defined as

$$L(u_k) \triangleq \log\left(\frac{P(u_k = +1 \mid y)}{P(u_k = -1 \mid y)}\right). \tag{2.10}$$

Taking into account and incorporating the trellis, let S be the set of all 2^m constituent encoder states (m is the memory) and $s_k \in S$ be the state of the encoder at time k. Furthermore, let S^+ be the set of ordered pairs (s',s) corresponding to all the state transitions $(s_{k-1} = s') \rightarrow (s_k = s)$ caused by data input $u_k = +1$, and S^- be similarly defined for $u_k = -1$. This may be written as [33],

$$L(u_k / \mathbf{y}) = \log\left(\frac{\sum_{S^+} \tilde{\alpha}_{k-1}(s') \bullet \gamma_k(s',s) \bullet \tilde{\beta}_k(s)}{\sum_{S^-} \tilde{\alpha}_{k-1}(s') \bullet \gamma_k(s',s) \bullet \tilde{\beta}_k(s)}\right), \tag{2.11}$$

where, the $\tilde{\alpha}'s$ are computed recursively as,

$$\tilde{\alpha}_k = \frac{\sum_{s'} \tilde{\alpha}_{k-1}(s')\gamma_k(s',s)}{\sum_s \sum_{s'} \tilde{\alpha}_{k-1}(s')\gamma_k(s',s)}, \tag{2.12}$$

with initial conditions $\tilde{\alpha}_0(0) = 1$ and $\tilde{\alpha}_0(s \neq 0) = 0$. (These conditions ensure that the decoder starts in state 0). The 'backward' recursion values $\tilde{\beta}$'s are computed as,

$$\tilde{\beta}_{k-1}(s') = \frac{\sum_{s'} \tilde{\beta}_k(s)\gamma_k(s',s)}{\sum_s \sum_{s'} \tilde{\alpha}_{k-1}(s')\gamma_k(s',s)}, \tag{2.13}$$

with boundary conditions $\tilde{\beta}_N(0) = 1$ and $\tilde{\beta}_N(s \neq 0) = 0$. (The encoder is expected to end in the state 0 after N input bits, implying that the last m input bits, the termination bits, are also selected). The probability $\gamma(s',s)$ in (2.11), (2.12) and (2.13) is defined as,

$$\gamma(s',s) = p(s_k = s, y_k / s_{k-1} = s'), \tag{2.14}$$

and represents the branch transition probabilities used by the MAP algorithm. They are of particular interest and essentially measure the probability of channel outputs given a particular state transition along a branch in the encoder trellis. The computation of branch

transition probabilities depends on the channel, so they play an important role later in the design of concatenated turbo space-time coded systems.

Assuming a memoryless Gaussian channel with BPSK modulation, it is shown from [33] that for a systematic code such as a RSC code,

$$\begin{aligned}\gamma(s',s) &= P(u_k)\,p(y_k/u_k) \\ &= \exp\left[\frac{1}{2}u_k\left(L^e(u_k)+L_c y_k^s\right)+\frac{1}{2}L_c y_k^p x_k^p\right] \\ &= \exp\left[\frac{1}{2}u_k\left(L^e(u_k)+L_c y_k^s\right)\right]\bullet\gamma_k^e(s',s),\end{aligned} \tag{2.15}$$

where,

$$L_c \triangleq \frac{4E_c}{N_0}, \tag{2.16}$$

and where

$$\gamma^e(s',s) = \exp\left[\frac{1}{2}L_c y_k^p x_k^p\right]. \tag{2.17}$$

In (2.16) and (2.17) x_k^p and y_k^p are the individual bits within the transmitted and received codewords y_k and x_k, $E_c = rE_b$ is the energy per channel bit, $\sigma^2 = N_0/2E_c$ is the noise variance and a is the fading amplitude (where a=1 for non-fading AWGN channels).

Iterative Turbo Decoding Principles

Combining (2.15) with (2.11) it can be shown that, for a systematic code such as a RSC code, the output from the MAP decoder can be re-written as

$$L(u_k/\mathbf{y}) = L(u_k) + L_c y_k^s + L_e(u_k), \tag{2.18}$$

where, we can see that the a-posteriori LLR $L(u_k/\mathbf{y})$ calculated with the MAP algorithm can be thought of as comprising of three terms - $L(u_k), L_c y_k^s$ and $L_e(u_k)$. The a-priori LLR term $L(u_k)$ comes from $P(u_k)$ in the expression of the branch transition probability $\gamma(s',s)$ (2.15). In most cases we will have no independent or a-priori knowledge of the

likely value of the bit u_k, however, in the case of an iterative turbo decoder, each component decoder can provide the other decoder with an estimate of the a-prior LLR $L(u_k)$. The second term is $L_c y_k^s$ in (2.18) is the soft output of the channel for the systematic bit u_k, which is directly transmitted across the channel and received as y_k^s. The final term in (2.18), $L_e(u_k)$, is derived using the constraints imposed by the code used, from the a-priori information sequence $L(u_k)$ and the received channel information sequence $\mathbf{y}$, excluding the received systematic bit y_k^s and the a-priori information $L(u_k)$ for the bit u_k. Hence, it is called extrinsic LLR for the bit u_k, and (2.18) shows that the extrinsic information from the MAP decoder can be obtained by subtracting the a-priori information $L(u_k)$ and the received systematic channel input $L_c y_k^s$ from the soft output $L(u_k / \mathbf{y})$ of the decoder.

This iterative process continues with ever-updating extrinsic information to be exchanged between the two component decoders, and with every iteration on the average, the BER of the decoded bits will fall. Due to complexity reasons usually around six to eight iterations are carried out, as no significant improvement in performance is obtained with higher number of iterations. After the last iteration stage, we obtain the computation of the output from the turbo decoder, given by the de-interleaved a-posteriori LLRs of the second component decoder given by,

$$L_i(u_k) = L_c y_k^s + L_{21}^e(u_{P^{-1}[k]}) + L_{12}^e(u_k), \tag{2.19}$$

where, i is the number of iterations used. The sign of the a-posteriori LLRs gives the hard decision output, i.e., whether the decoder believes the transmitted data bit u_k was +1 or -1, and the magnitude of these LLRs, which gives the reliability or in other words the confidence the decoder has in its decision.

2.7 Performance Analysis of Turbo Codes

In order to carry out the performance evaluation of turbo codes there are two main approaches adopted for this purpose. Simulation results of turbo codes have shown that turbo codes can produce low error rates at astonishingly low signal-to-noise ratios if the information blocks used are large and permutations are selected randomly [35,36]. In addition to simulation results, it is also useful to have theoretical bounds that establish decoder performance in the range where obtaining sufficient data from simulation is impractical.

This section discusses the transfer function bounding techniques to obtain upper bounds on the bit-error rate for maximum likelihood decoding for turbo code constructed with random permutation. The bound makes use of the so called uniform interleaver, which averages the performance of the codes over all possible interleavers. This concept was originally proposed by Benedetto et al [41]. The approach is similar to the conventional transfer function bounding technique as applied to convolutional codes [42], wherein the error probability is upper bounded by a union bound that sums the contributions from error paths of different encoded weights.

Much like transfer function bounds for convolutional codes, we assume the transmission of the all-zero codeword and evaluate the probability of the decoder selecting some alternative codeword. However, transfer function bounds for turbo codes as indicated in [35], differ from those of convolutional codes in many respects. First, these bounds require a term-by-term joint enumerator for all possible combinations of input and output weights. Second, because turbo codes are block codes, it is necessary to enumerate compound error events that can include more than one excursion from the all-zero state during the fixed block length, N as shown in Fig. 2.9. Third, since there are good and bad random interleavers from a stand point of code performance, the bounds make use of the uniform interleaver, which essentially averages out the effect of the interleaver on the bound. Finally, the bounds presume a maximum-likelihood decoder operating on the

encoded data even though the iterative decoding procedure used in practice will not necessarily converge to the maximum likelihood codeword.

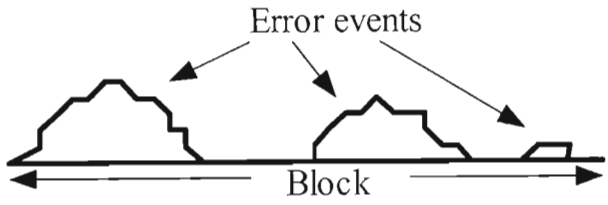

Fig. 2.9 Example of compound error events

2.7.1 Turbo Encoder Structure

Two exemplary turbo encoders from Fig. 2.10 (a) and Fig. 2.10 (b) can be used for this section. The encoder diagram in Fig. 2.10 (a) is systematic, and the remaining parity bits are produced by two identical constituent recursive convolutional encoders with generator polynomials, g_a / g_b where, $g_a(D) = 1 + D + D^2$ and $g_b(D) = 1 + D^2$. In octal notation, the composite encoder has generators $(1, 7/5, 7/5)$. It is assumed as previously mentioned in the chapter, that the two code fragments of memory $v = 2$, start in the all-zero state and are driven back to the all-zero state through the transmission of tail bits. Note that we assume tail-bit transmission for both encoders.

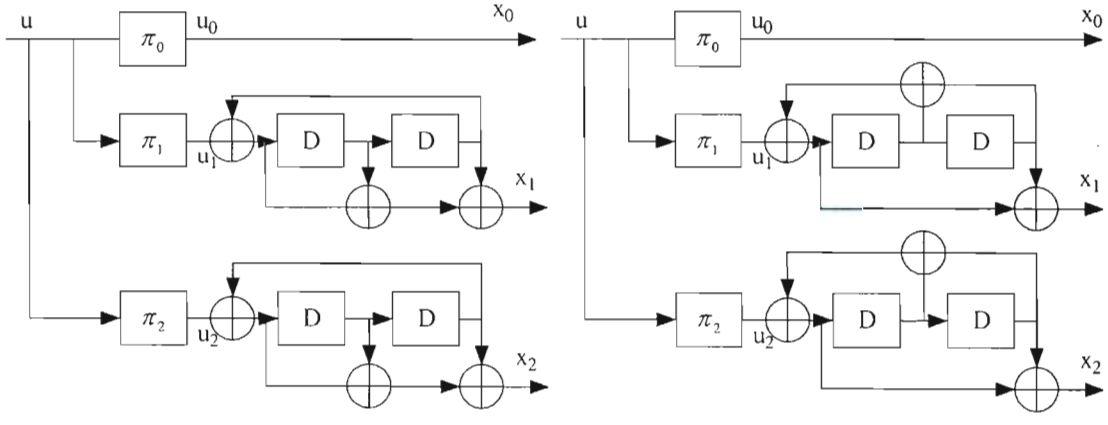

Fig. 2.10: (a) the (1, 7/5, 7/5) code and (b) the (1, 5/7, 5/7) code.

2.7.2 Union Bound

This section briefly discusses the union bound method of analyzing the performance of coded systems. This bounding technique is computationally very intensive and so a number of approximations have to be taken into account. Generally speaking, the performance of a given code is upper bounded using the union bound. The union bound states that the probability of the union of n_E error events E_i, is less than or equal to the sum of the individual probabilities of each error event. This can be mathematically represented as follows,

$$P(\bigcup_{i=1}^{n_E} E_i) \leq \sum_{i=1}^{n_E} P(E_i). \tag{2.20}$$

It is clear from the above equation that the union bound will always give an upper bound on the code's performance. The conventional bound on the probability of codeword error, P_w is given by

$$P_w \leq \sum_d t(d) P_2(d), \tag{2.21}$$

where, $t(d)$ represents the number of codewords of weight d and $P_2(D)$ is the probability of selecting an incorrect codeword that differs from the correct codeword in d bit positions. The weight enumerator $t(d)$ is typically obtained via the transfer function of the convolutional code. Using the notion of a uniform interleaver, the weight enumerator, $t(d)$, is replaced by an average weight enumerator, $\overline{t(d)}$, yielding an average upper bound on P_w as shown below,

$$\overline{P_w} \leq \sum_d \overline{t(d)} P_2(d). \tag{2.22}$$

Since $\overline{t(d)}$ reflects the averaging over all possible interleavers of length N, $\overline{t(d)}$ is given by,

$$\overline{t(d)} = \sum_{i=1}^{N} \binom{N}{i} p(d/i), \tag{2.23}$$

where, $\binom{N}{i}$ is the number of input sequences of length N and weight i, and $p(d/i)$ represents the probability that an input sequence of weight i yields an output

codeword of weight d, when averaged over all possible interleavers. Substituting (2.23) into (2.22), we obtain

$$\begin{aligned}\overline{P_w} &\le \sum_d \left(\sum_{i=1}^{N} \binom{N}{i} p(d/i) \right) P_2(d) \\ &= \sum_{i=1}^{N} \binom{N}{i} \sum_d p(d/i) P_2(d) \\ &= \sum_{i=1}^{N} \binom{N}{i} E_{d/i}\{P_2(d)\},\end{aligned} \tag{2.24}$$

where, the summand represents the average upper bound on the probability of an error event of input weight i, given that the all-zero codeword is transmitted, a decoded codeword of input weight i corresponds to an error event with i bit errors. Thus, we define the probability of bit error, P_b as the average number of bit errors per codeword which is shown,

$$P_b = \frac{1}{N} \sum_{i=1}^{N} iP\{error\ event\ of\ weight\ i\}. \tag{2.25}$$

Directly from this result, we obtain an average upper bound on the probability of bit error, given by,

$$\overline{P_b} \le \sum_{i=1}^{N} \frac{i}{N} \binom{N}{i} E_{d\backslash i}\{P_2(d)\}. \tag{2.26}$$

If we express the output weight d, of a turbo codeword in terms of the output weights, d_0, d_1 and d_2, of the constituent code fragments, we have $d = d_0 + d_1 + d_2$, and assuming the permutations are selected randomly and independently, we arrive at

$$p(d_0, d_1, d_2 \mid i) = p_0(d_0 \mid i) p_1(d_1 \mid i) p_2(d_2 \mid i), \tag{2.27}$$

where, the conditional probabilities in the right side of (2.27) corresponds to the individual code fragments. Next, we must determine the conditional probabilities for the respective code fragments. As we are dealing with systematic encoders, for the systematic fragment, assuming no puncturing, we have,

$$\begin{aligned}p_0(d_0 \mid i) &= \begin{cases} 1 & i = d_0 \\ 0 & i = d_0 \end{cases} \\ &= \delta(i, d_0).\end{aligned} \tag{2.28}$$

For a given i and d, we may compute $p_j(d_j \mid i), j = 1,2$, by counting the number of possible paths of length N through the decoding trellis of code fragment j which start and end in the all-zero state and have total input and output weights i and d_j, respectively. Given this count, which we denote by $t_j(i,d_j)$, the conditional probability is given by,

$$p_j(d_j \mid i) = \frac{t_j(i,d_j)}{\binom{N}{i}} \tag{2.29}$$

Hence (2.23) can be rewritten as,

$$\overline{t(d/I_1,I_2)} = \sum_{i}^{N} \sum_{d_1} \sum_{d} \binom{N}{i} P(i,d_1,d_2/i,I_1,I_2) \tag{2.30}$$

Therefore the complete expression for the word and bit error probabilities substituting in (2.22) are given as,

$$\overline{P}_w = \sum_{d=d_{\min}}^{3N} \underbrace{\sum_{i} \sum_{d_1} \sum_{d_2}}_{d=i+d_1+d_2} \binom{N}{i} P(d_1/i) P(d_2/i) P_2(d)$$

and (2.31)

$$\mathrm{P_b} \le \sum_{d=d_{\min}}^{3N} \underbrace{\sum_{i} \sum_{d_1} \sum_{d_2}}_{d=i+d_1+d_2} \frac{i}{k} \binom{N}{i} P(d_1/i) P(d_2/i) P_2(d).$$

2.7.3 State Transition Matrix

The state diagrams for the example (7/5) and (5/7) code fragments are shown in Fig.2.11. Transitions from states are labeled with the appropriate input and output bit, as well as monomials to enumerate accumulated path length (L), input weight (I), and output weight (D).

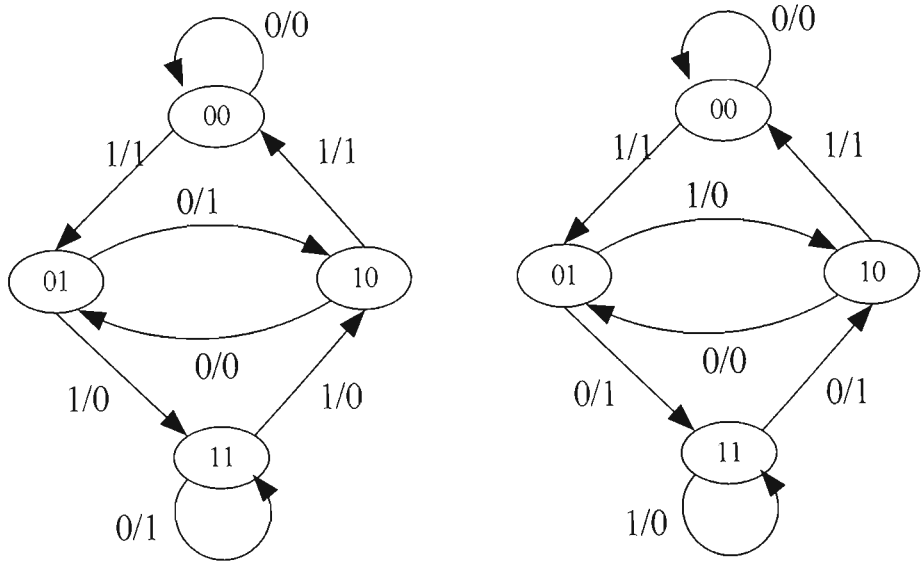

Fig.2.11: State diagrams for (7/5) and (5/7) code fragments

The code fragments may be equivalently described by a state transition matrix. The state transition matrix for the (7/5) and (5/7) code fragments respectively are given below,

$$\mathbf{A}_{7/5}(L,I,D)=\begin{pmatrix} L\,LID & 0 & 0 \\ 0 & 0 & LD\,LI \\ LID\,L & 0 & 0 \\ 0 & 0 & LI\,LD \end{pmatrix}, \tag{2.32}$$

and for the (5/7) code fragment,

$$\mathbf{A}_{5/7}(L,I,D)=\begin{pmatrix} L\,LID & 0 & 0 \\ 0 & 0 & LI\,LD \\ LID\,L & 0 & 0 \\ 0 & 0 & LD\,LI \end{pmatrix}. \tag{2.33}$$

This state transition matrix representation is obtained by replacing each edge label shown in Fig.(2.11a) and Fig.(2.11b) with a monomial $L^{l}I^{i}D^{d}$, where l is always equal to 1, and i and d are either 0 or 1, depending on whether the corresponding input and output bits are 0 or 1, respectively. By doing this we can summarize the information of the state diagrams in these state transition matrices $\mathbf{A}(L,I,D)$.

2.7.4 Transfer Function

The transfer function for the code fragment $T(L,I,D)$, is defined [35] as,

$$T(L,I,D)=\sum_{l\geq 0}\sum_{i\geq 0}\sum_{d\geq}t(l,i,d)L^{l}I^{i}D^{d}. \tag{2.34}$$

This function enumerates the input and output weight associated with all paths of all possible lengths through the state diagram of the code fragment which both start and end in the all-zero state. The weight enumerator $t(l,i,d)$ indicates the number of paths of length l with input weight i and output weight d which start and end in the all-zero state. As described in [35], the transfer function $T(l,i,d)$, is given by the $(0,0)$ element of the matrix raised to the power of the interleaver length. Hence, this can be represented as,

$$(I+\mathbf{A}(L,I,D)+\mathbf{A}(L,I,D)^{2}+\cdots)\mathbf{A}(1,1,D)^{\nu}, \tag{2.35}$$

where the term $\mathbf{A}(1,1,D)^{\upsilon}$ expresses the contribution of the tail-bit transmission in which neither path length nor input weight are accumulated.

To compute the coefficients $\{t(N,i,d)\}$, which are required for the performance bounding techniques described earlier, the transfer function can be obtained by noting that,

$$\mathbf{I}+\mathbf{A}+\mathbf{A}^{2}+\mathbf{A}^{3}+\cdots=(\mathbf{I}-\mathbf{A})^{-1}, \tag{2.36}$$

and, therefore, $T(L,I,D)$ is the (0, 0) element of the matrix

$$\left[\mathbf{I}-\mathbf{A}(L,I,D)\right]^{-1}\mathbf{A}(L,I,D)^{\upsilon}. \tag{2.37}$$

Using (2.37) and by omitting the termination factor $\mathbf{A}(L,I,D)^{\upsilon}$, we can get the following approximation for the example above mentioned (7/5) code as,

$$T(L,I,D)\approx\frac{1-LD-L^{2}D+L^{3}\left(D^{2}-I^{2}\right)}{1-L(1+D)+L^{3}\left(D+D^{2}-I^{2}-I^{2}D^{3}\right)-L^{4}\left(I^{4}D^{2}-I^{2}D^{4}+D^{2}-I^{2}\right)}. \tag{2.38}$$

Given $T(L,I,D)$, one can extract recursive equations from which the coefficients $t(l,i,d)$ can be calculated shown in (2.39), starting with $t(0,0,0)$, until $\{t(N,i,d)\}$ are obtained over a reasonable range of i and d .

$$\begin{aligned} t(l,i,d) &= t(l-1,i,d-1)+t(l-1,i,d) \\ &+t(l-3,i-2,d-3)+t(l-3,i-2,d)-t(l-3,i,d-2)-t(l-3,i,d-1) \\ &+t(l-4,i-4,d-2)-t(l-4,i-2,d-4)-t(l-4,i-2,d)+t(l-4,i,d-2) \\ &+\delta(l,i,d)-\delta(l-1,i,d-1)-\delta(l-2,i,d-1)+\delta(l-3,i,d-2)-\delta(l-3,i-2,d). \end{aligned} \tag{2.39}$$

Assuming the use of a uniform interleaver, we may compute $p_j(d_j \mid i), j=1,2$ from (2.29) for each code fragment and (2.27) for the entire code.

In practice the computation of (2.37) requires the algebraic inversion of SxS matrix of three dimensional polynomials, where $S \equiv 2^{\upsilon}$ is the number of states in the code fragment. The complexity of this calculation obviously grows with S and requires the capability to perform rational polynomial arithmetic. In [43], it was observed that they propose a new method by which the desired enumerators $t(N,i,d)$ may be found in a less complex manner. First, we note that the desired enumerators $t(N,i,d)$ may be found exclusively in the $(0,0)$ element of the matrix

$$\mathbf{A}(L,I,D)^N \mathbf{A}(1,1,D)^{\upsilon}. \tag{2.40}$$

In this case, since all the elements of $\mathbf{A}(L,I,D)^N$ contain L^N term, we may omit the monomial L entirely and, therefore compute

$$\mathbf{A}(1,I,D)^N \mathbf{A}(1,1,D)^{\upsilon}, \tag{2.41}$$

or in simplified notation,

$$\mathbf{A}(I,D)^N \mathbf{A}(1,D)^{\upsilon}. \tag{2.42}$$

Normally, you would employ the method whereby, you would ignore the termination term $\mathbf{A}(1,D)^{\upsilon}$ for the moment. Then calculate $\mathbf{A}^2$, then compute $\mathbf{A}^4 = \mathbf{A}^2 \bullet \mathbf{A}^2$, and so on until $\mathbf{A}^N$ is obtained. The larger the frame lengths involved the more complex the

calculations become. Alternatively, since we desire only the $(0,0)$ element of $\mathbf{A}(I,D)^N$, let us define a^T to be the first row of $\mathbf{A}$, and note that the product $a^T\mathbf{A}$ is just the first row of the matrix $\mathbf{A}^2$. If we apply these identity recursively (i.e. $a^T(k) = a^T(k-1)\mathbf{A}$) N times, we obtain the first row of $\mathbf{A}^N$. This method greatly reduces the intensive computational methods required previously. Having successfully computed the first row of $\mathbf{A}(I,D)^N$, we may apply the same method υ times to compute the first row of $\mathbf{A}(I,D)^N\mathbf{A}(1,D)^\upsilon$.

When successively multiplying polynomials in the above mentioned methods, it is possible for resulting polynomial degrees to get very large, especially when N is large. This growth in degree can be controlled by discarding any polynomial components with input degree (exponent of I) or the output degree (exponent of D) that exceed prescribed thresholds. This can be observed from [43] where the union bound becomes insignificant for $i < 10$, regardless of the block size and the error probability decreases rapidly for increasing d, which justifies the discarding of components with large output distances.

2.7.5 EXIT Charts and Density Evolution

Convergence analysis of iterative decoding algorithms for turbo codes has received much attention recently due to its useful application to predicting code performance, its ability to provide insights into the encoder structure, and usefulness in helping with the code design. Several methods have been proposed to analyze the convergence of the iterative decoders for binary turbo codes [119 - 122].

In particular, the extrinsic information transfer (EXIT) method [119]. The EXIT chart is a tool for studying the convergence of turbo decoders without simulating the whole decoding process. The chart is generated by a single component decoder by minimizing the *a-priori* input (as if generated by the other decoder) and measuring the decoder output. EXIT chart was introduced in [119] and, was extended to non-binary decoders. These

methods are based on the assumptions that the interleaver is long enough and the extrinsic information for each bit/symbol is mutually independent.

The analysis of iterative decoders for concatenated codes with short blocks is an unsolved problem. However, for very large block sizes, such analysis is possible under certain assumptions [120]. An asymptotic (as block size goes to infinity) analysis of iterative decoding can be based on the method of density evolution proposed by Richardson and Urbanke [122]. Their analysis tracks the probability density function (pdf) of the extrinsic information messages as this density evolves from iteration to iteration. They used this method to compute iterative decoding thresholds for low density parity check (LDPC) codes over a binary input AWGN channel.

2.8 Simulation and Analytical Results

In this section we present simulation results for convolutional and turbo codes using Binary Phase Shift Keying (BPSK) over AWGN channels. The MAP decoding algorithm is used to estimate the most likely transmitted information. In the case of convolutional codes shown in Fig. 2.12, the frame length is 32768 bits in an AWGN channel and the code used is (7/5) convolutional code. The convolutional code used was a single recursive, memory of order two, code. The performance of these codes is shown for low signal to noise ratios. Here decoding is done for only a single iteration.

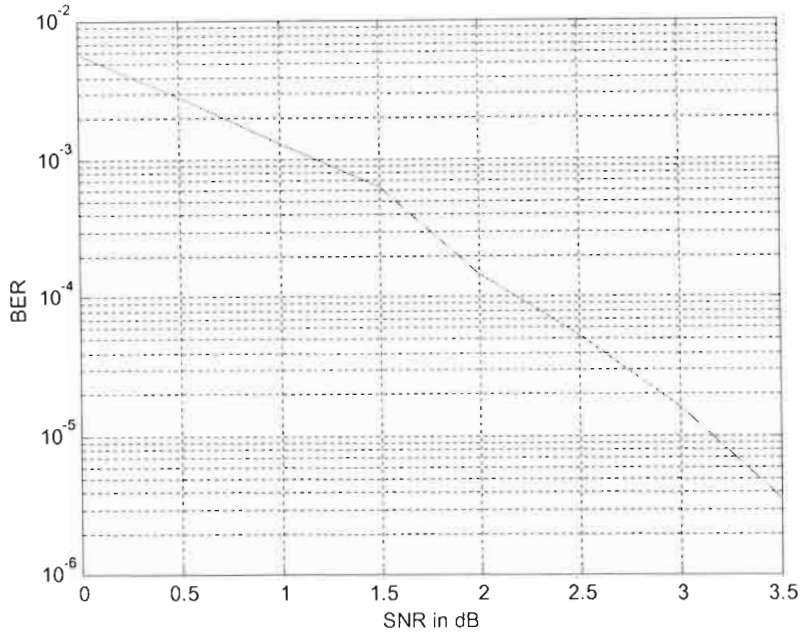

Fig.2.12: Convolutional Code (7/5), 4 state, BPSK, N=32768

Next the simulation performance for the turbo codes was observed for a parallel concatenation of two RSC (7/5) encoders having frame lengths N=1024 bits for a 4 state, BPSK type modulations. The number of iterations involved was restricted to 8 iterations, after which there was no significant improvement in performance. These results can be observed in Fig. 2.13 shown below. The results show the astonishing capability of these codes. The actual results which Berrou et al obtained which approached the Shannon limit was using a (37,21) RSC code and long block sizes of 65,232 bits and about 18 iterations [14]. But from a theoretical point of view, it shed light on what these types of codes are capable of achieving. It can be seen that the performance of the code improves with iterations, and the BER curves are lowered. We also provide the effect of increasing the interleaver size on the performance of turbo codes. We use RSC (5/7) rate ½ turbo codes to illustrate this example in Fig. 2.14.

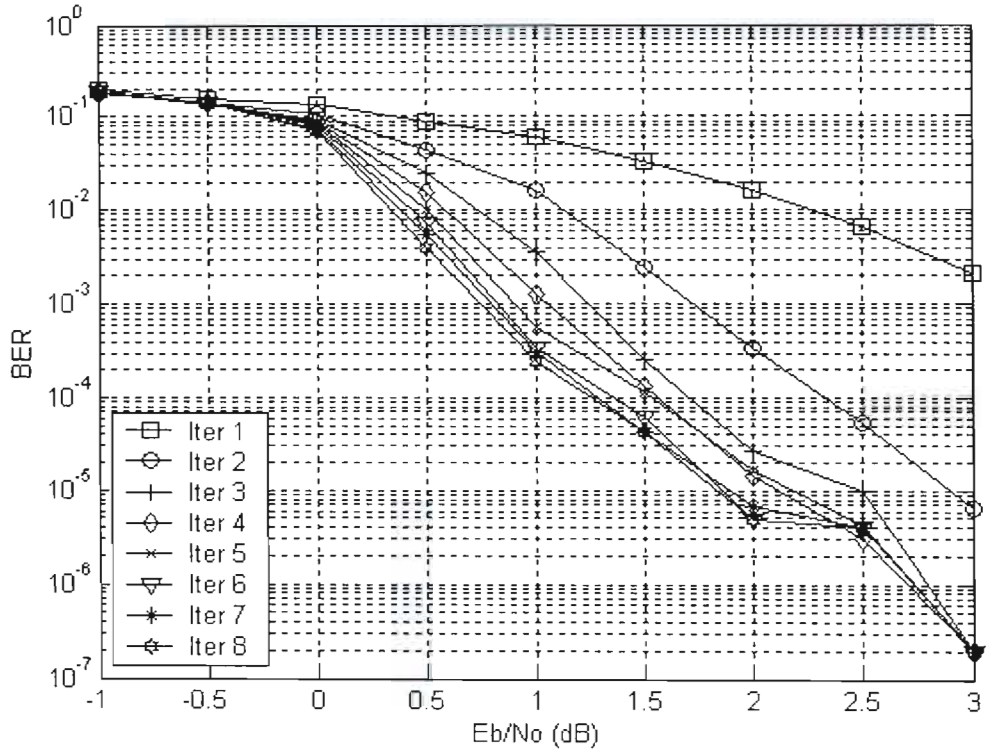

Fig. 2.13: Results for Turbo codes, R=1/3,v=2, (7/5), N=1024 bits, 8 iterations.

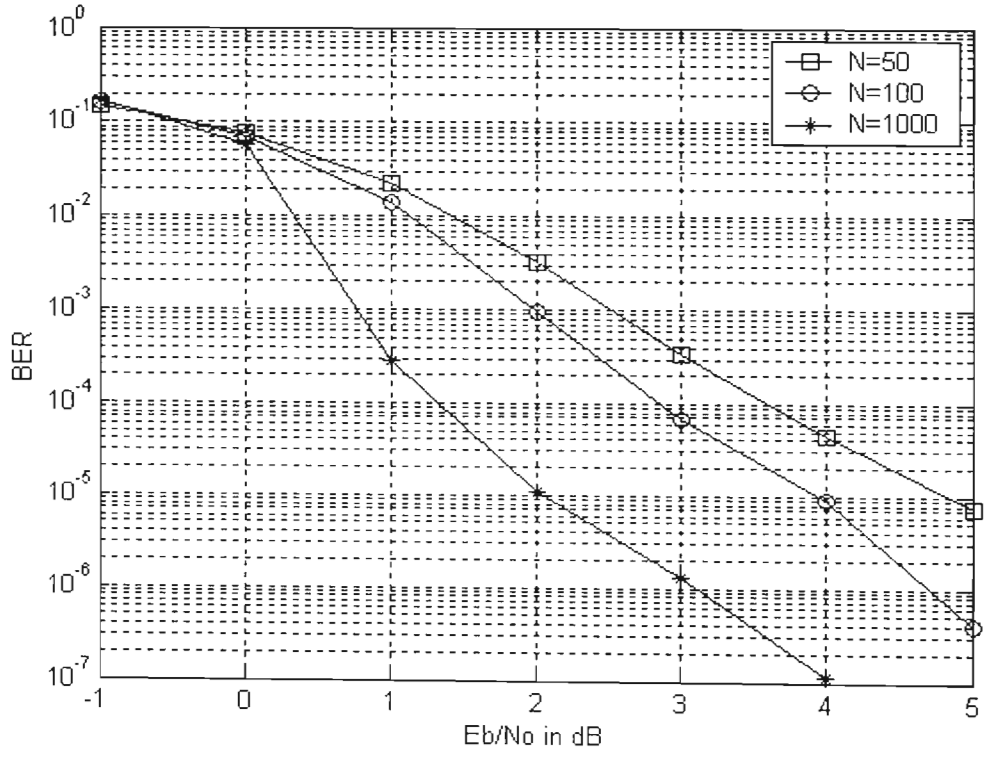

Fig. 2.14: Results for Turbo codes, R=1/2, (5/7), 8 iterations.

In order to fully understand the actual performance of turbo codes, analytical methods using the transfer function bounding techniques were also employed and union upper bounds were also obtained. As turbo codes are affected by error floor problems it is not possible to obtain accurate results for these codes at large SNRs due to time and memory constraints and exponential increase in decoding complexity, so it is necessary to use these bounding techniques in order to their performances at high SNRs. In Fig. 2.15 we can observe the Union bound for turbo codes of frame lengths N=10, N=50 and N=100 for (7/5) and (5/7) codes. It is seen that the (5/7) codes have marginal improvement in performance. Here we set limiting criteria for i and d to 30. In Fig. 2.16 we show the Union bounds on turbo codes using (5/7) codes in comparison with the simulation results.

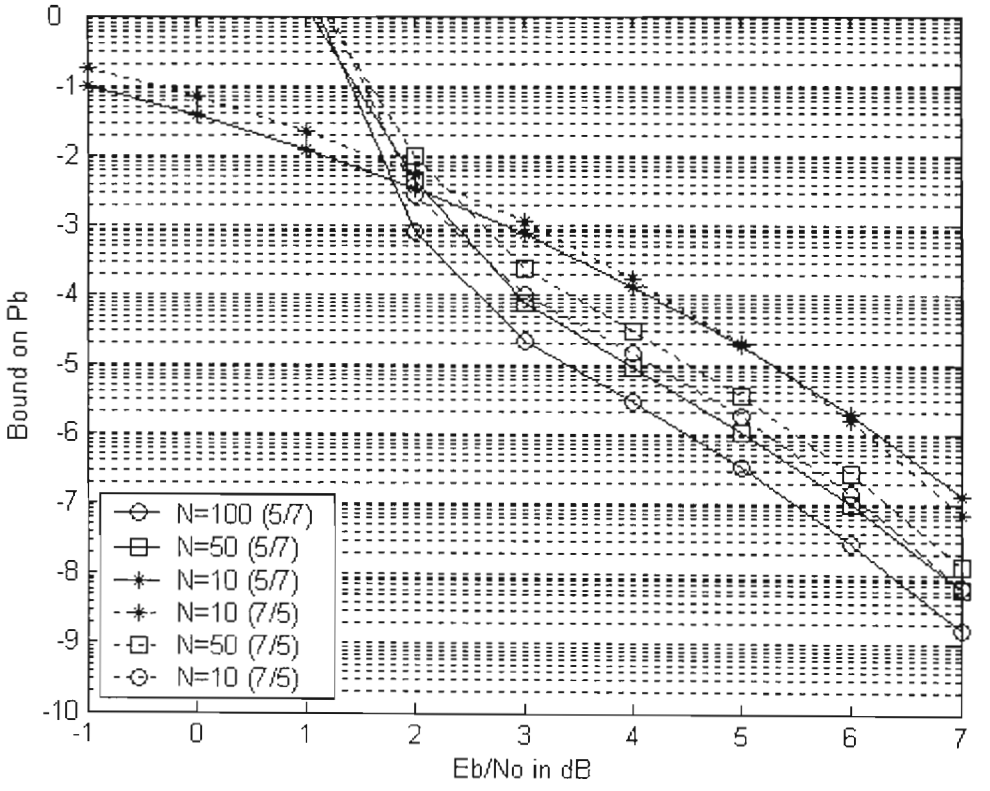

Fig. 2.15: Comparison of Union bounds for R=1/3, RSC (1, 5/7, 5/7) and (1, 7/5, 7/5) codes

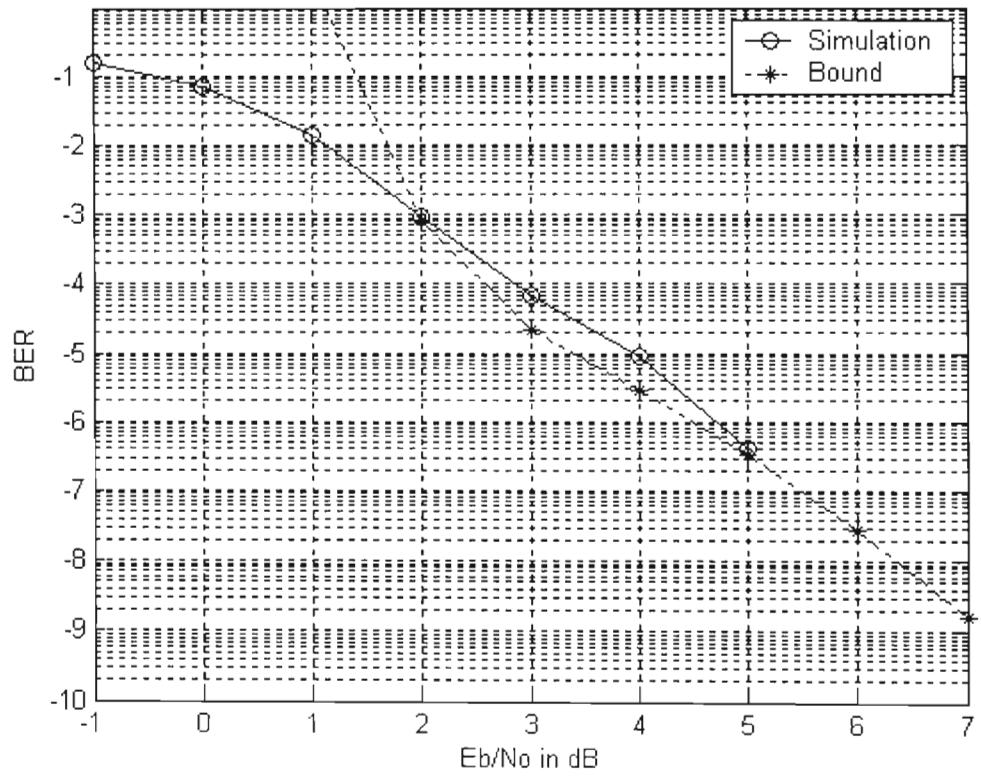

Fig. 2.16: Comparison of analytical and simulation results for an N=100, (1 5/7, 5/7) code.

Thus we are able to observe the performance capabilities of turbo codes through simulation and analysis, which provides an insight into the capability of these types of codes and the possibility of applying this turbo principle on various different types of codes and especially in particular to Space-Time codes.

2.9 Conclusion

In this chapter we have presented an overview of turbo codes, beginning with some background on the history of coding and error control coding. A brief description of convolutional codes and the different types of CCs were discussed. The specific parallel concatenated turbo code was investigated using two RSC codes. We described the MAP

decoding algorithm and present the iterative decoding procedure. A look at the performance analysis of turbo codes based on simulation and the transfer function bounding techniques are also investigated in order to broaden the understanding of these codes.

CHAPTER 3

SPACE-TIME CODING TECHNIQUES

3.1 Introduction

Communicating over the wireless link is highly challenging and the main challenge in achieving reliable communications lies in the severe conditions that are encountered when transmitting information over the link. It is well known that next generation wireless networks feature high data rate communications. This initiated research toward spectrally efficient transmission. While most of the techniques are being developed to improve single antenna channel capacity, another aspect of research seeks to increase channel capacity by using multiple (transmit and/or receive) antennas. These studies shed new light on the design of spectrally efficient coding/modulation [44]. The idea is to squeeze as much information as possible onto the wireless channel, then use the diversity provided by the antennas, together with the signal structure, to extract the information at the receiver.

In the next section we introduce the concepts of MIMO channels, followed by some insight into the channel capacity attainable by the use of these systems. A brief discussion on the various types of space-time coding schemes employed is introduced, along with

some of the current literature in this field is also provided. Space-time trellis coding techniques in particular are discussed in broad detail along with their system model, encoding and decoding techniques are provided. AWSTTC techniques are also investigated at length and its main features are also discussed. The performance analyses of these codes are also dealt with in section 3.6. Section 3.7 looks at the various results obtained from simulation and analysis for the various space-time trellis coded systems. Finally, in section 3.8, we look at the implementation complexity involved in implementing turbo codes, space-time codes and their concatenated versions in hardware.

3.2 MIMO System Model

Wireless transmission is impaired by signal fading and noise interference. The ever increasing requirements on data rate and quality of service for wireless communication systems call for new techniques to improve link reliability. Schemes which use multiple transmit and receive antennas for communication over a wireless channels are usually called Multiple-Input Multiple-Output (MIMO) schemes. MIMO channels exploit the diversity in both space (antenna) and time domains, thus significantly increasing the system capacity and improving reliability of the wireless link. The superior performance of MIMO systems depend heavily on the nature of the underlying multipath environment. The MIMO architecture has the ability to exploit the multiple scattering present in the environment in order to realize the substantial gains in both link and network capacities. To effectively evaluate the performance of a MIMO transmission scheme, models which account for all the major effects of wireless channels on various signals are required.

The basic model of a MIMO system or multi-element arrays (MEAs) as is often referred is shown in Fig. 3.1, and is based on the model described in [16, 17]. The basic model shows a single point to point wireless communication system with n_T transmit and n_R receive antennas. The overall transmitted power and channel bandwidth are constrained and the channel model is presented in complex baseband form.

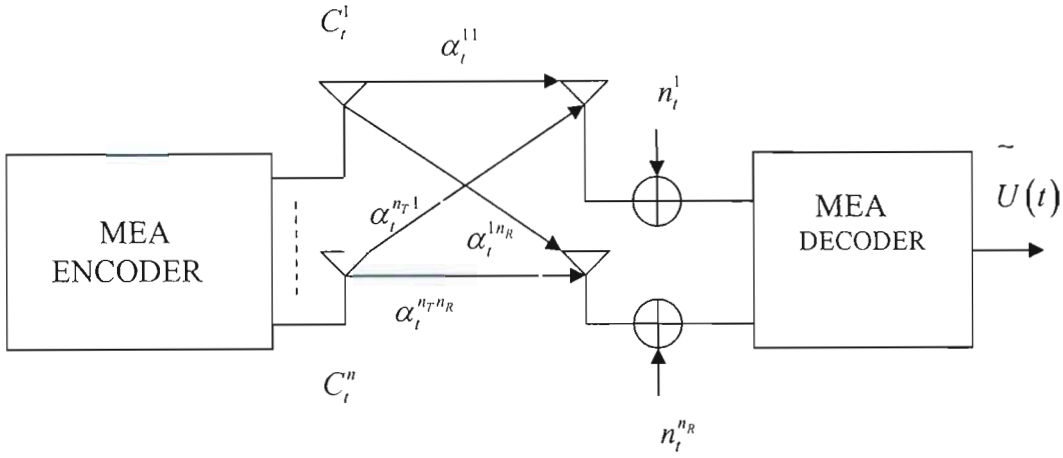

Fig. 3.1: Block Diagram of MIMO System

The stream of input bits $u(t)$ are passed on a frame by frame basis into the MIMO encoder, which produces n_T output symbols C_t^i where $i = \{1 \cdots n_T\}$. Each of these symbols are then individually modulated to produce signals $\sqrt{E_s C_t^i}$ which are simultaneously transmitted over n_T transmit antennas. The average energy E_s of each constellation is set to unity and the symbols C_t^i are normalized in magnitude. The MIMO channel for a system with n_T transmit and n_R receive antennas can be represented as, (3.1) where, α^{ij} is the path gain between the receive antenna i and transmit antenna j.

The signal received on receive antenna $j = \{1 \cdots n_R\}$ after matched filtering is a noisy superposition of the n_T transmitted signals and can be expressed as follows,

$$r_t^j = \sqrt{E_s} \sum_{i=1}^{n_T} C_t^j \alpha_t^{ij} + \eta_t^j. \tag{3.1}$$

The Rayleigh fading process is assumed to be frequency flat as the total system bandwidth is narrow. The complex path gain from transmit antenna i to receive antenna j is denoted by α_t^{ij}. This is modeled as zero-mean complex Gaussian random sequence with variance 0.5 per dimension. Spatially uncorrelated fading is ensured by sufficient separation of the antenna elements. This assumption holds if the antenna elements are separated by more than half a wavelength [16]. The term η_t^j represents the noise

introduced at the receive antenna j and is also zero-mean complex Gaussian random sequence with variance $N_0/2$ per dimension, where $N_0/2$ is the two-sided noise power spectral density. The MIMO decoder then tries to reconstruct an estimate of the original input data to produce the decoded bit stream $\hat{u}(t)$.

The most commonly used channel model for MIMO systems is quasi-static and rapid Rayleigh fading channels at all antenna elements. In this dissertation both quasi-static and rapid Rayleigh fading channel models are considered. In a quasi-static fading channel the path gains remain constant for the entire frame duration but are independent from one frame to another. In rapid fading channel the path gains are uncorrelated in time but are assumed to remain constant for the symbol duration. These schemes were employed in [16, 17, 18, 20, 45, 46] where novel signal processing schemes for MIMO systems were introduced. These methods showed an effective approach to achieving those increased data rates and larger channel capacities over wireless channels by employing these coding techniques appropriate to multiple transmit and receive antennas, namely space-time coding.

The availability of CSI or knowledge of the path gains between each transmit and receive antenna pair affects the performance of the MIMO system. The CSI is generally estimated using pilot symbols. In [47] various cases of CSI or no CSI at the transmitter and/or receiver were discussed. These include the cases of no CSI at transmitter or receiver (blind schemes), CSI at the receiver (feedforward) and CSI at both transmitter and receiver (feedback schemes). The rest of the dissertation will focus on schemes where perfect CSI at the receiver can be assumed unless where specifically stated.

3.3 Channel Capacity

Information theory provides means to explore the ultimate limits of reliable data transmission. The most important quantity in this context is the channel capacity. From

Shannon's coding theorem, discussed previously in section (2.1) it is known that for data rates below the channel capacity, arbitrarily small error probability can be achieved if the codewords are allowed to be sufficiently long, whereas this is impossible for rates exceeding capacity. Hence channel capacity is a convenient measure to analyze the potential gain of MIMO systems compared to single-input single-output systems [48].

Channel capacity [3] is the average mutual information $I(X;Y)$, maximized over the input probabilities $P(x_i)$ and is denoted by $\widetilde{C}$ with unit bits per input symbol with $I(X;Y)$ calculated using log to the base 2. This quantity which is expressed in (3.2) is only dependent on the characteristics of the channel, and not on the characteristics of the information source.

$$\widetilde{C} = \max_{P(x_i)} I(X;Y). \tag{3.2}$$

For a single Tx/Rx channel the capacity is given by Shannon's classical formula;

$$\widetilde{C} = W \log_2 \left(1 + snr \bullet |g|^2\right) bits/s, \tag{3.3}$$

where W is the bandwidth and g is the fading gain (the realization of a complex Gaussian random variable). For a MIMO channel of n inputs and m outputs the capacity is given by,

$$\widetilde{C} = W \log_2 \det\left[\mathbf{I}_m + \left(\frac{snr}{n}\right)\mathbf{G}\mathbf{G}^*\right] bits/s, \tag{3.4}$$

where, I_m is the identity matrix of order m, snr is the signal to noise ratio, G is the MIMO channel matrix and $*$ denotes the conjugate transpose operation. The ratio $\widetilde{C}/W$ is referred to as the normalized channel capacity and is denoted by C. Fundamental limits for MEA systems were presented in [49] for an AWGN channel and in [50] for a quasi-static fading channel with no CSI at the transmitter or receiver. Fundamental limits for the most commonly studied case of no CSI at the transmitter and perfect CSI at the receiver were derived in [16] for a quasi-static fading Rayleigh fading channel.

We consider a MIMO system with n transmit and m receive antennas, over a fast fading Rayleigh channel, assuming that the channel parameters are known at the receiver but not at the transmitter. In this case $m = n = N_R = N_T$, so that the asymptotic capacity is given by [49] and can be represented in the closed form in (3.5), and can be observed in Fig. 3.2.

$$\lim_{n\to\infty} \frac{C}{Wn} = \log_2 \frac{P}{\sigma^2} - 1 + \frac{\sqrt{1+\frac{4P}{\sigma^2}} - 1}{2\frac{P}{\sigma^2}} + 2\tanh^{-1}\frac{1}{\sqrt{1+\frac{4P}{\sigma^2}}}, \tag{3.5}$$

where, the total received power per antenna is equal to the total transmitted power, and the SNR is equal to the ratio of the total transmitted power and the noise power per receive antenna. An approximated bound can also be used as follows,

$$\lim_{n\to\infty} \frac{C}{Wn} \geq \log_2 \frac{P}{\sigma^2} - 1. \tag{3.6}$$

The capacity curves obtained by using the bound in (3.6) are shown in Fig. 3.3, using the signal to noise ratio as a parameter, varying between 0 and 30dB. The bound shows that the capacity increases linearly with the number of antennas and logarithmically with the SNR.

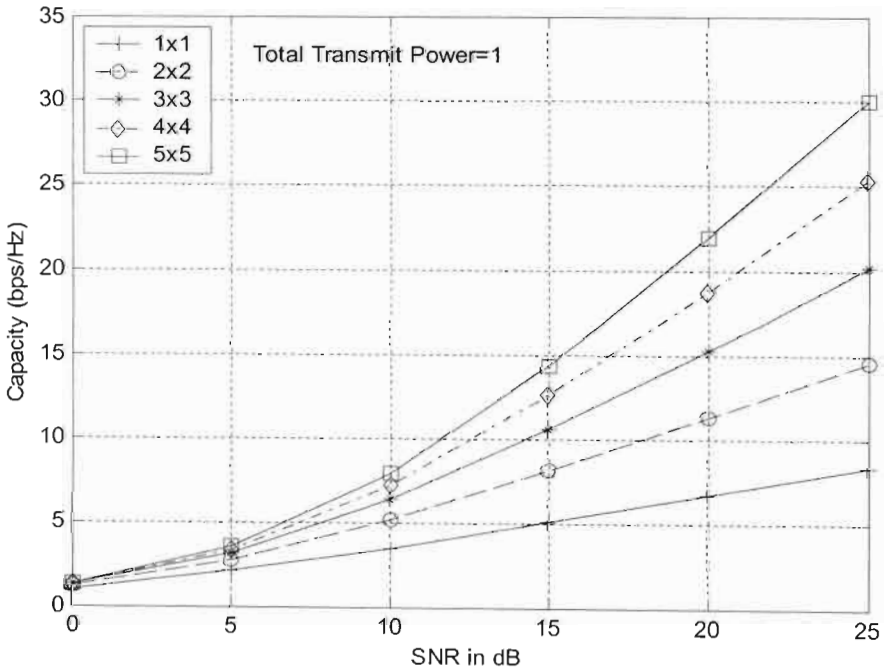

Fig. 3.2: Capacity increase for different antenna configurations.

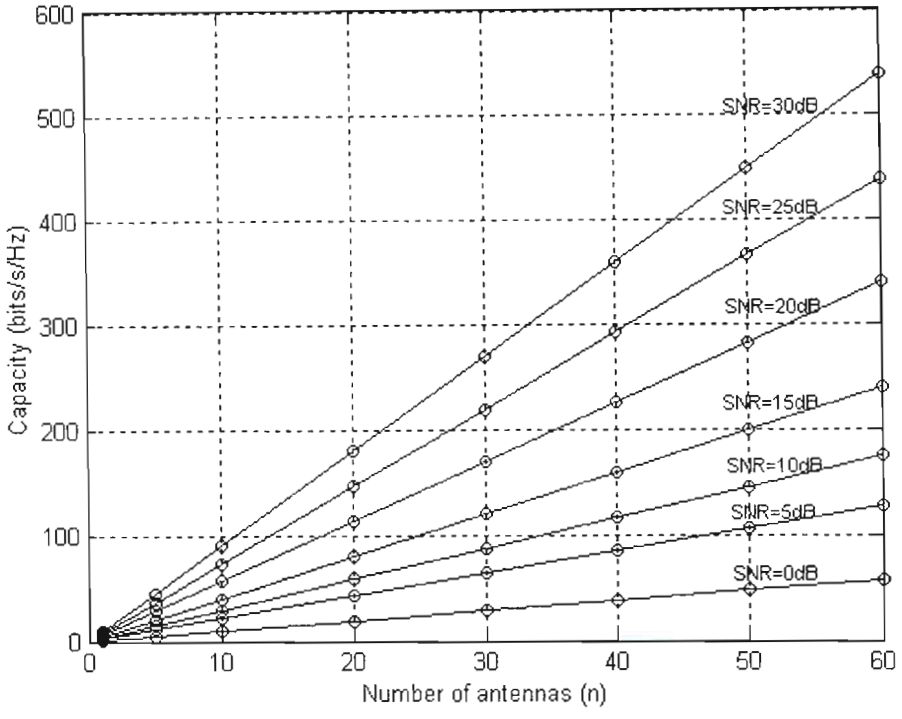

Fig. 3.3: Logarithmic Variation of Capacity at different SNR values for increase of number of antennas.

Considering correlation factors

If we consider a special case when $m = n$ and $\mathbf{G} = \mathbf{I}_n$ which represents completely uncorrelated parallel sub-channels then (3.4) reduces to,

$$\widetilde{C} = W \log_2 \det\left[1 + \left(\frac{snr}{n}\right) I_n\right] bits/s, \tag{3.7}$$

which, can be reduced to,

$$C = n \log_2 \left(1 + \frac{snr}{n}\right) \ bits/s/Hz. \tag{3.8}$$

Since we assume that all received powers are equal, we define $\sigma_j = \sum_i \left|g_{ij}\right|^2 = 1$, then the capacity,

$$C = \log_2 \det\left(I + \frac{snr}{n} R \right), \tag{3.9}$$

where, R is the normalized channel correlation matrix $\left(|r_{ij}| \le 1\right)$ whose components are defined by,

$$r_{ij} = \frac{1}{\sqrt{\sigma_i \sigma_j}} \sum_k g_{ki} g_{ij}^{*}. \tag{3.10}$$

Therefore the capacity for the channel taking into account the presence of correlation is given by [118],

$$C \cong n \log_2\left(1 + \frac{snr}{n}\left(1 - |r|^2\right)\right) + \log_2\left(\frac{1 + snr/n}{1 + \frac{snr}{n}\left(1 - |r|^2\right)}\right), \tag{3.11}$$

where, r is the correlation coefficient. The effect of correlation in these channels can be observed in Fig. 3.4 and Fig. 3.5, obtained by using (3.11).

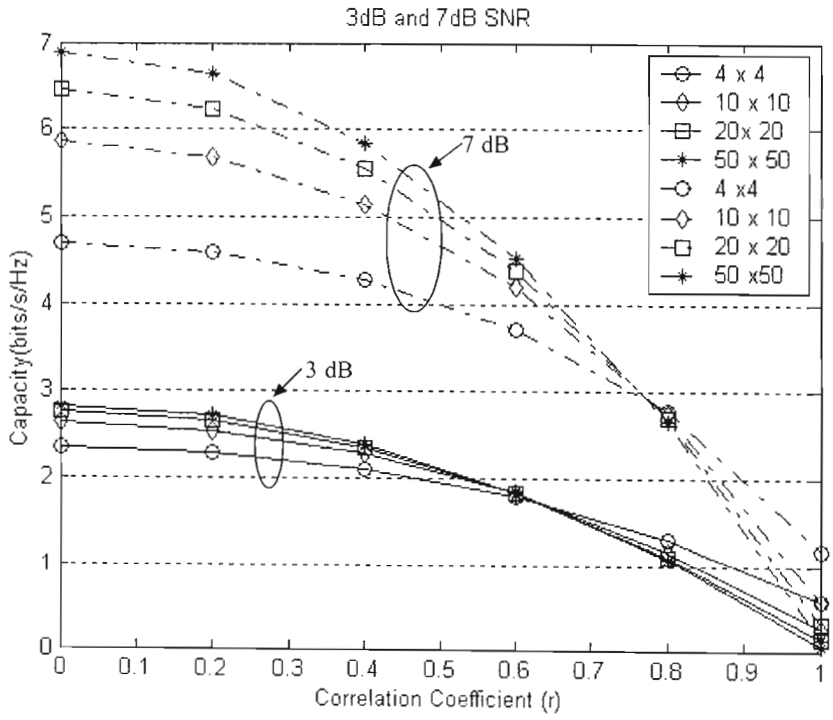

Fig. 3.4: Effect of Correlation coefficient on Capacity at SNRs of 3dB and 7dB.

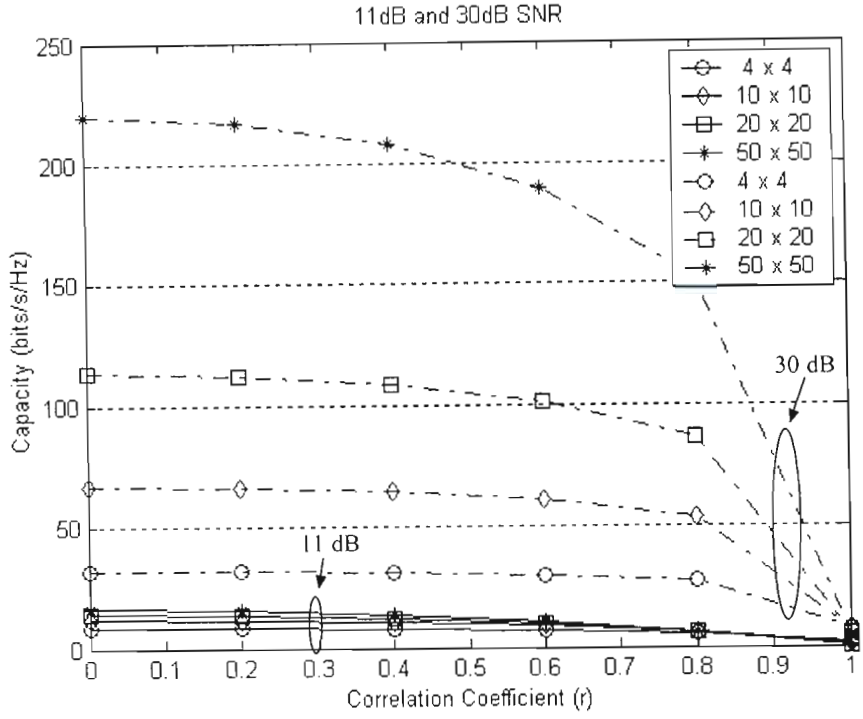

Fig. 3.5: Effect of Correlation coefficient on Capacity at SNRs of 11dB and 30dB.

Thus in general it is seen that the individual capacities of the single-input single-output channels add up to the total capacity of MIMO channel, while single-input single-output systems gain $1 bit/s/Hz$ in capacity every 3dB, the growth rate is m times as high in the MIMO case yielding a remarkable improvement especially for high [16] as can be seen in Fig. 3.2.

3.4 Space-Time Coding Schemes

Communicating over a wireless link is highly challenging due to the complex time-varying propagation medium. Consider a wireless link with a single transmit and receive antenna. The transmitted signal that is launched into the wireless environment arrives at the receiver along a number of distinct paths referred to as multipaths. These paths arise from scattering and reflection of radiated energy from objects such as buildings hills and trees. Each of these paths has a distinct and time-varying path delay, angle of arrival, and

signal amplitude. Due to the constructive and destructive interference of the multipaths the received signals can vary as a function of frequency, time and space. These variations are collectively referred to as fading and cause deterioration in link quality. Moreover the links suffer from co-channel interference (CCI) which distorts the desired signal and hence leads to low system performance.

Wireless systems must be designed to mitigate fading and interference to ensure a reliable link. The development of algorithms with a reasonable BER performance and complexity compromise is required to realize MIMO gains in practice. Current transmission schemes over MIMO channels typically fall into two categories: data rate maximization or diversity maximization schemes, although there are ongoing efforts towards their unification. The set of schemes aimed at realizing joint encoding of multiple transmit antennas are called space-time codes.

3.4.1 Current Literature

Wireless systems are developing rapidly to provide voice, data and multimedia messaging services, which require reliable wireless channels with large capacities. Owing to the huge increase in capacity of multi-antenna systems, a considerable amount of work has been done in the field since the pioneering papers of Teletar [49], Foschini and Gans [16]. They showed that the capacity of multi-antenna systems far exceeds that of single antenna systems in fading environments. Subsequently the investigations led to the proposal of a novel transmit–receive architecture called Bell Laboratories Layered Space-Time (BLAST) architecture [18]. The initial idea of combining coding, antenna diversity, and the delay diversity schemes was proposed by Wittenben [51]. The scheme used two transmit antennas and transmitted the same information from both antennas simultaneously but with a delay of one symbol interval.

Recently, driven by the desire to support high data rates for a wide range of bearer services, Tarokh *et al.* [17] proposed Space-time trellis codes in 1998. Their approach

focused on merging antenna diversity with proper channel coding and derived the design criteria for STTC codes over slow non-selective fading channels. But it was seen that their decoding complexity rose exponentially with transmission rate for a fixed number of transmit antennas. In addressing the issue of decoding complexity Alamouti [45] discovered a remarkable scheme that used two transmit antennas along with a simple decoding algorithm. This proposal motivated Tarokh et al. [46], to generalize Alamouti's scheme to an arbitrary number of transmit antennas using the theory of orthogonal designs, leading to the concept of Space-Time Block Codes. Then Bauch *et al.* [52, 53], Agarwal [54], and Naquib *et al.* [22] extended the research of STBCs and STTCs from considering narrow–band channels to dispersive channels. It is also seen that in recent years, large number of research proposals have been published which propose new code constructions or perform systematic searches for different convolutional STTC or some variant of the design proposed by Tarokh *et al.* Examples of such work can be found in [55, 56, 57, 58, 59]. These new code constructions provide an improved coding advantage, however only marginal gains were obtained and generally for systems employing more than a single receive antenna. A more detailed survey on the evolution of space-time coding techniques can be found in [60, 61].

Various methods have been used in literature to analyze the performance of STTCs in Rayleigh fading channels. The union bound was generally used to analyze the code's performance, where a number of different enumeration methods and bounds on the pair-wise error probability (PWEP) of each error event have been proposed. In the first performance investigation of STTCs [17], analytical bounds and design criteria were proposed for slow and fast fading channels. It was pointed out that in slow fading channels, the critical parameters are the rank and determinant of the codeword distance matrix, while in fast fading channels, the important parameter are the symbol-wise Hamming distance and product distance. Based on these criteria, new 4-PSK and 8-PSK STTCs have been reported [57, 59, 62, 63] for slow fading, and in [64] for fast fading channels. The development of performance bounds for STTCs has been considered with the union bound, evaluated using the PWEPs was shown [65-68]. In [69] the union bound on the codes performance was calculated using the distance spectrum of the code. The

distance spectrum is defined as the enumeration of product measures of significant pair-wise error events. The analytical bounds in [68] were tighter than those in [69, 70] for both quasi-static and rapid fading. The performance bounds in [71] are also quite effective as the bounds are derived by limiting the conditional union bound before averaging over the fading process.

Now that we have reflected on the underlying phenomena making it possible for MIMO systems employing space-time coding strategies to support greatly enhanced performance, we turn to a more detailed exploration of what researchers in the field have done with this available potential. The next section looks at a system level overview of the various space-time coding techniques that have been proposed in the literature.

3.4.2 Layered Space-Time Codes

It is understood that extremely large spectral efficiencies can be achieved on a wireless link if the number of transmit and receive antennas is large. However, space-time coding schemes have a potential drawback that the maximum likelihood decoder complexity grows exponentially with the number of bits per symbol, thus limiting the achievable data rates. This motivates the design of suboptimal space-time schemes with low complexity and still achieving a good portion of the spectral efficiencies predicted by theory. A class of space-time codes based on a layered architecture on a low complexity decoding scheme that meets the above mentioned requirements was proposed by Foschini and Gans [16]. This led to the development of BLAST architecture which was a test bed system [18]. BLAST used an 8 element array on both ends of the wireless link that proved to increase significantly the capacity of the wireless link. The BLAST approach exploits multipath, whereby it uses the scattering characteristics of the propagation environment to enhance, rather than degrade, transmission accuracy by treating the multiplicities of scattering paths as separate parallel subchannels. BLAST accomplishes this by splitting a single user's data stream into multiple substreams and using the array of transmit antennas to simultaneously launch the parallel substreams. All the substreams

are transmitted in the same frequency band, so spectrum is used very efficiently. Since the user's data is being sent in parallel over multiple antennas, the effective transmission rate is increased roughly in proportion to the number of transmit antennas used. The receiver uses N_R antennas to separate and detect the N_T transmitted signals. The separation process involves a combination of interference suppression and cancellation, and the separated signals are then decoded by using conventional decoding algorithms developed for one dimensional component codes.

There are a number of various layered space-time (LST) architectures, depending on whether error control coding is used or not and the way modulated symbols are assigned to transmit antennas. An un-coded LST structure, known as vertical layered space-time (VLST) is also used. At a given time t, the transmitter sends the t^{th} column from the transmission matrix, one symbol from each antenna. In a horizontal layered space-time (HLST) the sequence is first encoded by a channel code and subsequently demultiplexed into N_T sub-streams which are modulated, interleaved and sent to N_T transmit antennas. A better performance is offered by the diagonal layered space-time (DLST) [16], in which a modulated codeword of each encoder is distributed among the N_T antennas among the diagonal of the transmission array. The entries below the diagonal are padded by zeroes, which is done by delaying the i^{th} row by (i-1) time slots and replace the entries below the diagonal by zero. Spatial interleaving which is a cyclic shift mechanism is carried out after this. At the transmission stage each diagonal is transmitted on each antenna. Lastly a threaded layered space-time (TLST) structure [56] is obtained from the HLST scheme by introducing a spatial interleaver prior to the time interleaver.

3.4.3 Space-Time Block Codes

The Alamouti scheme referred to in section 3.4.1 is historically the first Space-Time Block Code (STBC) to produce full diversity for systems with two transmit antennas [15, 45, 46]. The key feature of the scheme is that it achieves a full diversity gain with a

simple maximum-likelihood decoding algorithm and has orthogonality between the sequences generated by the two transmit antennas. STBC are defined by a mapping operation of a block of input symbols into space and time domains, creating orthogonal sequences that will be transmitted from different transmit antennas. Although STBC codes give the same diversity gain as STTC for the same number of transmit antennas, they provide zero or minimal gain. Here we look at a brief review of the basics of STBCs. A broader in depth study can be found in [72].

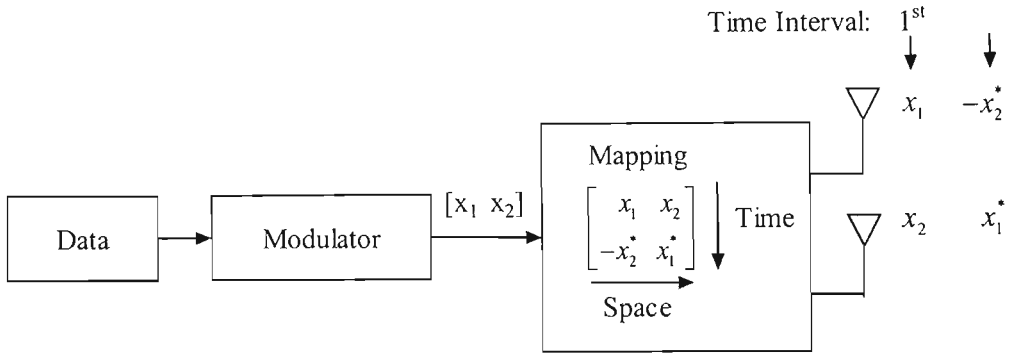

Fig. 3.6: Block diagram of STBC Encoder.

Fig. 3.6 shows block diagram of Alamouti's STBC encoder with two transmit antennas and a single receive antenna. At each time slot t, signals $C_t^i, i = 1,2 \cdots\cdots N_T$ are transmitted simultaneously from the N_T transmit antennas. The channel is assumed to be a flat fading channel and the path gain form transmit antenna i to receive antenna j is defined to be $\alpha_{i,j}$. The path gains are modeled as samples of independent complex Gaussian random variables with variance 0.5 per dimension. The channel is assumed to be quasi-static so that the path gains are constant over a frame of length l and vary from one frame to another. The input symbols to the encoder are divided into two groups of two symbols each. At a given symbol period, the two symbols in each group $\{C_1, C_2\}$ are transmitted simultaneously from the two antennas. The STBC is defined by $p \times n$ transmission matrix $\mathbf{G}$. The entries of the matrix $\mathbf{G}$ are linear combinations of the variables $X_1, X_2 \cdots X_K$ and their conjugates. For example, $\mathbf{G}_2$ represents a code which utilizes two transmit antennas and is defined by,

$$G_2 = \begin{pmatrix} X_1 & X_2 \\ -X_2^* & X_1^* \end{pmatrix}. \tag{3.12}$$

Maximum likelihood decoding of any space-time block code can be achieved using only linear processing at the receiver. At time t the signal r_t^j, received at antenna j, is given by,

$$r_t^j = \sum_{i=1}^{N_T} \alpha_{i,j} C_t^i + \eta_t^j, \tag{3.13}$$

where, the noise samples η_t^j are independent samples of a zero-mean complex Gaussian random variable with variance $N_T/(2SNR)$ per complex dimension. The average energy of the symbols transmitted from each antenna is normalized to be one. Assuming perfect channel state information is available, the receiver computes the decision metric

$$\sum_{t=1}^{l} \sum_{j=1}^{m} \left| r_t^j - \sum_{i=1}^{n} \alpha_{i,j} C_t^i \right|^2, \tag{3.14}$$

over all code words

$$C_1^1 C_1^2 \cdots C_1^{N_T} C_2^1 C_2^2 \cdots C_2^{N_T} \cdots\cdots C_l^1 C_l^2 \cdots C_l^{N_T}, \tag{3.15}$$

and decides in favour of the code word that minimizes the sum. The maximum likelihood detection amounts to minimizing the decision metric

$$\sum_{j=1}^{N_R} \left(\left| r_1^j - \alpha_{1,j} s_1 - \alpha_{2,j} s_2 \right|^2 + \left| r_2^j + \alpha_{1,j} s_2^* - \alpha_{2,j} s_1^* \right|^2 \right), \tag{3.16}$$

over all possible values of s_1 and s_2. The symbol s_i represents the possible symbols from either BPSK or QPSK at time $t = 1$ or $t = 2$. Due to the quasi-static nature of the channel, the path gains are constant over two transmissions. The minimizing values are the receiver estimates of s_1 and s_2, respectively. It is important to note that there is no memory between consecutive blocks and the typical block length is very short. Thus, a very limited coding gain is expected.

3.4.4 Space-Time Trellis Coded Modulation

Although STBC can achieve a maximum possible diversity advantage with a simple decoding algorithm, and was very attractive because of its simplicity, it could not provide any coding gain. Also it was observed that some non-full rate STBCs can introduce bandwidth expansion. The consideration of a joint design of error control coding, modulation, transmit and receive diversity to develop an effective signaling scheme, called Space-Time Trellis Codes (STTC) was introduced to overcome these issues.. This scheme is able to combat the effects of fading, and was a real breakthrough in the field of space-time coding [15].

Space-Time Trellis coding was originally proposed by Tarokh et al. from AT&T Research Labs [17], where codes were developed for two transmit antennas and various signal constellations. Since the original STTC were introduced by Tarokh et al, there has been extensive research aiming at improving the performance of the original STTC designs. The original STTC designs were hand crafted (according to the proposed design criteria) and therefore are not optimum designs. These new proposed code constructions provide an improved coding advantage over the original scheme by Tarokh et al, however only marginal gains were obtained in most cases. The STTC architecture will be discussed in greater detail in the next section. It is well known that STTCs achieve greater coding gains than STBCs [22] and in [73] STTCs were shown to outperform Layered Space-Time codes.

Recently, a new class of space-time codes called Super-Orthogonal Space-Time Trellis Codes (SOSTTC) [21] was introduced, that combine set-partitioning with a super set of orthogonal space-time block codes in such a way as to provide full diversity with increased rate and improved coding gain over previous space-time trellis code constructions in quasi-static Rayleigh fading channels. The idea can be basically defined as a combination of space-time block codes with a trellis code to come up with a new structure that guarantees the full diversity and increased rate. The result also provides a systematic method to design space-time trellis codes for any given rate and number of

states, unlike the conventional STTCs which had handcrafted code designs. We will have a more detailed description of the performance of this code and its attributes in chapter 4.

3.5 Space-Time Trellis Codes (STTC)

Space-time coding schemes combine the channel code design and the use of multiple transmit and receive antennas. The encoded data is split into N_T streams that are simultaneously transmitted using N_T transmit antennas. The received signal is a linear superposition of these simultaneously transmitted symbols corrupted by noise and fading. Space-time decoding algorithms as well as channel estimation techniques are incorporated at the receiver in order to achieve diversity advantage and coding gain.

Space-Time Trellis Codes were originally proposed by Tarokh et al [17] from AT&T research labs, which combine the design of channel coding with the symbol mapping onto multiple transmit antennas. These codes are designed to obtain maximum diversity gain and provide the best trade off between constellation size, data rate, trellis complexity and diversity advantage. The encoder is composed of N_T different generator polynomials to determine the simultaneously transmitted symbols. The receiver is based on channel estimation of the fade coefficients and Maximum Likelihood Sequence Estimation (MLSE) decoder, which computes the lowest Euclidean distance metric to extract the most likely transmitted sequence.

3.5.1 System model

Space-time trellis codes can be considered to function in a similar manner to convolutional encoders. The connection weights and output symbols form part of an M-ary alphabet. The system under consideration can be assumed to employ a STTC with N_T transmit and N_R receive antennas. While the transmitter has no knowledge about the

channel, it is assumed that the receiver can recover the CSI perfectly [17]. We can consider the encoder structure of a STTC shown in Fig. 3.7. It can be described in discrete time using feedforward implementation. At each instant, k input bits $(U_t^1 \cdots U_t^k)$ are shifted into the STTC encoder. Each M-ary output symbol C_t^i for each of the two transmit antennas is generated by multiplying the input bits and those in the shift registers S_1 and S_2 by their corresponding weights and modulo m-addition. The space-time trellis coded modulation with M points in the signal set can achieve a bandwidth efficiency of m bits/s/Hz, where the memory $m = \log_2 M$. Consider the QPSK case, where $m = 2$ and $M = 4$ having two transmit and a single receive antenna. At each time instant t, the number of output symbols per antenna is 1 which translates to a bandwidth efficiency of 2 bits/s/Hz.

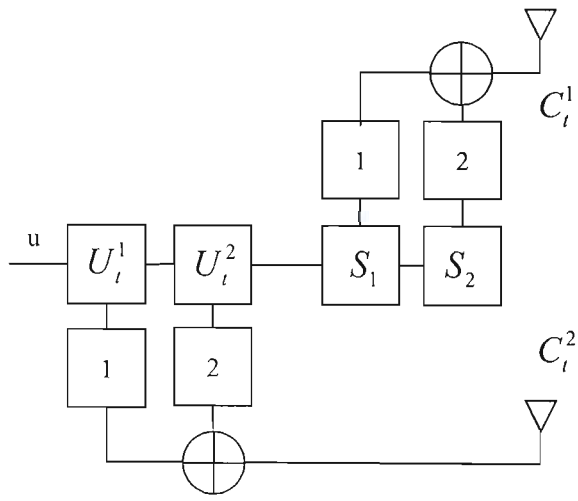

Fig. 3.7 STTC Encoder

A trellis diagram can be drawn to completely illustrate the space-time trellis code. The trellis shown in Fig. 3.8 consists of $2^m = 4$ states represented by state nodes and there are 4 branches leaving from each state corresponding to four different input patterns. Each branch is labeled as $U_t^1 U_t^2 / C_t^1 C_t^2$, where U_t^1 and U_t^2 are pair of encoder input bits and C_t^1 and C_t^2 represents two coded QPSK symbols transmitted from antennas 1 and 2 respectively.

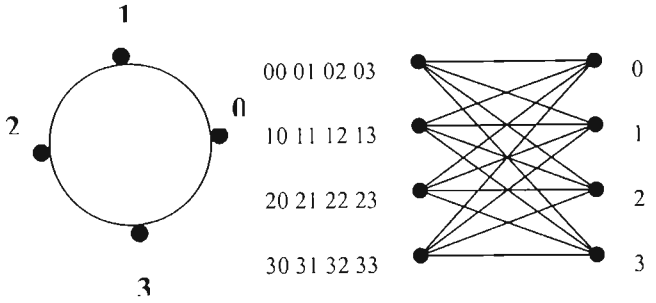

Fig.3.8 (a.) 4PSK Constellation (b) STTC 4-State

The channel over which the system propagates the symbols using the multiple transmitters is identical to that described in section 3.2 and the received signal on receive antenna j at time t, r_t^j is given by (3.1), where L is the frame length. As mentioned earlier, perfect CSI is assumed to be known at the receiver. The Viterbi algorithm can be employed at the receiver side to estimate the most likely information stream using the branch metric for the state transition with output symbols $q_t^1 \cdots q_t^{N_T}$, given by,

$$m = \sum_{l=1}^{L} \sum_{j=1}^{N_R} \left| r_t^j - \sum_{i=1}^{N_T} \alpha_t^{i,j} g_t^{N_T} \right|^2 . \tag{3.17}$$

The function of the decoder is to estimate the likelihood of the received signal by calculating the Euclidean distance between this signal and M^{N_T} possible signals. The Viterbi algorithm performs this task and computes the path with the lowest accumulated metric as shown in (3.17). In this dissertation, both quasi-static (slow) and rapid (fast) channels will be considered. For quasi-static fading channels it is assumed that the fading coefficients are constant during a frame and vary from one frame another independently. For fast fading channels, the fading coefficients are constant within each symbol period and vary from one symbol to another independently.

3.5.2 Adaptively Weighted Space-Time Trellis Codes

The Shannon capacity of communication systems using multi-element arrays at the transmitter and/or the receiver has attracted much research activity recently. It was

determined that with perfect CSI at the transmitter or receiver, the capacity of MEA array was shown in [49] to be $n = \min(N_T, N_R)$ times that of Single Input Single Output (SiSo) non interfering channels. Recent work in [74] on multiple antenna channel capacity with partial CSI at the transmitter has shown some interesting results. It was found that unlike single antenna systems where exploiting CSI at transmitter does not significantly enhance the Shannon capacity, for multiple antenna systems, that capacity improvement through even partial CSI can be substantial when perfect channel parameters are perfectly known at the transmitter.

The design criteria for STTCs have been proposed in [17, 57, 58]. However, all of them have been derived for a system with no CSI available at the transmitter. If perfect or partial CSI is made available at the transmitter the system can further enhance the performance and capacity. Transmit diversity methods fall into two categories, namely open loop and closed loop methods. Space-Time Transmit diversity (STTD) is an open loop technique in which the symbols are encoded into N_T symbol streams that are transmitted along N_T antennas simultaneously. Transmit adaptive array is a closed loop transmit diversity technique in which mobile users feedback the estimated optimal transmit weights depending on the different modes of operation, the amplitude and/or phase of the transmit weights are adaptively weighted based on the channel conditions.
Novel STTCs, known as Adaptively Weighted Space-Time Trellis Codes (AWSTTC) are a form of STTCs whereby the STTC is combined with the weighting of transmitted signals [75]. It can be seen that this scheme provides significant coding gain over the schemes which use systems with a single receive antenna.

The system model we consider here consists of a MIMO system with $N_T = 2$ transmit antennas and one receive antenna over quasi-static fading channels. In this scheme perfect channel state information is assumed at the transmitter side and using the knowledge of the path gain values, the corresponding weights are determined and the encoder produces weighted symbols which are transmitted on both transmit antennas.
The transmit signal matrix, denoted by C_{m}, can be written as,

$$C_w = \begin{vmatrix} w_1 c_1(1) & .... & w_1 c_1(l) \\ \vdots & \ddots & \vdots \\ w_n c_n(1) & .... & w_n c_n(l) \end{vmatrix} = \begin{vmatrix} c_1^w(1) & ... & c_1^w(l) \\ \vdots & \ddots & \vdots \\ c_n^w(1) & ... & c_n^w(l) \end{vmatrix} \tag{3.18}$$

where, $c_i^w(t) = w_i c_i(t)$; and $c_i(t)$, $t = 1 \cdots\cdots l$; and $i = 1 \cdots\cdots n$ is the modulated signal on antenna i at time t; l represents the length of the frame, and n represents the number of transmit antennas; and w_i is the weighting coefficient for transmit antenna i given by,

$$w_i(t) = h_i \left(\sum_{i=1}^{n} |h_i|^2 \right)^{-1/2}, \tag{3.19}$$

and the average energy of the signal is equal to 1.The encoder structure for the adaptive weighted scheme is shown in Appendix A.1.1 [75].

It is similar to the encoder structure of Tarokh's scheme except that the weighting is changed and the transmitted signals are different on each antenna and is shown in the trellis diagram also in Appendix B. The received signal can be expressed as

$$r = hc_w + n \tag{3.20}$$

where $r = [r_1 r_2 \cdots r_l]$; which is the received signal at time t, t=1,...l. And h is the channel matrix given by $h = [h_1 \cdots h_n]$ and n is a noise vector which is a zero mean complex Gaussian random variable with two-sided noise power spectral density $N_0/2$ per dimension. From [57] the method of determining the generator matrix is used to obtain the generator matrix for the Tarokh, Seshadri and Calderbank (TSC) scheme and the adaptively weighted scheme.

3.6 Performance Analysis of STTC

3.6.1 Introduction

In this section, we look at the performance of STTCs using two analytical means. First we look at the pairwise error probabilities, and then transfer function bound technique using truncated evaluation in the closed form. This is followed by the performance analysis of STTCs in Rayleigh fading channels based on the work in [76], which is a modification of [68]. The enumeration method used is a modification of state transition matrix method [35, 43]. The analytical results obtained are then compared with simulation results.

3.6.2 Pairwise Error Probability for STTCs

The pairwise error probability (PWEP) is an important component for any performance analysis of a coded modulation. For an STTC encoder, if we assume that a valid codeword of length L, and symbols $c=\left(c_1^1 c_1^2 \cdots c_1^{N_T} c_2^1 c_2^2 \cdots c_2^{N_T} \cdots c_l^1 c_l^2 \cdots c_l^{N_T}\right)$ was transmitted. A maximum likelihood receiver might decide erroneously in favor of another codeword $e=\left(e_1^1 e_1^2 \cdots e_1^{N_T} e_2^1 e_2^2 \cdots e_2^{N_T} \cdots e_l^1 e_l^2 \cdots e_l^{N_T}\right)$. Hence the PWEP $P(c,e)$ is the probability that the decoder selects as its estimate an erroneous sequence e when the transmitted sequence was in fact c. The channel is modeled by a $N_R \times N_T$ channel matrix, denoted by H. The elements of H, denoted by $h_{i,j}$ where, $1 \le i \le N_T$ and $1 \le j \le N_R$ are constant during one frame and vary independently from one frame to another.

Let $r(r \le N_T)$ denote the rank of the $N_T \times l$ code difference matrix $B(c,e)$ defined as,

$$B(c,e)=\begin{pmatrix} e_1^1-c_1^1 & \cdots\cdots & e_l^1-c_l^1 \\ \vdots & & \vdots \\ e_1^{N_T}-c_1^{N_T} & \cdots\cdots & e_l^{N_T}-e_l^{N_T} \end{pmatrix}, \tag{3.21}$$

and λ_i be the eigenvalues of the distance matrix $A(c,e)=B(c,e)B^*(c,e)$ where, $B^*(c,e)$ denotes the transpose conjugate of $B(c,e)$. The conditional pairwise error probability has the upper bound [17] given by,

$$P(c\to e/H)\le\frac{1}{2}\exp\left(-d^2(c,e)E_S/4N_O\right), \tag{3.22}$$

where, $d^2(c,e)$ is given by,

$$d^2(c,e)=\sum_{j=1}^{N_R}\sum_{t=1}^{l}\left|\sum_{i=1}^{N_T}h_{i,j}\left(c_t^i-e_t^i\right)\right|^2 \tag{3.23}$$

and E_S is the energy per symbol at each transmit antenna. This is just a standard approximation to the Gaussian tail function which can be related as $h_{i,j}=\beta_{i,j}/\sqrt{2}\sigma$ which is with zero mean and variance 0.5 per dimension. The conditional pairwise error probability is further expressed as [44],

$$P(c\to e/H)\le\frac{1}{2}\exp\left(-\sum_{j=1}^{N_R}\sum_{i=1}^{N_T}\lambda_i\left|\beta_{i,j}\right|^2\bullet\frac{E_s}{4N_O}\right), \tag{3.24}$$

in which $|\beta_{i,j}|$ follows a Rayleigh distribution with the probability distribution function,

$$P\left(\left|\beta_{i,j}\right|\right)=2\left|\beta_{i,j}\right|\exp\left(-\left|\beta_{i,j}\right|^2\right). \tag{3.25}$$

Now, if we average (3.24) with respect to independent Rayleigh distribution of $|\beta_{i,j}|$, we get the Chernoff bound [17],

$$P(c\to e)\le\left(\frac{1}{\prod_{i=1}^{N_T}\left(1+\lambda_i\frac{E_S}{4N_O}\right)}\right)^{N_R}, \tag{3.26}$$

$$P(c \to e) \le \left(\prod_{i=1}^{r} \lambda_i \right)^{-N_R} \left(\frac{E_S}{4N_O} \right)^{-rN_R}. \tag{3.27}$$

Thus, a diversity advantage of rN_R and a coding advantage of $(\lambda_1 \lambda_2 \cdots \lambda_r)^{1/r}$ are achieved. The above analysis leads us to an idea for the design criteria of space-time codes for quasi-static fading.

(i.) The Rank Criterion: Maximize the diversity advantage rN_R, when the code difference matrix $B(c,e)$ is full rank over all pairs of distinct codewords c and e.

(ii.) The Determinant Criterion: maximize the minimum pairwise coding advantage $(\lambda_1 \lambda_2 \cdots \lambda_r)^{1/r}$ taken over all pairs of distinct codewords c and e.

In [77] a new bound was proposed which is asymptotically tight at high SNRs and uniformly tighter than the Chernoff bound was introduced, and is shown below in (3.28),

$$P(c \to e) \le \binom{2rN_R - 1}{rN_R - 1} \left(\frac{E_S}{N_O} \right)^{-rN_R} \left(\prod_{i=1}^{r} \lambda_i \right)^{-N_R}. \tag{3.28}$$

The analysis is simplified by setting $E_S = 1$ and considering the number of transmit antennas in the calculation of E_S / N_O from the SNR in dB as,

$$\frac{E_S}{N_O} = \frac{1}{N_T} 10^{SNR/10}. \tag{3.29}$$

3.6.2.1 PWEP in Rayleigh Fading Channels

In rapid fading channels, the path gains $\alpha_t^{i,j}$ are uncorrelated in time and space. For the time instance i when $c_t \neq e_t$ the expression for the eigenvalues in [68] is equivalent to that derived in [17] and is given as,

$$\lambda_i = |c_i - e_i|^2. \tag{3.30}$$

Here the number of time instances that $c_t \neq e_t$ is the rank r of the codeword difference covariance matrix (CDCM). For rapid fading channels the upper bound on the PWEP can

be calculated by substituting the eigenvalues λ_i and r into (3.27) and (3.28). A diversity gain of rN_R and coding gain of $\prod\prod\lambda_i$ is achieved. For the case of quasi-static fading channels $\alpha_t^{i,j}$'s are only spatially uncorrelated as they are constant for a whole frame. From [68] the eigenvalues of the codeword difference covariance matrix (CDCM) are equivalent to the Hermitian matrix $H(c,e)$ derived in [17]. This matrix can be represented with elements H_{pq} and is given by,

$$H_{pq} = \sum_{t=1}^{L}\left(c_t^p - e_t^p\right)\overline{\left(c_t^q - c_t^q\right)}. \tag{3.31}$$

Again the upper bound on the PWEP can be obtained by using the eigenvalues λ_i and rank r of $H(c,e)$ in (3.27) and (3.28). In this case diversity gain of rN_R and coding gain of $\left(\prod\prod\lambda_i\right)^{1/r}$ is achieved.

3.6.2.2 Coding Gain for AWSTTC

For the case of adaptively weighted space-time trellis codes, we look at the performance in terms of coding gain over the corresponding space-time trellis codes. Now consider the two schemes, which both have full diversity order, in order to quantify the coding gain by looking at the error events with path lengths of 2 as it is the shortest distance for an event to occur. The difference matrix from (3.21) becomes,

$$B = \begin{bmatrix} (1+j0)-(1+j0) & (-1+j0)-(1+j0) \\ (0+j1)-(0+j2) & (1+j0)-(1+j0) \end{bmatrix}. \tag{3.32}$$

Since $A = BB^H$, so $A = \begin{bmatrix} 4 & 0 \\ 0 & 2 \end{bmatrix}$, and the eigenvalues $|A-\lambda I| = 0$, are $\lambda_1 = 2$ and $\lambda_2 = 4$.

Taking log of (3.27), we can write, $P_k \sim -MNa_k - Nb_k$ where $k = 1,2$ representing the weighted code and TSC code respectively and,

$$a_k = \log\left(\frac{E_s}{4N_0}\frac{1}{M}\right) \text{ and } b_k = \log\left(\prod_{m=1}^{M}\lambda_m\right). \tag{3.33}$$

Since the diversity gain is the same and we are interested in the coding gain, the gains are $b_1 = \log(8) = 0.9031$ and $b_2 = \log(4) = 0.6201$ [115], so the asymptotic gain is given as,

$$Asymptotic\ Gain = 10\log\left(\frac{gain_{AWSTTC}}{gain_{TSC}}\right) = 3dB \tag{3.34}$$

For a given SNR, $\Delta a = 0$, and $\Delta P \sim -MN\Delta a - N\Delta b = -N\Delta b$. Here $\Delta b > 0 \Rightarrow \Delta P < 0$. and therefore code 1 which is the adaptively weighted scheme outperforms the TSC scheme. It is seen that the asymptotic gain is approximately 3dB. It is seen that [57, 58] had approximately 1.5dB gain form analysis, and was only significant for systems with more than one receive antenna. Thus it is seen that the AWSTTC scheme has a visible and significant coding gain over other systems with single receive antenna.

3.6.3 Transfer Function Bounds

In order to compute the upper bound on the average bit error probability, we perform the following steps;

i.) we add over all error events weighting each information bit errors associated with that event,

ii.) statistically average this sum over all possible transmitted sequences, and

iii.) divide by the number of input bits per transmission.

The process can be expressed as,

$$P_b(e) \le \frac{1}{n_c} c\sum_{c} P(c)\sum_{c\neq e} n(c,e)P(c,e), \tag{3.35}$$

where $P(c)$ is the probability that the sequence c is transmitted, and $n(c,\hat{e})$ is the number of information bit errors occurring by choosing $\hat{e}$ instead of c. For a large class of trellis codes, a symmetry property exists such that the correct sequence c can always be chosen

as the all-zeros sequence, thus avoiding the necessity of averaging over all possible transmitted sequences. Codes of this type are referred to as uniform error probability (UEP) codes. Then we have,

$$P_b(e) \le \frac{1}{n_c} \sum_{c \ne \hat{e}} n(c,\hat{e}) P(c,\hat{e}). \tag{3.36}$$

Considering only a number of events yields an approximation (i.e. truncation of the upper bound). Thus, we have,

$$P_b(e) \cong \frac{1}{n_c} \sum_{k=1}^{K} n(c,\hat{e}) P(c,\hat{e}), \tag{3.37}$$

where, K is the length of the error event. Error events can be defined as paths corresponding to codewords that diverge at time t_1, from a specific state and remerge at time t_2 to the same specific state. These error events can be classified into types according to the number of bit errors present in each of them.

The transfer function bounding method is an efficient method for computing the weighted sum in the union bound and based on the exact PWEP [78]. It is given by,

$$P_b(e) \le \int_0^{\pi/2} \left[\frac{1}{n_c} \frac{\partial}{\partial I} T(D(\theta), I)|_{I=1} \right] d\theta. \tag{3.38}$$

In order to compute the transfer function, the error state diagram obtained from the trellis code is required. This is obtained by splitting the zero state into initial and final stages and removing the path between these stages, then by labelling all branches with the corresponding weight profiles of the form $D(\theta)I^2$. This can be done using Mason's gain formula shown below,

$$T = \frac{1}{\Delta} \sum_i F_i \Delta_i, \tag{3.39}$$

where, F_i : gain of the i^{th} forward path and Δ_i : determinant of signal flow graph after removing all nodes along the i^{th} forward path. A broader discussion of this method can be found in [24]. Since we assume QPSK signalling there are four possibilities, $S_{m,l} = \{0,1,2,3\}$ which implies that the possible estimates $\hat{e}_{m,l} = \exp\left(j\frac{2\pi}{4} S_{m,l} \right)$

can be determined. Hence we define a distance term λ, which can take values $\lambda = (2,4,6,8)$, from the equation (3.40),

$$\lambda = \sum_{m=1}^{M} \left| C_{m,l} - \hat{e}_{m,l} \right|^2 . \tag{3.40}$$

By obtaining the λ values, we are able to determine the Bhattacharyya parameter $D(\theta)$, given by,

$$D_\lambda(\theta) = \left(1 + \frac{1}{\sin^2 \theta} \frac{E_s}{4N_O} \right)^{-N} . \tag{3.41}$$

So for a 4-state, QPSK STTC code, a state transition diagram can be found in appendix A.1, and a corresponding state transition matrix can be derived based on this approach as shown below,

$$A(D_\lambda(\theta), I) = \begin{bmatrix} D_0(\theta)I^0 & D_2(\theta)I^1 & D_4(\theta)I^1 & D_2(\theta)I^2 \\ D_2(\theta)I^0 & D_4(\theta)I^1 & D_6(\theta)I^1 & D_4(\theta)I^2 \\ D_4(\theta)I^0 & D_6(\theta)I^1 & D_8(\theta)I^1 & D_6(\theta)I^2 \\ D_2(\theta)I^0 & D_4(\theta)I^1 & D_6(\theta)I^1 & D_4(\theta)I^2 \end{bmatrix} . \tag{3.42}$$

Using this approach we can determine the transfer function in a closed form expression as,

$$T(D_\lambda(\theta), I) = \frac{(I+I^2)D_2^2(\theta) + ID_4^2(\theta) - (I^2+I^3)[D_2^2(\theta)D_8(\theta) + D_4^3(\theta) - 2D_2(\theta)D_4(\theta)D_6(\theta)]}{1-(I+I^2)D_4(\theta) - ID_8(\theta) + (I^2+I^3)[D_4(\theta)D_8(\theta) - D_6^2(\theta)]} . \tag{3.43}$$

Now in order to reduce the complexity, we will evaluate an approximation based on a truncation method, taking into account only a small number of error events. For a case where the length of the error event is K=2, by examining the trellis code we can determine that there are three error events of length 2; two of them of Type I and one of them of Type II, defined as

$$P(c,\hat{e})_I = \frac{1}{\pi} \int_0^{\pi/2} \left(\frac{\sin^2 \theta}{\sin^2 \theta + \bar{\gamma}/2} \right)^{2N} d\theta \qquad P(c,\hat{e})_{II} = \frac{1}{\pi} \int_0^{\pi/2} \left(\frac{\sin^2 \theta}{\sin^2 \theta + \bar{\gamma}} \right)^{2N} d\theta . \tag{3.44}$$

Noting that Type I contributes a total of 3 bit errors and Type II contributes 1 bit error, we obtain,

$$P_b(e) \cong \frac{1}{2}\left[3P(c,\hat{e})_I + P(c,\hat{e})_{II}\right]. \tag{3.45}$$

Hence after differentiating (3.43), and considering only the error events of length 2 and for high SNR case it can be reduced to (3.46) shown below,

$$\left.\frac{\partial}{\partial I}T(D_\lambda(\theta),I)\right|_{I=1} \cong 3D_2^2(\theta) + D_4^2(\theta). \tag{3.46}$$

Substituting (3.46) in (3.38), we obtain the closed form for the bound,

$$\begin{aligned} P_b(e) &\cong \frac{1}{\pi}\int_0^{\pi/2}\frac{1}{2}\left[3\left(\frac{\sin^2\theta}{\sin^2\theta+\bar{\gamma}/2}\right)^{2N}+\left(\frac{\sin^2\theta}{\sin^2\theta+\bar{\gamma}}\right)^{2N}\right]d\theta \\ &= \frac{3}{4}\left\{1-\sqrt{\frac{\bar{\gamma}/2}{1+\bar{\gamma}/2}}\sum_{k=0}^{2N-1}\binom{2k}{k}\left(\frac{1}{4\left(1+\bar{\gamma}/2\right)}\right)^k\right\}+\frac{1}{4}\left\{1-\sqrt{\frac{\bar{\gamma}}{1+\bar{\gamma}}}\sum_{k=0}^{2N-1}\binom{2k}{k}\left(\frac{1}{4\left(1+\bar{\gamma}\right)}\right)^k\right\}. \end{aligned} \tag{3.47}$$

This is now an approximated bound and no longer an upper bound. Similarly bounds can be obtained for larger number of error events.

3.6.4 Union Bound for Rapid Fading

Here we employ the method used in [76] to determine the union bound for rapid and quasi-static channels in the next section. For rapid fading channels the PWEP given by (3.28) required the number of epochs r for which $c_t \neq e_t$ and the product of the Eigen values λ_i. Thus an error event can be described by three parameters; an input weight i, an eigenvalue product p and the rank r. Each λ_i is simply the Euclidean distance between the individual symbol vectors $\underline{c_i}$ and $\underline{e_i}$. This product can be calculated on an epoch by epoch basis, but the state transition method accumulates the sum of error event parameters not the product. If the Euclidean distances between symbol vectors are converted to the log domain, multiplication is now equivalent to addition as shown below,

$$\prod_i a_i = \exp\left(\sum_i \ln a_i\right). \tag{3.48}$$

The state transition matrix takes the form $A(I,P,R)$ with the elements $A_{sf}(I,P,R)$ and is initialized as follows. If a transition from state s to state f exists then $A_{sf}(I,P,R)$ is calculated as shown below, otherwise it is set to zero.

$$A_{sf}(I,P,R) = I^i P^p R^r, \tag{3.49}$$

$$\begin{aligned} p &= \begin{cases} 0 & if\ \underline{c}_{00} = \underline{c}_{sf} \\ \ln\left|\underline{c}_{00} - \underline{c}_{sf}\right|^2 & otherwise \end{cases} \\ r &= \begin{cases} 0 & if\ \underline{c}_{00} - \underline{c}_{sf} \\ 1 & otherwise \end{cases}. \end{aligned} \tag{3.50}$$

For the 4-state Tarokh STTC given in appendix A.1.1, the initial state transition matrix is given below,

$$A(I,P,R) = \begin{bmatrix} 1 & IP^{\ln 2}R & IP^{\ln 4}R & I^2P^{\ln 2}R \\ P^{\ln 2}R & IP^{\ln 4}R & IP^{\ln 6}R & I^2P^{\ln 4}R \\ P^{\ln 4}R & IP^{\ln 6}R & IP^{\ln 8}R & I^2P^{\ln 6}R \\ P^{\ln 2}R & IP^{\ln 4}R & IP^{\ln 6}R & I^2P^{\ln 4}R \end{bmatrix}. \tag{3.51}$$

After the calculation of $A(I,P,R)^L$ element $(0,0)$ is a polynomial of the form,

$$N(I,P,R) = \sum_{i,p,r} n(i,p,r) I^i P^p R^r, \tag{3.52}$$

and the union bound on the frame error rate (FER) and BER can be calculated as follows.

$$P_f \leq \sum_{i,p,r} n(i,p,r) \exp(-N_R p) \gamma(r, N_R), \tag{3.53}$$

$$P_b \leq \sum_{i,p,r} \frac{i}{kL} n(i,p,r) \exp(-N_R p) \gamma(r, N_R). \tag{3.54}$$

The exponential term converts the sum of Euclidean distances in the log domain to the desired product of Euclidean distances. The $\gamma(.)$ term is replaced by (3.27) when the new bound on the PWEP is used and by (3.28) when the Chernoff bound on the PWEP is used. In order to limit the number of terms in each polynomial, a limiting function $(plim)$ is calculated whereby, a term is excluded if $p \geq plim$. An important feature of this bound is that $N(I,P,R)$ is calculated independently of the SNR and the number of receive antennas,

hence the FER and BER of the STTC can be calculated for any SNR and N_R with only a single $N(I,P,R)$ calculation.

3.6.5 Union Bound for Quasi-Static Fading

In quasi-static fading channels the PWEP (3.31) is calculated using the rank r and the non-zero eigenvalues λ_i of the Hermitian matrix $H(c,e)$. For convenience this matrix is expressed as $\boldsymbol{h}$ with complex elements h_{pq}. Each element of $\boldsymbol{h}$ is an accumulation of terms over the entire frame where each term can be calculated on an epoch by epoch basis which lends itself to accumulation using the state transition matrix method.

An error event can now be described by an input weight i and a matrix $\boldsymbol{h}$. The state transition matrix takes the form $A(I,H)$ and is initialized as follows. If a transition from state s to state f exists, $A_{sf}(I,\mathbf{H})$ is calculated as shown below otherwise it is set to zero.

$$A_{sf}(I,\mathbf{H}) = I^i H_{11}^{h_{11}},\ldots,H_{pq}^{h_{pq}},\ldots,H_{N_T,N_T}^{h_{N_T,N_T}}, \tag{3.55}$$

$$h_{pq} = (c_{00}^{p} - c_{sf}^{p})\overline{(c_{00}^{q} - c_{sf}^{q})}. \tag{3.56}$$

For the 4-state Tarokh STTC given in appendix A.1.1, the initial state transition matrix is given below where $j=\sqrt{-1}$.

$$A(I,\mathbf{H}) = \begin{bmatrix} 1 & IH_{22}^2 & IH_{22}^4 & I^2H_{22}^2 \\ H_{11}^2 & IH_{11}^2H_{12}^2H_{21}^2H_{22}^2 & IH_{11}^2H_{12}^{2-2j}H_{21}^{2+2j}H_{22}^4 & I^2H_{11}^2H_{12}^{-2j}H_{21}^{2j}H_{22}^2 \\ H_{11}^4 & IH_{11}^4H_{12}^{2+2j}H_{21}^{2-2j}H_{22}^2 & IH_{11}^4H_{12}^4H_{21}^4H_{22}^4 & I^2H_{11}^4H_{12}^{2-2j}H_{21}^{2+2j}H_{22}^2 \\ H_{11}^2 & IH_{11}^2H_{12}^{2j}H_{21}^{-2j}H_{22}^2 & IH_{11}^2H_{12}^{2+2j}H_{21}^{2-2j}H_{22}^4 & I^2H_{11}^2H_{12}^2H_{21}^2H_{22}^2 \end{bmatrix}. \tag{3.57}$$

It is important to note that h_{pq} is complex and hence $A_{sf}(I,\mathbf{H})$ is a polynomial of dimension N_T^2+1 with complex coefficients. This computation can be simplified somewhat by noting that $A_{sf}(I,\mathbf{H})$ is equivalent to a polynomial of dimension $2N_T^2+1$ with

real coefficients where H_{pq} and exponent h_{pq} are divided into their real and imaginary parts.

After calculation of $A(I,\mathbf{H})^L$ the polynomial of interest is element $(0,0)$ and is expressed as follows.

$$N(I,\mathbf{H}) = \sum_{i,h} \mathrm{I}^i H_{11}^{h_{11}} \cdots H_{N_T,N_T}^{h_{N_T,N_T}}. \tag{3.58}$$

The union bound on the FER and BER can be calculated as shown below where the λ_j's are the non-zero eigenvalues and r the rank of the matrix $\boldsymbol{h}$. This matrix is constructed from the error event parameters $\{h_{11},\ldots,h_{N_T,N_T}\}$. The FER for the Chernoff and new Chernoff are shown,

$$\begin{aligned} P_f &\le \sum_{i,h} n(i,\boldsymbol{h}) \left(\prod_{j=1}^{r} \lambda_j\right)^{-N_R} \left(\frac{E_S}{4N_0}\right)^{-rN_R}, \\ &\text{or} \\ P_f &\le \sum_{i,h} n(i,\boldsymbol{h}) \left(\prod_{j=1}^{r} \lambda_j\right)^{-N_R} \binom{2rN_R-1}{rN_R-1} \left(\frac{E_S}{N_0}\right)^{-rN_R} \end{aligned} \tag{3.59}$$

and the BER for the Chernoff and new Chernoff are shown,

$$\begin{aligned} P_b &\le \sum_{i,h} \frac{i}{kL} n(i,\boldsymbol{h}) \left(\prod_{j=1}^{r} \lambda_j\right)^{-N_R} \left(\frac{E_S}{4N_0}\right)^{-rN_R}. \\ &\text{or} \\ P_b &\le \sum_{i,h} \frac{i}{kL} n(i,\boldsymbol{h}) \left(\prod_{j=1}^{r} \lambda_j\right)^{-N_R} \binom{2rN_R-1}{rN_R-1} \left(\frac{E_S}{N_0}\right)^{-rN_R} \end{aligned} \tag{3.60}$$

From the above equations it can be seen that the contribution of an error event to the union bound is inversely proportional to the eigenvalue product. For this reason the limiting factor is defined as,

$$f(\boldsymbol{h}) = \prod_{j=1}^{r} \lambda_j, \tag{3.61}$$

where all the terms with $f(\boldsymbol{h}) \ge h_{\lim}$ are excluded from the polynomial.

Once again it is important to note $N(I,\mathbf{H})$ is calculated independently of the SNR and the number of receive antennas therefore the FER and BER of the STTC can be calculated for any SNR and N_R with only a single $N(I,\mathbf{H})$ calculation.

3.7 Analytical and Simulation Results

In this section the FER performance of various 2 bits/s/Hz, Tarokh STTCs (TSC) [17] and adaptively weighted STTCs (AWSTTCs) [75] are investigated for both quasi-static and rapid fading channels. For these STTCs $k=2$ input bits, $N_T=2$ transmit antennas and use QPSK modulation. Simulation results are presented for the STTCs using 4-state and 16-state codes for $N_R=1$ and $N_R=2$ receive antennas. The frame size is chosen to be 260 bits or 130 transmissions in all cases. The trellis diagrams for these codes are given in appendix B.

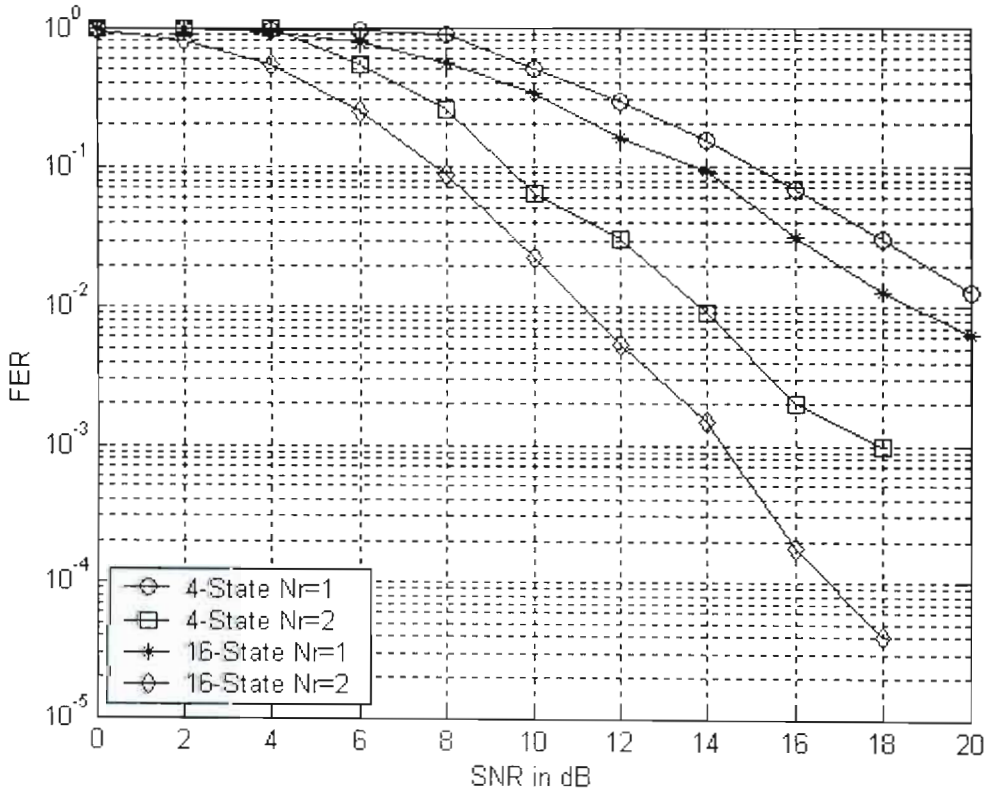

Fig. 3.9: FER for Tarokh STTC in quasi-static fading ($N_T=2,k=2,M=4$).

In Fig. 3.9 the performance of various STTCs in a quasi-static fading channel is shown. It is clear that the system performance increases with the number of states and by increasing the number of receive antennas. The diversity gain determines the slope of the curve and the coding gain determines the horizontal offset or shift of the curve. In Fig. 3.10 the performance of various STTCs is investigated in rapid fading channels. Here it is observed that an increase in the number of states of the code results in a greater improvement of FER performance than in quasi-static fading channels. Once again it is clear that increasing the number receive antennas improves the system performance.

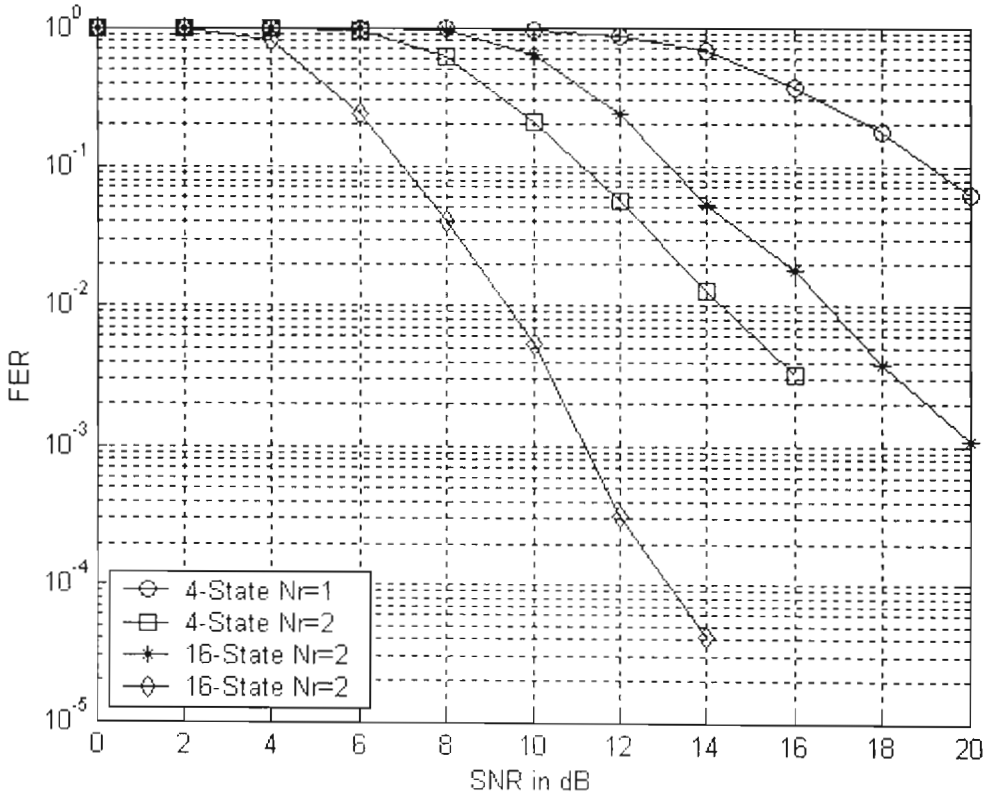

Fig. 3.10: FER for Tarokh STTC in rapid fading ($N_T = 2, k = 2, M = 4$).

Fig. 3.11 shows the performance of the AWSTTC code in comparison with the TSC scheme in quasi-static fading channel. The adaptively weighted space-time trellis codes with CSI at the transmitter has shown to perform better in terms of coding gain than the standard TSC scheme and has also shown significant coding gain in comparison with

other systems with a single receive antenna and comparable complexity. It is observed that there is a coding gain of 2dB over the TSC scheme under similar system parameters. Fig. 3.12 compares the performance of AWSTTC code in rapid fading channels. It is seen that there is still a significant gain over the TSC scheme in this channel.

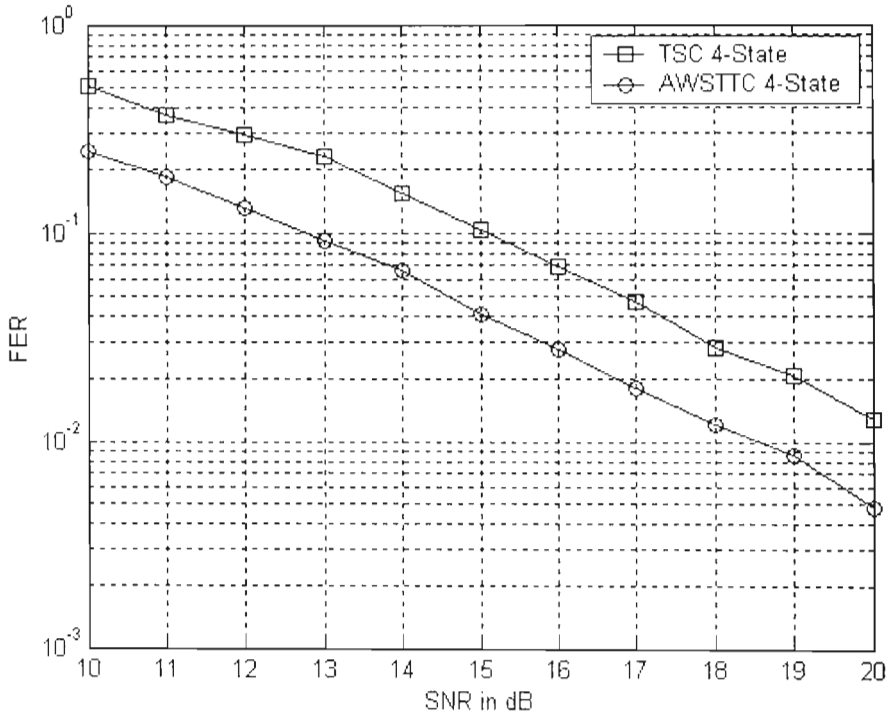

Fig. 3.11: Comparison of FER results of TSC and AWSTTC in quasi-static fading.

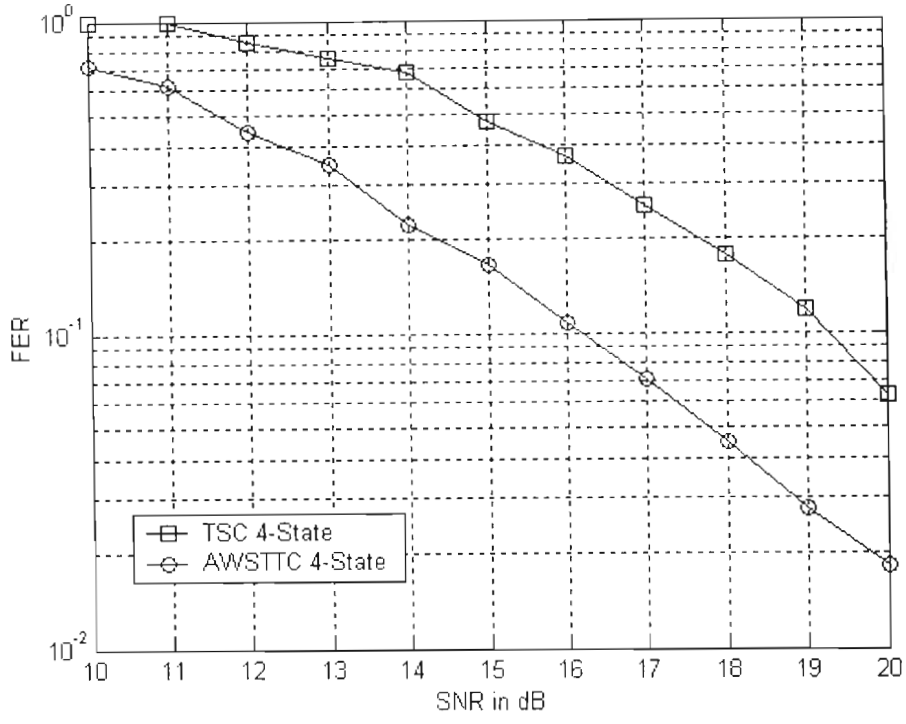

Fig. 3.12: Comparison of FER results of TSC and AWSTTC in rapid fading.

In considering the analytical results obtained, we compare them with the simulation results in order to assess their accuracy or tightness. The Q-PSK, 4-state STTCs with 2 transmit antennas are considered, namely the STTC of Tarokh [17]. The channel conditions considered are rapid and quasi-static Rayleigh fading models as described in section (3.2). The FERs and BERs (where provided) are plotted against the SNR per receive antenna. In all cases the input bits are 260 bits corresponding to L=130 transmissions from each antenna. In the following figures, the labels simulation, Chernoff, and New refer to the simulation results, the union bound using the Chernoff bound on the PWEP, and the union bound using the new bound on the PWEP. The number following the bound name is the limiting factor which is *plim* in the case of rapid fading and *hlim* in the case of quasi-static fading as described in section 3.6.3 and 3.6.4.

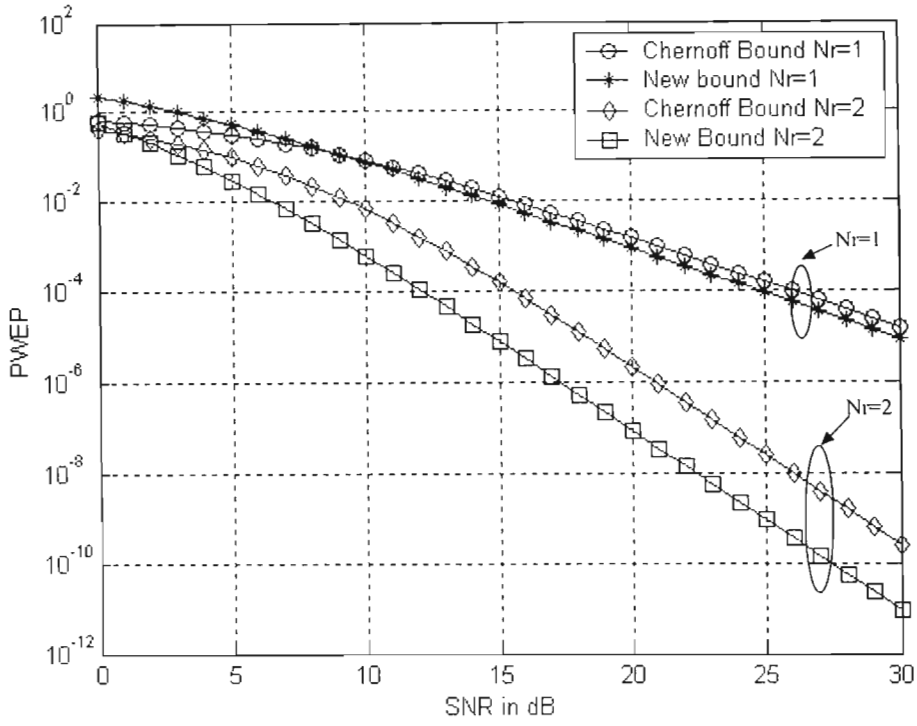

Fig. 3.13: Comparison of Chernoff and New bounds on the PWEP for STTCs

In Fig. 3.13 the TSC scheme is considered. Here the PWEP bound for the Chernoff bound and new bound are shown for $N_R = 1$ and $N_R = 2$ receive antennas. The variation in the bounds can be clearly observed in $N_R = 2$ curves. The union bound using the Chernoff bound and the new bound on the PWEP are compared for a value of *plim* as 10. It can be seen in Fig. 3.14 where we first consider the rapid fading case that the Chernoff bound is fairly loose even at high SNRs, whereas the new bound is very tight at high SNRs. It can be observed that as more number of error events is considered the bound still converges which indicates that in rapid fading channels there are dominant error events.

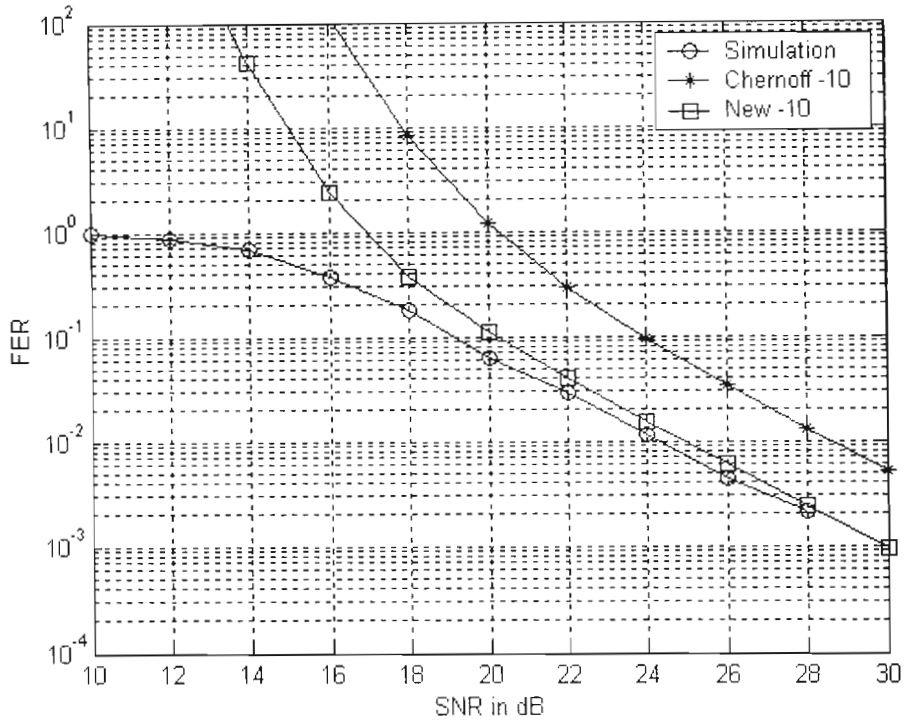

Fig. 3.14: Chernoff and New bound for Tarokh STTC in rapid fading with $N_R = 1$.

It can be observed that the new bound and simulation results show good agreement. It is seen that there is a divergence of the bound at low SNRs is observed, which is in accordance with the behaviour of the union bound. In Fig. 3.15 the results for the Chernoff and New bounds are presented in quasi-static channels. It was observed that there was no convergence, as the number of error events is increased (increase of *hlim*), even at high SNRs. We show $hlim = 4$ as an example in the plot in Fig. 3.15. The reason is due to the fact that there are no dominant error events in quasi-static fading channels. The bound in this channel was also found to be loose under these channel conditions.

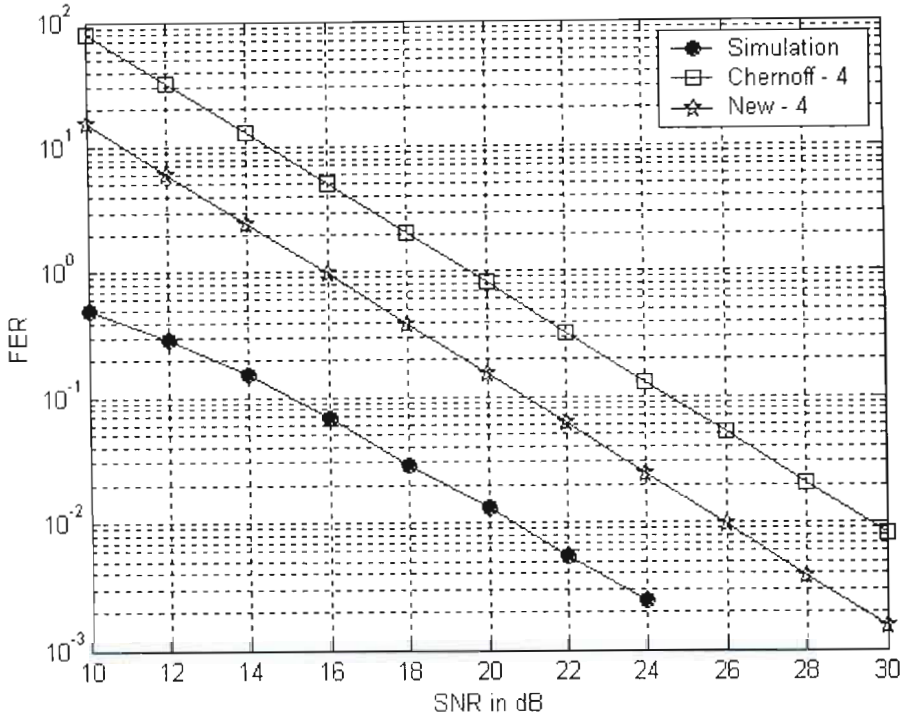

Fig. 3.15: Chernoff and New bound for Tarokh STTC in quasi-static fading with $N_R = 1$.

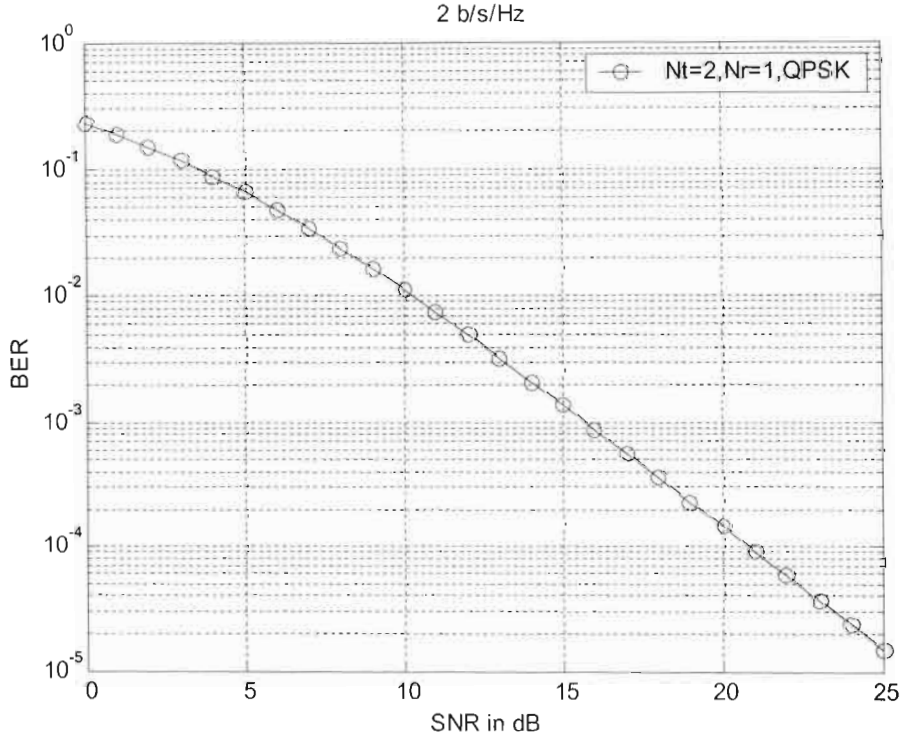

Fig. 3.16: Truncated Transfer function bound in quasi-static fading channel.

In Fig. 3.16 the bounds using the transfer function bounding approach is used, whereby error events of length ($N = 2$) are taken into consideration. This means that the bound is approximated as it only takes into account the possible error events of length 2, unlike all of them in the union bound case. Nevertheless, the bound gives a good performance of STTCs in quasi-static fading channels.

3.8 Implementation Complexity

Turbo codes and Space-Time codes have shown very good performances in their respective fields of near Shannon capacity coding and high data rate coding schemes. It can be seen that though these two schemes seem to offer incredible performance gains from a theoretical point of view, the fact remains that it becomes increasingly complicated to implement such schemes on hardware for actual real-time systems. As both these codes are computationally intensive, we investigate the implementation individually and investigate the feasibility of their concatenated schemes.

With the increasing technological advances in the processing speeds and capabilities of digital signal processors (DSP), fairly complex algorithms can be processed with ease. State of the art fixed point processors have acceleration hardware and special instruction sets to speed up the execution of various algorithms. In turbo decoding for instance the MAP algorithm is preferred as it gives the best performance. However, the MAP algorithm has huge memory requirements and processing delays. It is due to this fact that the less complex viterbi based decoder and the soft-output viterbi algorithm (SOVA) based decoders have been widely implemented, with a trade-off in performance. In order to shed light in the implementation hurdles which have to be overcome before such schemes are deployed in the next generation systems, the processing speeds and features of top performing DSP kits are studied and the complexity of their implementation based on the number of instruction cycles is studied.

3.8.1 Complexity Issues

The computational complexity of a turbo decoder is dominated by the MAP module implementation [79, 80]. This is because all of the states must be updated at each trellis stage, and most of the time is spent on the metric update. Thus normalization and precisions become important issues, due to the iterative nature of the decoding. As discussed in section 2.6, the MAP algorithm computations are based on the logarithmic function of a sum of exponentials, and such an expression can be computed as the sum of two terms using Jacobean logarithm as a maximum exponent and correction term as shown in (3.62),

$$\log\left(e^{L_1} + e^{L_2}\right) = \max\left(L_1 L_2\right) + \log\left(1 + e^{|L_1 - L_2|}\right). \tag{3.62}$$

If the correction term is omitted and only the max term is used to compute the alpha, beta and extrinsic LLR values, the max-log-MAP is obtained.

We consider a C6200 compiler that has eight functional units, of which two are multipliers and log-MAP instructions can not be carried out on them. The remaining six units can execute basic 32-bit arithmetic logic unit (ALU) operations as well as some specialized instructions. The tables provided in appendix C provides the analysis of optimized C code and the operations required to perform log-gamma, log-alpha and log-beta computations [80]. The final cycle count requirements for one trellis stage of MAP decoding is shown in table 3.1 below,

Table 3.1: Cycle Count for single trellis stage

LOOP	CYCLES/TRELLIS STAGE
Log-Gamma	2.5
Log-Alpha	8
Log-Beta	8
Extrinsic LLR	10
TOTAL	28.5

The entire turbo decoding process requires two MAP decoders, two interleaver/deinterleavers, as well as some entry or exit overheads (~10%). Then for a frame length of 1024 bits and 8 iterations requires:

[28.5 cycles/stage/iteration/MAP * 1024 stages * 8 iterations * 2MAPS
+ 0.5cycles/stage/iteration/interleaver * 1024stages * 8 iterations * 2 interleavers]*1.10

≈ 522650 cycles @300MHz.

The STTC are decoded using the Viterbi algorithm and so is relatively less complex than the turbo code, as it has much less memory requirements. The sliding window approach in Viterbi decoding drastically reduces the memory requirements as the backward recursion converges after 4 to 5 times the constraint length of the encoders. The number of instruction cycles required for a Viterbi is shown below [81],

Table 3.2: Cycle Count for Viterbi

IMPLEMENTAION METHOD	CYCLES
C-Code	6612
C6205 Assembly	329

For a frame length of 260 bits, the number of instruction cycles for the whole frame would be 329 * 260 = 85540 cycles@200MHz.

3.8.2 Processor Performances

DSP technology has made tremendous strides due to advances in semiconductor processing that allow more memory and compute resources to be integrated on one chip, and architectural enhancements that let the processors do more during each clock cycle. A list of the top performing DSP processors is shown in Table 3.3.

Table 3.3: List of top performing DSP kits.

PROCESSOR TYPE	CYCLE TIME (ns)	CLOCK RATE (MHz)	Turbo Decoder Comp. Time (ms)	Max. Sampling Frequency (KHz)
TMS320C6411	3	300M	2	500
TMS320C67xx	1	1 G	0.6	1.67K
MOTOROLA ADSP BF561	1.3	750M	0.75	1.34K
SHARC ADSP TS201S	1.7	600M	0.6	1.05K

From the above example, the decoding can be computed in 522620 instruction cycles. If for example the TMS320C67xx is used, the computational time is 0.522ms. If we allow approximately 0.574ms for the decoder computation and any other computations, the maximum sampling can be determined to be 1742Hz. For the concatenated scheme which uses an outer turbo code and an inner STTC code using a SOVA decoder, the complexity can be calculated to be at least of the order of 608,190 cycles [82]. The maximum sampling time for the C67xx will be 0.608ms or a maximum sampling frequency of 1.644 KHz. This implies only low data rates can be processed when using the concatenated scheme. It is seen that several factors affect the processing requirements for the systems discussed. These factors include constraint lengths, coding rates and convergence times. Longer constraint lengths require more data memory for transition register storage and more program memory space for metric updating.

3.9 Conclusion

In this chapter we presented the generalized system model of a MIMO system with multi-element arrays at both ends of the wireless link. The importance of channel capacity and efforts to achieve that capacity are studied. Theoretical results for the capacity of MIMO systems were given for various combinations of multiple transmit and receive antennas, and the effects of channel correlation was investigated. Various types of coding for multi-antenna systems were briefly described. Current trends in research in space-time coded systems were discussed briefly. STTCs provide the best trade-off in terms of complexity

and performance. AWSTTCs show improved performance over STTCs, but owing to their closed nature are not feasible for implementation on concatenated platforms. Simulation and analytical results for the various schemes were studied in quasi-static and rapid fading Rayleigh channels. The original bound on the PWEP from [17] and a new bound from [77] were presented. The application of the union bound to the analysis of coded systems and methods to simplify the complexity of the calculation using error events were discussed. The transfer function bounding approach for quasi-static channels was also presented. The bounds were compared with simulation results in both fading cases. A look at the implementation complexity of turbo coded and space-time systems was investigated. The feasibility of implementation of a concatenated system was investigated.

CHAPTER 4

SUPER-ORTHOGONAL SPACE-TIME TRELLIS CODES

4.1 Introduction

Space-Time Trellis Codes have been introduced in [17] to improve the error performance of wireless systems using multiple transmit antennas. It has been shown that such codes provide full diversity gain as well as additional SNR advantage, called the coding gain. Tarokh *et al.* [17], derived design criteria to improve space-time code error performance. They also proposed code design rules for achieving full diversity for two transmit antennas. Using these code design rules, examples of codes with full diversity are constructed in [17] in which coding gains are not necessarily optimized.

A simple code providing full diversity for two transmit antennas is introduced by Alamouti in [45] where transmitted symbols can be separately decoded based on a linear processing at the receiver. In [46] STBC is presented which is a generalization of Alamouti's scheme to an arbitrary number of transmit antennas. Although orthogonal space-time block codes (OSTBC) provide full rate and full diversity with a very simple design, they do not provide any coding gain and can not guarantee full rate, diversity for

more than two transmit antennas. This is in contrast to STTC that provide full diversity as well as significant coding gains, but at a cost of higher decoding complexity.
Since there is no general rule for designing codes that provide diversity as well as coding gain, it is unclear how to design new codes for different number of states or different rates. Also, it is not clear as to how to improve the performance of the codes, i.e. how to maximize the coding gain. There have been significant efforts to improve the performance of the original STTC codes in [57, 58, 59, 84]. While very interesting codes have been proposed in the literature, the coding gain improvements are marginal for one receive antenna. Several schemes based on the concatenation of the STBC with an outer trellis code have been proposed [85], [86] to achieve satisfactory coding gains. The main disadvantage of these schemes is their rates which are below the possible maximum rate.

To solve this problem, Jafarkhani and Seshadri [21] proposed a new coding scheme which combines STBC with trellis codes and yet guarantees full rate. They also provide a systematic design criterion similar to the design criteria of trellis coded modulation (TCM).

In this chapter we first discuss the motivation behind the purpose of designing the new codes, and later discuss its salient features. Next the set partitioning criteria and the use of orthogonal design procedure is discussed. This is followed by specific design criteria for the case of rapid fading channels in section 4.3. Analytical methods using the CGD and MGF methods are used to analyse the performance of the codes in Rayleigh fading channels. Finally, the system performance is evaluated by some simulation and analytical results.

4.2 Super-Orthogonal Space-Time Trellis Codes

A new class of space-time codes called Super-Orthogonal Space-Time Trellis Codes (SOSTTC) is introduced in [21] which provide a new structure for STTC that guarantees full diversity and provide opportunity to maximize the coding gain. In order to go about

this the authors lay out a design method whereby they combine set-partitioning and a super set of orthogonal space-time block code in a systematic way to provide full diversity and improved coding gain over earlier STTC constructions. The super-orthogonal signal set is obtained by a constellation rotation. While providing full diversity and full rate, the structure of the new code allows an increase in the coding gain. Since the orthogonal designs have been used as building blocks in SOSTTCs, the decoding complexity remains low. In a nutshell, we can say that SOSTTCs are essentially STTCs transmitting STBC codewords in each trellis section. The set of available space-time block codewords are extended via rotations, while maintaining the orthogonality of the codewords. In this manner they develop a space-time trellis coding method which:
(i.) provides a larger coding gain than STTC for same diversity advantage and state size.
(ii.) has a systematic design method for SOSTTCs having a given diversity, rate and state size.

4.2.1 Motivation

In [45] a space-time block coding scheme was proposed which achieved a full rate and full diversity. This scheme can be used for $N = 2$ transmit antenna and any number of receive antennas. As described in section 3.4.3, the scheme transmits $2b$ bits every two symbol intervals, where the two dimensional $(2-D)$ constellation size is $L = 2^b$. The encoder then encodes the two symbols and transmits them according to the transmission matrix given by,

$$C(x_1 \;\; x_2) = \begin{pmatrix} x_1 & x_2 \\ -x_2^* & x_1^* \end{pmatrix}. \tag{4.1}$$

This scheme produces diversity gain, but no additional coding gain. In order to provide an additional coding gain, the concatenation of an outer trellis code with the space-time block code was proposed in [85] and [86]. This method created a four dimensional $(4-D)$ signal point by viewing each of the 2^{2b} orthogonal matrices generated by the space-time block code. The purpose of the outer code is to select one of the $(4-D)$ signal

points to be transmitted based on current state and $2b$ input bits. In their study in [85] they also concluded that for quasi-static fading channels, the trellis code used should be based on the set partitioning concepts of "Ungerboeck codes" for AWGN channels. However, the proposed schemes in [85] and [86] suffered from rate loss attributed to the fact that the schemes are not making use of all possible $(4-D)$ signal constellations.

To elaborate more on this let us consider other codes which provide behavior similar to those of (4.1) for identical parameters. The set of all such codes which use only x_1, x_2 and their conjugates with positive or negative signs are listed below as follows in (4.2),

$$\begin{bmatrix} x_1 & x_2 \\ -x_2^* & x_1^* \end{bmatrix}, \begin{bmatrix} -x_1 & x_2 \\ x_2^* & x_1^* \end{bmatrix}, \begin{bmatrix} x_1 & -x_2 \\ x_2^* & x_1^* \end{bmatrix}, \begin{bmatrix} x_1 & -x_2 \\ -x_2^* & x_1^* \end{bmatrix}$$
$$\begin{bmatrix} x_1 & x_2 \\ x_2^* & -x_1^* \end{bmatrix}, \begin{bmatrix} -x_1 & -x_2 \\ x_2^* & -x_1^* \end{bmatrix}, \begin{bmatrix} -x_1 & x_2 \\ -x_2^* & -x_1^* \end{bmatrix}, \begin{bmatrix} -x_1 & -x_2 \\ -x_2^* & x_1^* \end{bmatrix}. \tag{4.2}$$

The authors in [21] called the union of all these codes as "Super-orthogonal code" set U. It was evident that by using one of the constituent codes from U, e.g. the code in (4.1), one can not design all possible orthogonal $2x2$ matrices for a given constellation. Considering an example of BPSK constellation, it can be shown that one can build all possible $2x2$ orthogonal matrices using two of the codes in U. If we use the code in (4.1) we have,

$$\begin{pmatrix} 1 & 1 \\ -1 & 1 \end{pmatrix}, \begin{pmatrix} -1 & -1 \\ 1 & -1 \end{pmatrix}, \begin{pmatrix} -1 & 1 \\ -1 & -1 \end{pmatrix}, \begin{pmatrix} 1 & -1 \\ 1 & 1 \end{pmatrix}. \tag{4.3}$$

By using the following code from set U which represents a phase-shift of the antenna 1 by π,

$$\begin{pmatrix} -x_1 & x_2 \\ x_2^* & x_1^* \end{pmatrix}, \tag{4.4}$$

one can create other four possible distinct orthogonal $2x2$ matrices which are shown below in (4.5),

$$\begin{pmatrix} -1 & 1 \\ 1 & 1 \end{pmatrix}, \begin{pmatrix} 1 & -1 \\ -1 & -1 \end{pmatrix}, \begin{pmatrix} 1 & 1 \\ 1 & -1 \end{pmatrix}, \begin{pmatrix} -1 & -1 \\ -1 & 1 \end{pmatrix}. \tag{4.5}$$

Hence, by using more than one code from set U, we can create all possible $2x2$ orthogonal matrices. This allows the scheme to have a sufficient number of constellation matrices to design a trellis code with the highest possible rate. Also it allows for a systematic design of SOSTTC using the available knowledge about (TCM) [87] and multiple trellis coded modulation (MTCM) [88].

4.2.2 Super-Orthogonal Codes

In [21], the authors propose a clever and unique method of parameterized super-orthogonal codes, whereby they allow for the expansion of the number of available orthogonal matrices and ensure that they avoid expansion of the signal constellation which leads to increasing the peak-to-average power ratio. They propose a unique class of orthogonal designs as the transmission matrix shown below, in (4.6)

$$C(x_1, x_2, \theta) = \begin{pmatrix} x_1 e^{j\theta} & x_2 \\ -x_2^* e^{j\theta} & x_1^* \end{pmatrix}. \tag{4.6}$$

Here if $\theta = 0$, it provides the code in (4.1). The choice of θ is chosen such that for any choice of x_1 and x_2 from the original constellation points, the resulting transmitted signals are also from the same constellation. This is evident by an example where if we use L-PSK constellation signals, the constellation can be represented by $e^{j\frac{2\pi}{L}}$, for $l = 0,1\cdots,L-1$. One can pick $\theta = 2\pi l'/L$, where $l' = 0,1\cdots L-1$. In this case, the resulting transmitted signals are also members of the L-PSK constellation and, therefore do not expand the constellation signals. Since the transmitted signals are from a PSK constellation the peak-to-average power ratio of the transmitted signals are equal to one. In this way, there is no increase in the number of signals in the constellation, but also there is no need for an amplifier to provide a higher linear operation region.

For the case of BPSK constellation, we use $\theta = 0$, π and for the QPSK case, $\theta = 0, \frac{\pi}{2}, \pi, \frac{3\pi}{2}$. So by using $C(x_1, x_2, 0)$ and $C(x_1, x_2, \pi)$ for the BPSK constellation, one can generate all of the eight $2x2$ orthogonal matrices. In fact, $C(x_1, x_2, 0)$ is the code in (4.1) and $C(x_1, x_2, \pi)$ is the code (4.4). So in general a super-orthogonal code consists of the union of a few orthogonal codes, like the ones in (4.2) and the set of orthogonal codes is a subset of the set of super-orthogonal codes. Hence, in the design of full rate, full diversity trellis codes the expansion of the number of available orthogonal matrices ensure that there is no extension of the constellation alphabet of the transmitted signals. Another advantage is that the super-orthogonal codes are parameterized.

4.2.3 Set Partitioning

In this section we look at the set partitioning method adopted from Ungerboeck [93] to orthogonal codes and show how to maximize the coding gain. Let us denote the difference of the transmission matrices for codewords c_1 *and* c_2 by $B(c_1, c_2)$ and it's Hermitian, complex conjugate and transpose, by $B^H(c_1, c_2)$. According to [17], the diversity of such a code is defined by the minimum rank of the matrix $B(c_1, c_2)$. For a full diversity code, the minimum of the determinant of the matrix $A(c_1, c_2) = B(c_1, c_2)B^H(c_1, c_2)$ over all possible pairs of distinct codewords c_1 *and* c_2 corresponds to the coding gain. So in [21] the coding gain distance (CGD) between codewords c_1 *and* c_2 is defined as $d^2(c_1, c_2) = \det(A(c_1, c_2))$, where $\det(A)$ is the determinant of the matrix A . So in general, if a code has diversity less than the full diversity N , the distance can be defined as the harmonic mean of nonzero eigenvalues of $A(c_1, c_2)$. Then, the CGD is used instead of Euclidean distance to define a set partitioning similar to Ungerboeck's set partitioning in [87].

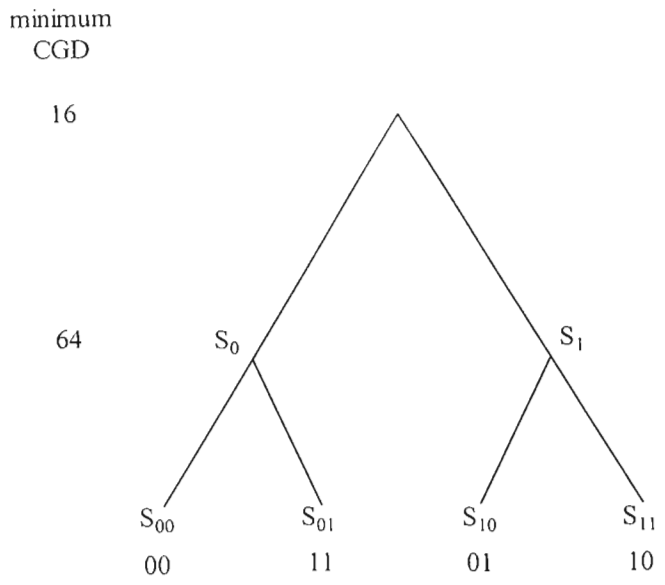

Fig. 4.1: Set partitioning for BPSK

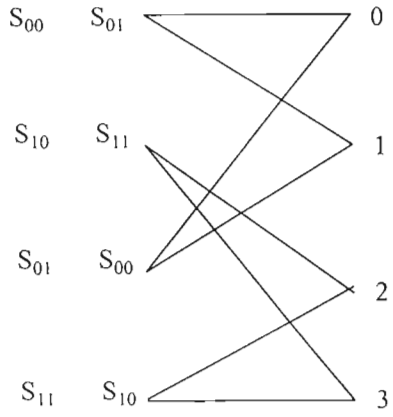

Fig. 4.2: Four-state trellis: Ungerboeck's set partitioning

Let us assume that we use a BPSK constellation using the code in (4.1), having a four-way partitioning of the orthogonal code as shown in Fig 4.1. At the root of the tree, the minimum determinant is 16. At the first level of partitioning, the highest determinant that can be obtained is 64. This is obtained by a set partitioning in which subsets S_0 and S_1 use different transmitted signal elements for different transmit antennas. At the next level of partitioning we have four sets S_{00}, S_{11}, S_{01} and S_{10} with only one element per set. Consider the trellis diagram shown in Fig. 4.2 which is constructed based on the set-partitioning with a rate $b/2$ bits/s/Hz for L-PSK constellation, where $L = 2b$. This is similar to codes

presented in [85, 86] which can only transmit at a rate which is half of the maximum possible rate. For an L-PSK constellation each signal can be represented by $s = e^{\frac{j2\pi l}{L}}$, $l = 0,1,\ldots,L$ or $s = e^{jl\omega}$ where $\omega = \frac{2\pi}{L}$. Now, we consider two distinct pairs of constellation symbols $\left(s_1^1 = e^{jk_1\omega}, s_2^1 = e^{jl_1\omega}\right)$ and $\left(s_1^2 = e^{jk_2\omega}, s_2^2 = e^{jl_2\omega}\right)$ with the corresponding code matrices c_1 and c_2 to calculate $B(c_1,c_2)$ and $A(c_1,c_2)$. We omit (c_1,c_2) from A and B for the sake of brevity. For parallel transitions in a trellis, we have (4.7) and (4.8) as shown below,

$$B = \begin{pmatrix} e^{jk_1\omega} - e^{jk_2\omega} & e^{jl_1\omega} - e^{jl_2\omega} \\ e^{-jl_2\omega} - e^{-jl_1\omega} & e^{-jk_1\omega} - e^{-jk_2\omega} \end{pmatrix}, \tag{4.7}$$

$$A = \begin{pmatrix} 4 - 2\cos\left[\omega(k_2 - k_1)\right] - 2\cos\left[\omega(l_2 - l_1)\right] & 0 \\ 0 & 4 - 2\cos\left[\omega(k_2 - k_1)\right] - 2\cos\left[\omega(l_2 - l_1)\right] \end{pmatrix}. \tag{4.8}$$

Using (4.8), one can show that

$$\det(A) = \left\{4 - 2\cos\left[\omega(k_2 - k_1)\right] - 2\cos\left[\omega(l_2 - l_1)\right]\right\}^2. \tag{4.9}$$

Now, if we have two codewords which differ in P pairs of constellation symbols, it can be shown that still $A_{12} = A_{21} = 0$. Also, if for the first codeword, we denote the set of constellation symbols as $\left(s_1^1, s_2^1\right)^p = \left(e^{jk_1^p\omega}, e^{jl_1^p\omega}\right)$, $p = 1,2,\ldots, P$ and for the second codeword, we denote the set of constellation symbols by $\left(s_1^2, s_2^2\right)^p = \left(e^{jk_2^p\omega}, e^{jl_2^p\omega}\right)$, $p = 1,2,\ldots, P$. Then we have,

$$\det(A) = \left\{\sum_{p=1}^{P} 4 - 2\cos\left[\omega\left(k_2^p - k_1^p\right)\right] - 2\cos\left[\omega\left(l_2^p - l_1^p\right)\right]\right\}^2. \tag{4.10}$$

Since (4.10) includes a sum of P terms and each of these terms is non-negative, the following inequality holds,

$$\begin{aligned}\det(A) &= \left\{\sum_{p=1}^{P} 4 - 2\cos\left[\omega\left(k_2^p - k_1^p\right)\right] - 2\cos\left[\omega\left(l_2^p - l_1^p\right)\right]\right\}^2 \\ &\geq \sum_{p=1}^{P}\left\{4 - 2\cos\left[\omega\left(k_2^p - k_1^p\right)\right] - 2\cos\left[\omega\left(l_2^p - l_1^p\right)\right]\right\}^2.\end{aligned} \tag{4.11}$$

Based on the coding distances calculated in (4.9) and (4.10), one can show that the coding gain of such a space-time trellis code is dominated by parallel transitions. It is observed from Fig 4.1 and [21] that as we go one level down the tree the minimum CGD increases (or remains the same).

Set Partitioning of Orthogonal Codes

This subsection provides a set partitioning for super-orthogonal codes and shows how to maximize the coding gain without sacrificing the rate. Similar to the case of orthogonal designs, it remains to do the set partitioning such that the CGD is maximized at each level of partitioning. Using (4.9) to calculate the CGD between a pair of codewords, it is apparent that increasing the Euclidean distance between the first signals of the codewords will increase the CGD. The CGD also increases as we increase the Euclidean distance between the second signals of the codewords. Therefore, the objective in set partitioning is to choose the codewords that contain signal elements with highest maximum Euclidean distance from each other as the leaves of the set-partitioning tree. For example, in the case of QPSK in Fig 4.2, $s = e^{\frac{j2\pi l}{2}}, l = 0,1,2,3$ are the QPSK signal constellation elements and $k = 0,1,2,3$ represents $s = 1, j, -1, -j$ respectively. The maximum CGD in this case is 64 when $|k_1 - k_2| = 2$ and $|l_1 - l_2| = 2$ in (9). This is the justification for the choice of leaf codewords in Fig 4.1. At the second level of the tree from the bottom, it is impossible to have both $|k_1 - k_2|$ and $|l_1 - l_2|$ equal to 2 in all cases. The next highest value for CGD is 16 when $|k_1 - k_2| = 2, |l_1 - l_2| = 0$ or $|k_1 - k_2| = 0$ and $|l_1 - l_2| = 2$. Hence, we group the sub trees in the second level such that the worst case is when $|k_1 - k_2| = 2, |l_1 - l_2| = 0$ or $|k_1 - k_2| = 0, |l_1 - l_2| = 2$. We keep grouping the sub trees to maximize the minimum CGD at each level of set partitioning.

4.2.4 Super-Orthogonal Space-Time Trellis Codes

Here we now build on the proposed set partitioning scheme to design full-diversity full-rate space-time trellis codes. In the new SOSTTC scheme, a constituent space-time block code is assigned to all transitions from a state. Every pair of codewords diverging from (or merging to) a state achieves full diversity because the pair is from the same orthogonal code and differs by rank 2. We illustrate this with a few examples on how to assign the block codes to different trellis structures. Figs 4.3 and 4.4 demonstrates examples of the SOSTTC 4-state and SOSTTC 2-state codes respectively. In these diagrams, $C(x_1,x_2,\theta)$ represents the particular member of our parameterized space-time block code which is used at the specific state. Also we have shown the corresponding sets from our set partitioning next to each state.

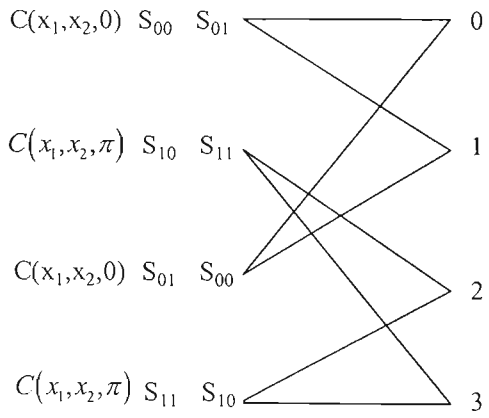

Fig. 4.3: A four-state code $r = 1b/s/Hz$ using BPSK or $r = 2b/s/Hz$ using QPSK

Fig 4.3 shows an example of the 4-state SOSTTC. In this example if we use BPSK and the corresponding set partitioning in Fig 4.1 the rate of the code is 1. When departing from state zero and two $C(x_1,x_2,0)$ is used and when departing from states 1 and 3 $C(x_1,x_2,\pi)$ is used. With this code structure, it is now possible to have eight possible orthogonal $2x2$ matrices which satisfy the $(4-D)$ signal point requirement, which ensures a full rate code. If we use QPSK constellation and the corresponding set partitioning in (5), the result is a 4-state SOSTTC at rate 2 b/s/Hz.

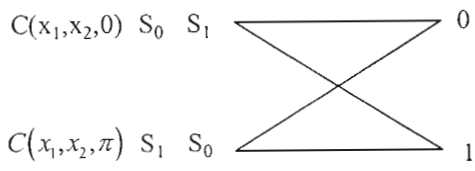

Fig. 4.4: A two-state code $r = 1b/s/Hz$ using BPSK or $r = 2b/s/Hz$ using QPSK

In Fig 4.4, the trellis diagram and transmission scheme for a 2-state trellis, where a rate 1 b/s/Hz is obtained if we use BPSK and 2 b/s/Hz, if we use QPSK constellation. It should be noted that there are no equivalent codes present in [17]. Thus it is seen that unlike the manual or hand crafted design strategy in [17], one can systematically design a code for an arbitrary trellis and rate using the set partitioning and code design strategy.

4.3 Code Design for Rapid Fading Channels

In [17], Tarokh et al. pointed out that in evaluating space-time code performance in quasi-static fading channels, the critical parameters are the minimum rank and the minimum determinant of the difference matrix between all possible transmitted and erroneously decoded symbols. In rapid fading channels, the important parameters are the symbol-wise Hamming distance and the sum-product distance. We consider Alamouti's orthogonal transmit scheme where s_0 and s_1 denote the transmitted symbols for the first symbol interval and $-s_1^*$ and s_0^* their corresponding conjugate values at the second symbol interval. Let

$$X = \left\{s_0, s_1, -s_1^*, s_0^*, \cdots\cdots s_{L-2}, s_{L-1}, -s_{L-1}^*, s_{L-2}^*\right\}, \tag{4.12}$$

and

$$Y = \left\{r_0, r_1, -r_1^*, r_0^*, \cdots\cdots r_{L-2}, r_{L-1}, -r_{L-1}^*, r_{L-2}^*\right\}, \tag{4.13}$$

be the transmitted and erroneously decoded symbol sequence with respect to the Alamouti's scheme. The pairwise error probability [89] is given by,

$$P(X \to Y) \le \prod_{i \in v} \left[1 + \frac{E_s}{4N_0} \left(|r_i - s_i|^2 + |r_{i+1} - s_{i+1}|^2 \right) \right]^{-2}, \tag{4.14}$$

where E_s is the symbol energy, $N_0/2$ is the variance per dimension of the zero-mean complex Gaussian noise sample and v is the set of all i for which $s_i \neq r_i$ or $s_{i+1} \neq r_{i+1}$. If the number of elements in v is denoted by n , (4.14) can be expressed as,

$$P(X \to Y) \le \frac{1}{\left[\left(\frac{E_s}{4N_0} \right)^n d_{prod}(n) \right]^2}, \tag{4.15}$$

where

$$d_{prod}(n) = \prod_{i \in v} \left(|r_i - s_i|^2 + |r_{i+1} - s_{i+1}|^2 \right). \tag{4.16}$$

Here $d_{prod}(n)$ is the product of distance sum of two consecutive symbols along the error event path, and is also known as sum-product distance ' n ' is the number of space-time symbols in which the two sequences differ, also called space-time symbolwise hamming distance. It is seen that the smallest n and the smallest $d_{prod}(n)$ dominates the error event probability [17]. Hence the code design criteria for fast fading channels can be summarized as follows,

(i). Maximize the minimum space-time symbolwise hamming distance n, between all pairs of distinct codewords. This corresponds to diversity maximization.

(ii.) Maximize the minimum product distance d_{prod} , along the path with minimum symbolwise hamming distance. This corresponds to coding gain maximization.

Next we look at the design methods introduced in [89] to improve the performance of SOSTTCs in rapid fading channels. We consider a specific system having two transmit and a single receive antenna, which uses BPSK signaling. This can be illustrated by the trellis diagram in Fig. 4.5 shown below,

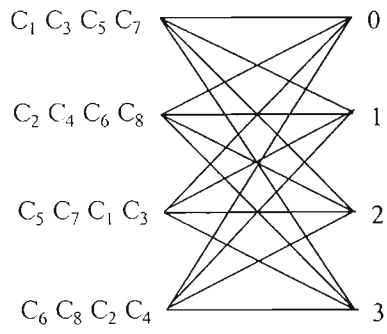

Fig. 4.5: 4-state BPSK SOSTTC for rapid fading channel

The idea adopted here to maximize the minimum space-time symbolwise hamming distance between all pairs of distinct transmission matrix sequences, is to avoid any parallel transitions between any state pair. So now, if two sequences diverge from a common state to different states, they have to go through at least two transitions before they merge to a common state. Therefore the shortest error event path will have two steps for a BPSK, 4-state code which still maintains full rate. To maximize the second design criteria, after exhaustive computer search [89], the transmission matrices are assigned to the trellis branches so that the minimum sum-product distances over all possible two-step transmission matrix sequence pairs is maximized. The expansion of $C_1 \cdots C_8$ can be found in appendix A.1.2.

4.4 Performance Analysis

The performance of SOSTTCs is investigated by two analytical means in the following section. Fist we look at the coding gain distance approach to determine the improved performance of these codes analytically in comparison with STTCs. Next we look at an MGF method which is a rigorous method of investigating the performance of these codes using evaluation through closed form expressions.

4.4.1 Coding Gain Distance Analysis

In order to determine the coding gain of the different super-orthogonal space-time trellis codes that are discussed in the previous section, we investigate how to determine the dominant path for coding gain distance (CGD) calculation in the trellis [21]. For our discussion we consider two specific examples, namely the BPSK and QPSK case for both 4-state and 2-state codes, and then illustrate by example the method adopted for CGD analysis.

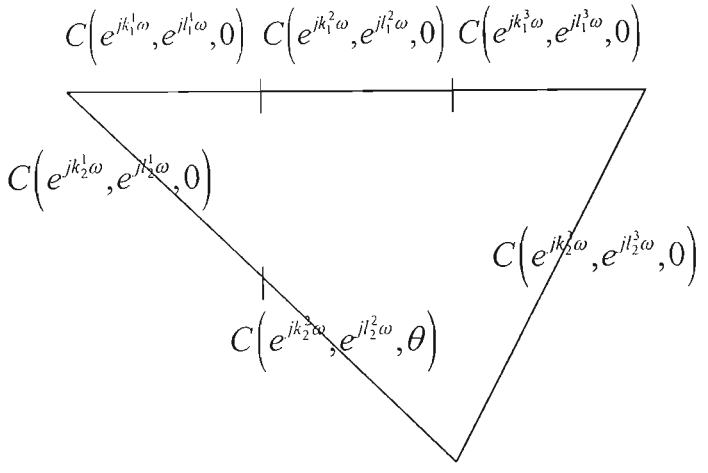

Fig. 4.6: Parallel paths differing in P = 3 transitions.

We first consider the 4-state SOSTTC shown in Fig. 4.3. It must be remembered that when there are parallel transitions between two states, we assign a different transition to each possible constellation matrix which is governed by the set partitioning rule. Any two codewords may differ in (P=1) trellis transition. As the trellis structure adopted for this code is similar to the TCM structure, it is impossible to have two codewords which differ in only two trellis transitions (P=2). This is due to the fact that if two codewords diverge from state zero, they have to go through at least three transitions to re-emerge. An example of such a path is illustrated by Fig. 4.6. Hence the smallest value P excluding parallel transitions is three. We first consider the case excluding parallel transitions. In a similar fashion to normal trellis codes exhibiting uniform error properties, we assume that the first codeword remains at state zero for the entire length of P, which in this case is three. For the second codeword, the first and third transitions (diverging and merging to

state zero) use $C(x_1,x_2,0)$ and the second transition uses $C(x_1,x_2,\theta)$ as can be seen in Fig. 4.3. Using trigonometry equations, it can be shown that,

$$\det(A)=(a+b_1+c)(a+b_2+c)-d, \tag{4.17}$$

where,

$$\begin{aligned} a&=4-2\cos\left[\omega\left(k_2^1-k_1^1\right)\right]-2\cos\left[\omega\left(l_2^1-l_1^1\right)\right]\\ c&=4-2\cos\left[\omega\left(k_2^3-k_1^3\right)\right]-2\cos\left[\omega\left(l_2^3-l_1^3\right)\right] \end{aligned} \tag{4.18}$$

For our specific example, since in our second transition of the second codeword case we use $(\theta=\pi)$ according to the trellis in Fig. 4.3, we have

$$\begin{aligned} b_1&=4+2\cos\left[\omega\left(k_2^2-k_1^2\right)\right]-2\cos\left[\omega\left(l_2^2-l_1^2\right)\right]\\ b_2&=4-2\cos\left[\omega\left(k_2^2-k_1^2\right)\right]+2\cos\left[\omega\left(l_2^2-l_1^2\right)\right]\\ d&=8\left(1+\cos\left[\omega\left(k_2^2-k_1^2+l_1^2-l_2^2\right)\right]\right). \end{aligned} \tag{4.19}$$

Since $a,b_1,b_2,c,d\geq 0$, we have

$$min\,det(A)\geq\left[min(a)+min(b_1)+min(c)\right]\cdot\left[min(a)+min(b_2)+min(c)\right]-max(d). \tag{4.20}$$

Now we evaluate the result showing that the minimum value of coding gain distance for length (P=3) is greater than the minimum value when (P=1) in order to prove that the minimum coding distance is dominated by the presence of parallel transitions. We first assume the case of a rate $r=1\ bit/s/Hz$ code using BPSK for the same trellis in Fig. 4.3. According to the general rule, we assume two codewords diverging from sate zero and re-emerging after P transitions to state zero. For parallel transitions (P=1) the CGD from (4.9) is as follows,

$$\det(A)=\left\{4-2\cos\left[\omega(k_2-k_1)\right]-2\cos\left[\omega(l_2-l_1)\right]\right\}^2. \tag{4.21}$$

Here $\omega=\pi$, $k_1=0$, $l_1=0$ *and* $k_2=1$, $l_2=1$, so

$$\begin{aligned} \det(A)&=\left\{4-2\cos\left[\pi(1-0)\right]-2\cos\left[\pi(1-0)\right]\right\}^2\\ \det(A)&=64. \end{aligned} \tag{4.22}$$

Hence, for $(P=1)$ case of the BPSK code, $min\,det(A)=64$. For the same code, considering the case where parallel transitions are excluded $(i.e., P=3)$, we have

From (4.18) $k_1=0,\ l_1=0$ *and* $k_2=0,\ l_2=1$

$$\begin{aligned} &\min a = 4-2\cos\left[\pi(0)\right]-2\cos\left[\pi(1-0)\right] \\ &\min a = 4-2(1)-2(1) \\ &\min a = 4. \end{aligned} \tag{4.23}$$

Similarly c is given by,

$$\begin{aligned} &\min c = 4-2\cos\left[\pi(0)\right]-2\cos\left[\pi(1-0)\right] \\ &\min c = 4-2(1)-2(1) \\ &\min c = 4. \end{aligned} \tag{4.24}$$

The min value of b_1, b_2 *and* d is obtained when $k_1=0,\ l_1=0$ *and* $k_2=1,\ l_2=1$, using (4.19)

$$\begin{aligned} &\min b_1 = 4+2\cos\left[\pi(1-0)\right]-2\cos\left[\pi(1-0)\right] \\ &\min b_1 = 4-2(-1)-2(-1) \\ &\min b_1 = 4 \end{aligned}$$

$$\begin{aligned} &\min b_2 = 4-2\cos\left[\pi(1-0)\right]+2\cos\left[\pi(1-0)\right] \\ &\min b_2 = 4-2(1)-2(1) \\ &\min b_2 = 4 \end{aligned} \tag{4.25}$$

$$\begin{aligned} &\max d = 8\left(1+\cos\left[\pi(1-0+0-1)\right]\right) \\ &\max d = 8\left(1+\cos[0]\right) \\ &\max d = 8(2) \\ &\max d = 16. \end{aligned}$$

Therefore the inequality (4.20) results in

$$\min \det(A) \geq 128. \tag{4.26}$$

Also for $k_2^1 = k_1^1 = l_1^1 = k_2^2 = k_1^2 = l_1^2 = l_2^2 = k_2^3 = k_1^3 = l_1^3 = 0$ and $l_2^1 = l_2^3 = 1$ in equation (4.17), we have $\det(A) = 128$ which means

$$\min(A) \leq 128. \tag{4.27}$$

Combining inequalities (4.26) and (4.27) provides

$$\min(A)=128, \tag{4.28}$$

which, is greater than 64.

Now in the case of QPSK constellation for $(P=1)$, the CGD is from (4.9) and is given by,

$$\det(A) = \left\{4-2\cos\left[\omega(k_2-k_1)\right]-2\cos\left[\omega(l_2-l_1)\right]\right\}^2. \tag{4.29}$$

Here $\omega=\pi/2$, $k_1=0$, $l_1=0$ *and* $k_2=3$, $l_2=1$ so,

$$\det(A)=\left\{4-2\cos\left[\frac{\pi}{2}(3-0)\right]-2\cos\left[\frac{\pi}{2}(1-0)\right]\right\}^2 \tag{4.30}$$

$$\det(A) = 16.$$

Using the equations (4.18) and (4.19), one can obtain the min values using identical steps of calculation as shown above, which is not shown here to avoid repetition. Thus, we can obtain $min\, a = \min c = 2$, $min\, b_1 = \min b_2 = 4$, and $max\, d = 16$. Therefore the inequality (4.20) results in

$$min\ det(A) \geq 48. \tag{4.31}$$

Also for

$$k_2^1 = k_1^1 = l_1^1 = k_2^2 = k_1^2 = l_1^2 = l_2^2 = k_2^3 = k_1^3 = l_1^3 = 0$$

and $l_2^1 = l_2^3 = 1$ in (4.17), we have $\det(A) = 48$ which means

$$\min(A) \leq 48. \tag{4.32}$$

Combining inequalities (4.31) and (4.32) provides

$$\min(A)=48,$$

which is greater than 16. It can be seen that the minimum CGD for this $2\,bit/s/Hz$ code is equal to 16, which is greater than 4, the CGD corresponding to space-time trellis code from [17].

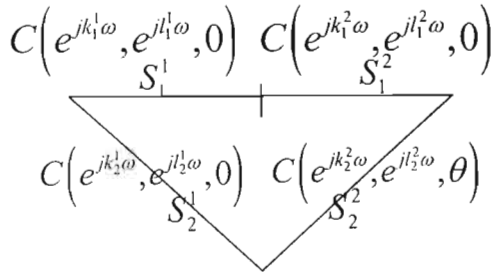

Fig. 4.7: Parallel paths differing in P = 2 transitions.

Now that we have considered specific codes for clarity of presentation, we can show similar results for any trellis for which it is possible to diverge from a state and merge to the same state in $(P=2)$ transitions. Fig. 4.7 shows an example of a $(P=2)$ transition. We build on the similar basic principles of our previous discussion and consider two separate codewords. The first case considered is $(P=1)$ for parallel transitions, and one can calculate the CGD from (9). For the next case which excludes parallel transitions, there are two codewords diverging from state zero and re-emerging after $(P=2)$ transitions. The first codeword stays at state zero. For the second codeword, the first transition diverging from state zero uses $C(x_1, x_2, 0)$ and the second transition re-emerging to state zero uses $C(x_1, x_2, \theta)$ as shown in Fig. 4.7. It can be shown that,

$$det\,(A) = (a+b_1)(a+b_2) - d = a^2 + a(b_1+b_2) + b_1 b_2 - d, \tag{4.33}$$

where,

$$\begin{aligned} a &= 4 - 2\cos\left[\omega\left(k_2^1 - k_1^1\right)\right] - 2\cos\left[\omega\left(l_2^1 - l_1^1\right)\right], \\ b_1 &= 4 - 2\cos\left[\omega\left(k_2^2 - k_1^2\right) + \theta\right] - 2\cos\left[\omega\left(l_2^2 - l_1^2\right)\right], \\ b_2 &= 4 - 2\cos\left[\omega\left(k_2^2 - k_1^2\right)\right] - 2\cos\left[\omega\left(l_2^2 - l_1^2\right) - \theta\right], \text{ and} \\ d &= (2 - 2\cos\theta)\left(2 - 2\cos\left[\omega\left(k_2^2 - k_1^2 + l_1^2 - l_2^2\right) + \theta\right]\right). \end{aligned} \tag{4.34}$$

We calculate the coding gain for BPSK code in Fig. 4.4. Again, we assume two codewords diverging from state zero and re-emerging after P transitions to state zero.

For parallel transitions $(P=1)$, as calculated from (4.9) previously the value of CGD is 64. For $(P=2)$, $min\ a = min\ b_1 = min\ b_2 = 4$ and $d=16$, so

$$\begin{aligned} min\ det(A) &= 16 + min\left[4(b_1+b_2)+b_1b_2-d\right] \\ min\ det(A) &= 16 + min\left[4(4+4)+16-16\right] \\ min\ det(A) &= 48 < 64. \end{aligned} \tag{4.35}$$

Therefore, $CGD = 48$ and the coding gain is dominated by paths with $(P=2)$ transitions and is equal to 6.92. For the QPSK case shown in Fig. 4.3, the CGD for parallel transitions $(P=1)$ is 16. For $(P=2)$ here, $min\ a = 2$, $min\ b_1 = min\ b_2 = 4$ and $d=16$, we have

$$\begin{aligned} min\ det(A) &= 4 + min\left[2(b_1+b_2)+b_1b_2-d\right] \\ min\ det(A) &= 4 + min\left[2(4+4)+16-16\right] \\ min\ det(A) &= 20 > 16. \end{aligned} \tag{4.36}$$

Hence the coding gain for the QPSK case in Fig. 4.3 is 4. It should be emphasized that the importance of picking the right set of rotations and subsets is vital in providing the maximum coding gain.

4.4.2 Performance using Moment Generating Function Approach

Here we use the key analytical method used in [83], in order to determine the performance of SOSTTCs. We assume a system with two transmit antennas and N_R number of receive antennas. Let $x_n = \left[x_1^{(n)}, x_2^{(n)}\right]^T$ be the vector representing a pair of complex symbols to be transmitted in the n^{th} transmission from the two transmit antennas, and the superscript T denotes the transpose operation. During the n^{th} transmission interval the channel can be described by a $N_R x 2$ matrix $C_n = \left[c_{ji}^{(n)}\right]$, where $c_{ji}^{(n)}$ is the channel fade coefficient between the i^{th} transmit antenna and the j^{th} receive antenna, and $c_{ji}^{(n)}$ is independent of one another. The vectors representing the two pairs of symbols successively transmitted over the channel in the n^{th} transmission interval is given by,

$$X_{n1} = \left[x_1^{(n)} e^{j\theta(n)}, x_2^{(n)} \right]^T, \tag{4.37}$$

and

$$X_{n2} = \left[\left(-x_2^{(n)}\right)^* e^{j\theta(n)}, \left(x_1^{(n)}\right)^* \right]^T. \tag{4.38}$$

The received signal for the corresponding transmission of X_{n1} and X_{n2} is given by,

$$\begin{aligned} y_l^{(n)} &= c_{l1}^{(n)} x_1^{(n)} e^{j\theta(n)} + c_{l2}^{(n)} x_2^{(n)} + n_l^{(n)} \\ y_{l+N_R}^{(n)} &= c_{l1}^{(n)} \left(-x_2^{(n)}\right)^* e^{j\theta(n)} + c_{l2}^{(n)} \left(x_1^{(n)}\right)^* + n_{l+N_R}^{(n)}, \end{aligned} \tag{4.39}$$

where $l = 1, 2, \ldots N_R$, and $n_l^{(n)}$ are i.i.d. complex zero mean Gaussian noise samples, each with variance σ^2 per dimension and are assumed to be independent of the channel gains. Assuming perfect CSI, the l^{th} receiver uses the pair of samples $y_l^{(n)}, y_{l+N_R}^{(n)}$ to create

$$\begin{aligned} \tilde{x}_l^{(n)} &= \left(c_{l1}^{(n)}\right)^* e^{-j\theta(n)} y_l^{(n)} + c_{l2}^{(n)} \left(y_{l+N_R}^{(n)}\right)^* \\ \tilde{x}_{l+N_R}^{(n)} &= \left(c_{l2}^{(n)}\right)^* y_l^{(n)} - c_{l1}^{(n)} e^{j\theta(n)} \left(y_{l+N_R}^{(n)}\right)^* \\ & \qquad\qquad l = 1, 2, \ldots, N_R \end{aligned} \tag{4.40}$$

which, is necessary for forming the maximum likelihood (ML) metric corresponding to the n^{th} transmission interval.

Fast Rician Fading Channels

This section looks at exactly evaluating the PWEP using ML metric. For each and every observation of N blocks ($2N$ Symbols), each described by (4.39), the ML metric corresponding to the correct path is given by,

$$m(Y, X) = \sum_{n=1}^{N} \sum_{l=1}^{L_R} \left[\left| y_l^{(n)} - \left(c_{l1}^{(n)} x_1^{(n)} e^{j\theta(n)} + c_{l2}^{(n)} x_2^{(n)} \right) \right|^2 + \left| y_{l+L_R}^{(n)} - \left(c_{l1}^{(n)} \left(-x_2^{(n)}\right)^* e^{j\theta(n)} + c_{l2}^{(n)} \left(x_1^{(n)}\right)^* \right) \right|^2 \right]. \tag{4.41}$$

Based on the realization of the channel over the entire N block observation, the PWEP is given by,

$$\begin{aligned} P\left(X \to \widehat{X} \mid C\right) &= \Pr\left\{m\left(Y,X\right) > m\left(Y,\widehat{X}\right) \mid C\right\} \\ &= \Pr\left\{m\left(Y,X\right) - m\left(Y,\widehat{X}\right) > 0 \mid C\right\}. \end{aligned} \tag{4.42}$$

Substituting the value of (4.41) in (4.42) simplifies to

$$\begin{aligned} P\left(X \to \widehat{X} \mid C\right) = \Pr\Bigg\{ Z \geq \sum_{n=1}^{N}\sum_{l=1}^{L_R}\Bigg[\Bigg| c_{l1}^{(n)}\left(\hat{x}_1^{(n)} e^{j\theta(n)} - x_1^{(n)} e^{j\theta(n)}\right) + c_{l2}^{(n)}\left(\hat{x}_2^{(n)} - x_2^{(n)}\right)\Bigg|^2 \\ + \Bigg| -c_{l1}^{(n)}\left(\hat{x}_2^{(n)} e^{-j\hat{\theta}(n)} - x_2^{(n)} e^{-j\theta(n)}\right)^* + c_{l2}^{(n)}\left(\hat{x}_1^{(n)} - x_1^{(n)}\right)^*\Bigg|^2\Bigg]\Bigg| C\Bigg\} \\ \triangleq \Pr\left\{Z \geq \mu \mid C\right\}, \end{aligned} \tag{4.43}$$

where Z is a conditionally zero mean Gaussian random variable with variance $\sigma_2^2 = 4\sigma^2\mu$. Hence the conditional PWEP can be expressed in terms of a Gaussian Q-function by,

$$P\left(X \to \widehat{X} \mid C\right) = Q\left(\sqrt{\frac{\mu}{4\sigma^2}}\right), \tag{4.44}$$

where μ can be written in matrix form as,

$$\mu = \sum_{n=1}^{N}\sum_{l=1}^{L_R}\left\| c_l^{(n)}\left(X_n - \widehat{X}_n\right)\right\|^2 = \sum_{n=1}^{N}\sum_{l=1}^{L_R}\left\| c_l^{(n)}\Delta_n\right\|^2, \tag{4.45}$$

with X_n and $\widehat{X}_n$ are the corresponding correct and incorrect signal matrices in the n^{th} block. The error signal matrix is shown in (4.46) below,

$$\Delta_n \triangleq X_n - \widehat{X}_n = \begin{bmatrix} x_1^{(n)} e^{j\theta(n)} - \hat{x}_1^{(n)} e^{j\hat{\theta}(n)} & \left(-x_2^{(n)}\right)^* e^{j\theta(n)} - \left(-\widehat{x_2^{(n)}}\right)^* e^{j\hat{\theta}(n)} \\ x_2^{(n)} - \hat{x}_2^{(n)} & \left(x_1^{(n)}\right)^* - \left(\hat{x}_1^{(n)}\right)^* \end{bmatrix}. \tag{4.46}$$

Assuming a rapid Rician fading, i.e. a fully interleaved environment the squared channel gain magnitudes $\left|c_{l1}^{(n)}\right|^2$ and $\left|c_{l2}^{(n)}\right|^2$ are i.i.d noncentral chi-square random variables with parameter K and mean square value Ω. Using the MGF for the SNR in a Rician channel as given in [90, (2.17)] we obtain for orthogonal STTCs,

$$P\left(X \to \hat{X}\right) = \frac{1}{\pi}\int_0^{\pi/2}\left\{\prod_{n=1}^{N}\left(\frac{(1+K)\sin^2\theta}{(1+K)\sin^2\theta + \frac{\bar{\gamma}_s}{4}d_n^2}\right)\times\exp\left[-\frac{K\frac{\bar{\gamma}_s}{4}d_n^2}{(1+K)\sin^2\theta + \frac{\bar{\gamma}_s}{4}d_n^2}\right]\right\}^{2L_R} d\theta, \quad (4.47)$$

where $\bar{\gamma}_s = \Omega E_S / N_0$, denotes the average symbol SNR. For the Rayleigh fading case (K=0) reduces to

$$\begin{aligned} P\left(X \to \hat{X}\right) &= \frac{1}{\pi}\int_0^{\pi/2}\prod_{n=1}^{N}\left(\frac{\sin^2\theta}{\sin^2\theta + \frac{\bar{\gamma}_s}{4}d_n^2}\right)^{2L_R} d\theta \\ &= \frac{1}{\pi}\int_0^{\pi/2}\left[\prod_{n=1}^{N}\left(\frac{\sin^2\theta}{\sin^2\theta + \frac{\bar{\gamma}_s}{4}d_n^2}\right)\right]^{2L_R} d\theta. \end{aligned} \quad (4.48)$$

The presence of cross product terms in μ of (4.45) making the rows of Δ_n orthogonal, and so for SOSTTCs, directly evaluating the average of the conditional PWEP in (4.44) over the channel is a bit more difficult and so μ becomes,

$$\begin{aligned} \mu \triangleq \sum_{n=1}^{N}\Bigg(&\sum_{l=1}^{L_R}\left|c_{l1}^{(n)}\right|^2\left[\left|x_1^{(n)}e^{j\theta(n)} - \hat{x}_1^{(n)}e^{j\hat{\theta}(n)}\right|^2 + \left|x_2^{(n)}e^{-j\theta(n)} - \hat{x}_2^{(n)}e^{-j\hat{\theta}(n)}\right|^2\right] \\ &+\sum_{l=1}^{L_R}\left|c_{l2}^{(n)}\right|^2\left[\left|x_1^{(n)} - \hat{x}_1^{(n)}\right|^2 + \left|x_2^{(n)} - \hat{x}_2^{(n)}\right|^2\right]\Bigg). \end{aligned} \quad (4.49)$$

In order to evaluate the unconditional PWEP, we first express μ in a compact matrix form. The $2N \times 2N$ matrix Δ is given by,

$$\Delta = \begin{bmatrix} \Delta_1 & 0 & \cdot & \cdot & 0 \\ 0 & \Delta_2 & 0 & \cdot & 0 \\ 0 & 0 & \cdot & \cdot & \cdot \\ \cdot & \cdot & \cdot & \Delta_{N-1} & 0 \\ 0 & 0 & \cdot & 0 & \Delta_N \end{bmatrix}. \quad (4.50)$$

For an entire block the channel gain vector corresponding to the l^{th} receive antenna is,

$$c_l = \left[c_{l1}^{(1)} \;\; c_{l2}^{(1)} \;\; c_{l1}^{(2)} \;\; c_{l2}^{(2)} \;\cdots\; c_{l1}^{(N)} \;\; c_{l2}^{(N)}\right]. \quad (4.51)$$

Then it can be shown that,

$$\mu = \sum_{l=1}^{L_R} c_l \Delta\left(c_l^* \Delta^*\right)^T = \sum_{l=1}^{L_R} c_l \Delta\left(\Delta^*\right)^T \left(c_l^*\right)^T, \tag{4.52}$$

whereupon the unconditional PWEP becomes

$$P\left(X \to \widehat{X} \mid C\right) = Q\left(\sqrt{\frac{E_S}{2N_0} \sum_{l=1}^{L_R} c_l \Delta\left(\Delta^*\right)^T \left(c_l^*\right)^T}\right). \tag{4.53}$$

If we now average over the channel because of the independence of the channel gain vectors c_l associated with N_R receivers, the unconditional PWEP can be expressed in terms of a single integral whose integrand is a product of MGFs associated with each of the receivers' i.e.

$$P\left(X \to \widehat{X}\right) = \frac{1}{\pi} \int_0^{\pi/2} \prod_{l=1}^{L_R} M_{\xi_l}\left(-\frac{1}{\sin^2\theta}\right) d\theta, \tag{4.54}$$

Where

$$\xi_l \triangleq \frac{E_S}{4N_0} c_l \Delta\left(\Delta^*\right)^T \left(c_l^*\right)^T, \tag{4.55}$$

is a quadratic form of complex variables with MGF

$$M_{\xi_l}(s) \triangleq E\left\{\exp\left(s\xi_l\right)\right\}. \tag{4.56}$$

In order to evaluate the above MGF in (4.56), the result in [91] is used and for Rayleigh channel $\bar{c}_l = 0$ and $k = 0$, we arrive at

$$M_{\xi_l}(s) = \left(\det\left[I - s\frac{\overline{\gamma_s}}{4}\Delta\left(\Delta^*\right)^T\right]\right)^{-1}. \tag{4.57}$$

If we assume that the channel gains have identical statistics, then $\prod_{l=1}^{L_R} M_{\xi_l}(s) = \left(M_{\xi_l}(s)\right)^{L_R}$ and hence for Rayleigh channel,

$$P\left(X \to \widehat{X}\right) = \frac{1}{\pi}\int_0^{\pi/2}\left(\det\left[I + \frac{\overline{\gamma_s}}{4\sin^2\theta}\Delta\left(\Delta^*\right)^T\right]\right)^{-L_R} d\theta. \tag{4.58}$$

For the evaluation of the determinant in (4.58), for the block diagram form of $\Delta\left(\Delta^*\right)^T$, we have

$$\det\left[I + \frac{\overline{\gamma_S}}{4(1+K)\sin^2\theta}\Delta\left(\Delta^*\right)^T\right] = \prod_{n=1}^{N}\det\left[I + A_n\right] \tag{4.59}$$

where

$$A_n = \frac{\overline{\gamma_S}}{4(1+K)\sin^2\theta}\Delta_n\left(\Delta_n^*\right)^T = \begin{bmatrix} a_{11}^{(n)} & a_{12}^{(n)} \\ a_{21}^{(n)} & a_{22}^{(n)} \end{bmatrix}, \tag{4.60}$$

with

$$\begin{aligned}
a_{11}^{(n)} &= \frac{\overline{\gamma_S}}{4(1+K)\sin^2\theta}\left[\left|x_1^{(n)}e^{j\theta(n)} - \hat{x}_1^{(n)}e^{j\hat{\theta}(n)}\right|^2 + \left|x_2^{(n)}e^{-j\theta(n)} - \hat{x}_2^{(n)}e^{-j\hat{\theta}(n)}\right|^2\right] \\
a_{12}^{(n)} &= \frac{\overline{\gamma_S}}{4(1+K)\sin^2\theta}\left[\left(x_1^{(n)}e^{j\theta(n)} - \hat{x}_1^{(n)}e^{j\hat{\theta}(n)}\right)\times\left(x_2^{(n)} - \hat{x}_2^{(n)}\right)^* - \left(x_2^{(n)}e^{-j\theta(n)} - \hat{x}_2^{(n)}e^{-j\hat{\theta}(n)}\right)^*\right. \\
&\quad \left.\times\left(x_1^{(n)} - \hat{x}_1^{(n)}\right)\right] \\
&= \left(a_{21}^{(n)}\right)^* \\
a_{22}^{(n)} &= \frac{\overline{\gamma_S}}{4(1+K)\sin^2\theta}\left[\left|x_1^{(n)} - \hat{x}_1^{(n)}\right|^2 + \left|x_2^{(n)} - \hat{x}_2^{(n)}\right|^2\right],
\end{aligned} \tag{4.61}$$

and thus

$$\det\left[I + \frac{\overline{\gamma_S}}{4(1+K)\sin^2\theta}\Delta\left(\Delta^*\right)^T\right] = \prod_{n=1}^{N}\left[\left(1+a_{11}^{(n)}\right)\left(1+a_{22}^{(n)}\right) - \left|a_{12}^{(n)}\right|^2\right]. \tag{4.62}$$

Finally the PWEP for the Rayleigh channel can be represented by,

$$\begin{aligned}
P\left(X \to \widehat{X}\right) &= \frac{1}{\pi}\int_0^{\pi/2}\left(\prod_{n=1}^{N}\left[\left(1+a_{11}^{(n)}\right)\left(1+a_{22}^{(n)}\right) - \left|a_{12}^{(n)}\right|^2\right]\right)^{-L_R} d\theta \\
&= \frac{1}{\pi}\int_0^{\pi/2}\left(\prod_{n=1}^{N}\left(1+a_{11}^{(n)} + a_{22}^{(n)} + \det A_n\right)\right)^{-L_R} d\theta.
\end{aligned} \tag{4.63}$$

We provide examples for the equations for determining the PWEP for a 2-state SOSTTC by evaluation of the PWEP using the closed form as in [83] and [90]. Consider a rate $r=1$, BPSK 2-state code, whose trellis diagram is shown in Fig 4.4. Here we have two sets, each containing two pairs of BPSK symbols assigned to each state. This means that as previously explained in section 4.2.4, there is a pair of parallel paths between each pair of states. Thus for an error event length N=1 in the case of fast fading Rayleigh channel the PWEP associated with the parallel paths is from (4.48), given by [83],

$$P\left(X \to \widehat{X}\right) = \frac{1}{\pi}\int_0^{\pi/2}\left(\frac{\sin^2\theta}{\sin^2\theta + 2\overline{\gamma_S}}\right)^{2L_R} d\theta. \tag{4.64}$$

This can be represented in the closed form as,

$$P\left(X \to \widehat{X}\right) = \frac{1}{2}\left\{1 - \sqrt{\frac{2\overline{\gamma_S}}{1+2\overline{\gamma_S}}} \times \sum_{k=0}^{2L_R-1}\binom{2k}{k}\left[\frac{1}{4\left(1+2\overline{\gamma_S}\right)}\right]^k\right\}. \tag{4.65}$$

Next we consider the case for an error event of length N=2 and have the all zero path as the correct one, then we would have, $x_1^{(1)} = x_2^{(2)} = 1$, $x_1^{(2)} = x_2^{(2)} = 1$, $\hat{x}_1^{(1)} = -1, \hat{x}_2^{(1)} = -1$, $\hat{x}_2^{(2)} = 1$ and $\theta^{(1)} = \hat{\theta}^{(1)} = 0$, $\theta^{(2)} = 0$, $\hat{\theta}^{(2)} = \pi$. Evaluating the matrix elements from (4.61) gives the values,

$$a_{11}^{(1)} = a_{11}^{(2)} = \frac{\overline{\gamma_S}}{\sin^2\theta},\ a_{12}^{(1)} = 0,\ a_{12}^{(2)} = -\frac{\overline{\gamma_S}}{\sin^2\theta},\ a_{22}^{(1)} = a_{22}^{(2)} = \frac{\overline{\gamma_S}}{\sin^2\theta}. \tag{4.66}$$

Thus from (4.63) we have

$$\begin{aligned} P\left(X \to \widehat{X}\right) &= \frac{1}{\pi}\int_0^{\pi/2}\left\{\left(1+\frac{\overline{\gamma_S}}{\sin^2\theta}\right)^2\left[\left(1+\frac{\overline{\gamma_S}}{\sin^2\theta}\right)^2 - \left(\frac{\overline{\gamma_S}}{\sin^2\theta}\right)^2\right]\right\}^{-L_R} d\theta \\ &= \frac{1}{\pi}\int_0^{\pi/2}\left(\frac{\sin^2\theta}{\sin^2\theta+\overline{\gamma_S}}\right)^{2L_R}\left(\frac{\sin^2\theta}{\sin^2\theta+2\overline{\gamma_S}}\right)^{L_R} d\theta. \end{aligned} \tag{4.67}$$

This can be simplified in the closed form expression considering the case where $(L_R = 1)$, simplifies to,

$$P(X \to \hat{X}) = \frac{1}{2}\left[1 - 4\sqrt{\frac{2\overline{\gamma_S}}{1+2\overline{\gamma_S}}} + \sqrt{\frac{\overline{\gamma_S}}{1+\overline{\gamma_S}}}\left(3 + \frac{1}{2(1+\overline{\gamma_S})}\right)\right]. \tag{4.68}$$

For the quasi-static Rayleigh fading case for error event path of length N=2, the PWEP is from (4.58) and is given by,

$$\begin{aligned} P(X \to \hat{X}) &= \frac{1}{\pi}\int_0^{\pi/2}\left(\frac{\sin^4\theta}{\sin^4\theta + 4\overline{\gamma_S}\sin^2\theta + 3\overline{\gamma_S}^2}\right)^{L_R} d\theta \\ &= \frac{1}{\pi}\int_0^{\pi/2}\left(\frac{\sin^2\theta}{\sin^2\theta + 3\overline{\gamma_S}}\right)^{L_R}\left(\frac{\sin^2\theta}{\sin^2\theta + \overline{\gamma_S}}\right)^{L_R} d\theta. \end{aligned} \tag{4.69}$$

This can be simplified as a closed form expression for a single receive antenna which simplifies to [83],

$$P(X \to \hat{X}) = \frac{1}{2}\left[1 - \frac{3}{2}\sqrt{\frac{3\overline{\gamma_S}}{1+3\overline{\gamma_S}}} + \frac{1}{2}\sqrt{\frac{\overline{\gamma_S}}{1+\overline{\gamma_S}}}\right]. \tag{4.70}$$

Evaluation of Approximate Bit Error Probability

In this section we evaluate in closed form an approximation to the average BEP $P_b(E)$ using the PWEPs derived in the previous section. We do an approximation method whereby we account only for error events of lengths N less than or equal to K. For a 2-state code assuming the transmission of the all zero sequence, there is a single error event path of length 1 and 4 error event paths of length 2. The single error event path of length 1 has a PWEP of Type I and contributes one bit error. There are 4 error event paths of length 2, which have PWEPs of Type II and the four paths contribute a total of 12 bit errors. Hence the approximate average BEP by considering only error event paths corresponding to K=2, can be mathematically represented as,

$$P_b(E) \cong \frac{1}{2}\left[P\left(X \to \widehat{X}\right)_I + 12P\left(X \to \widehat{X}\right)_{II} \right], \tag{4.71}$$

where, for a rapid fading channel $P\left(X \to \widehat{X}\right)_I$ and $P\left(X \to \widehat{X}\right)_{II}$ are given by the closed form expressions in (4.65) and (4.68) respectively. For the quasi-static fading case similar approximations can be used to evaluate the average BEP (K=2), which is still given by (4.71), where the error event path having PWEP of Type I is given by (4.71) where the error event path having PWEP is given by (4.65), but Type II is now given by (4.70) which is the closed form.

4.5 Simulation and Analytical Results

In this section we provide simulation results for the super-orthogonal space-time trellis codes using two transmit $(N_T = 2)$ and a single receive antenna. Results obtained are compared with those of existing space-time trellis codes in the literature when a comparable code exists. In all simulations, similar to that of chapter 3, a frame consists of 130 transmissions out of each transmit antenna. Simulation results are obtained for both quasi-static and rapid fading channels.

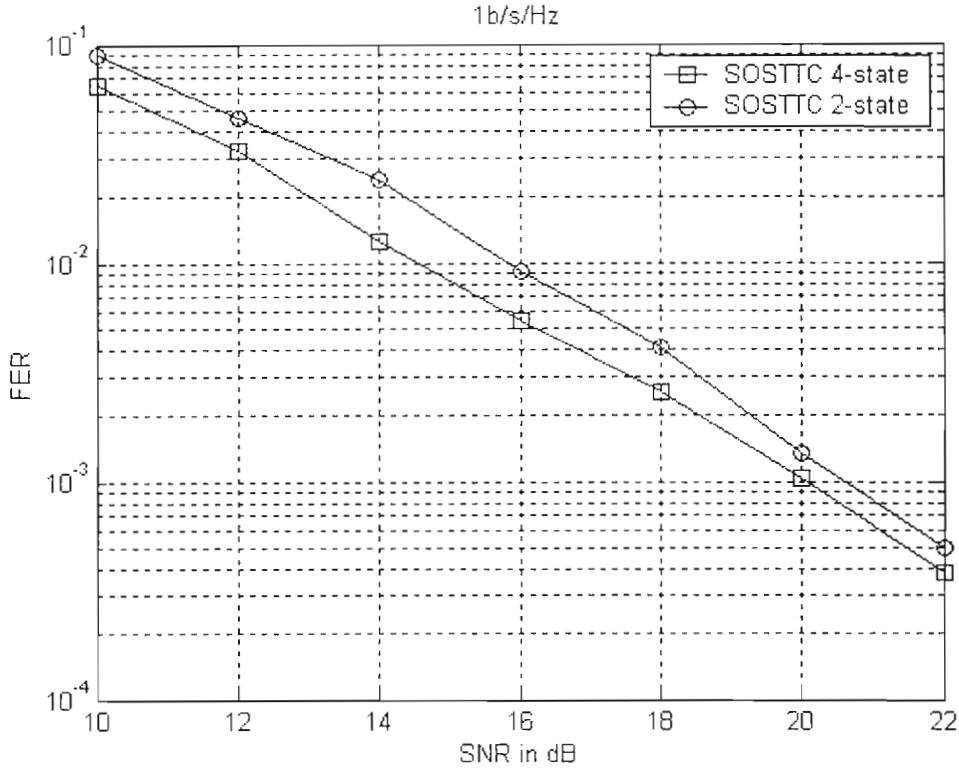

Fig. 4.8: FER for SOSTTC ($N_T = 2$, $N_R = 1$, $r = 1b/s/Hz$) (BPSK) in quasi-static fading.

Fig. 4.8 shows the frame error probability results versus SNR for the codes in Figs. 4.3 and 4.4 using BPSK and corresponding set partitioning in Fig. 4.1. Both these codes are full rate and the rate of transmission is $1b/s/Hz$. It is seen that the four state code has an improvement in performance due to more number of states.

Fig. 4.9 shows the simulation results for transmitting rate $r = 2b/s/Hz$ using QPSK constellation. The codes shown in Fig. 4.3 and Fig. 4.4 are denoted by SOSTTC 4-state and SOSTTC 2-states respectively. The corresponding results for Tarokh's code with the same rate and 4-state from [17] are also provided for comparison in performance. As can be seen from the figure, the 4-state SOSTTC outperforms the corresponding STTC by more than 2dB. The design of SOSTTC preserves the decoding simplicity of orthogonal designs. We obtain the results using both Viterbi and SISO decoding algorithms.

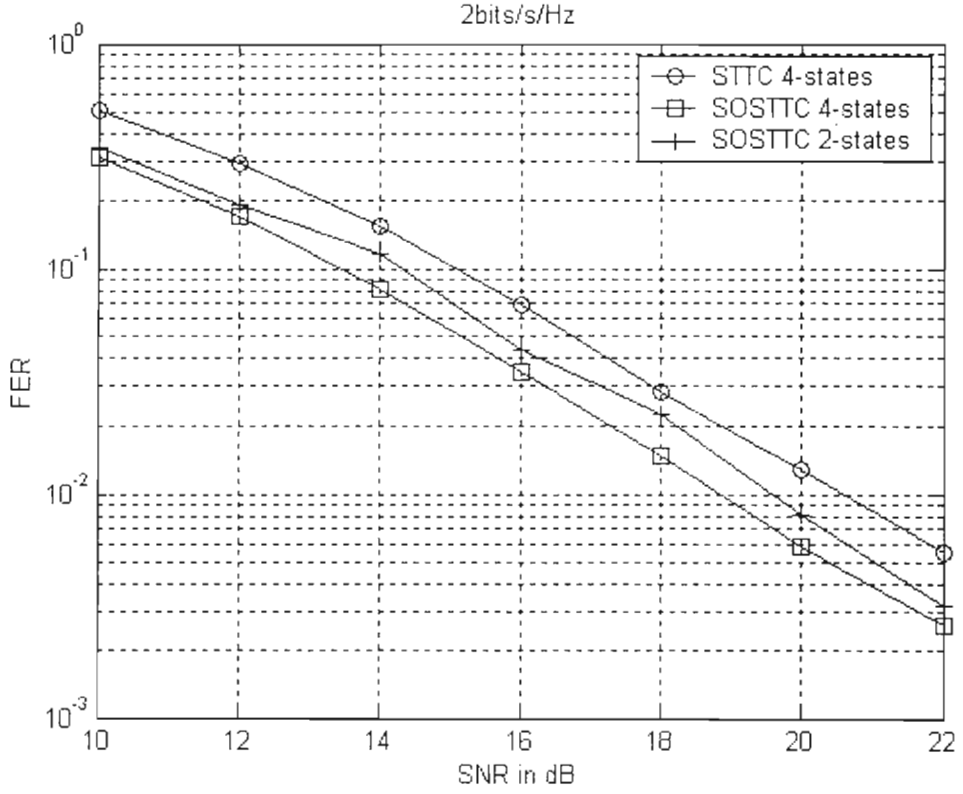

Fig. 4.9: FER for SOSTTC ($N_T = 2$, $N_R = 1$, $r = 2b/s/Hz$) (QPSK) in quasi-static fading.

Fig 4.10 shows the performance of SOSTTCs of rate $r = 1b/s/Hz$ in rapid Rayleigh fading channels. It can be seen that there is performance degradation in these channels in comparison with the quasi-static case. Fig. 4.11 shows the performance of SOSTTCs of rate $r = 2b/s/Hz$ in rapid fading channels [116]. It can be seen that as mentioned before there is performance degradation over their quasi-static case in comparison with Fig 4.9, but these codes maintain an improvement in performance over space-time trellis codes in the rapid faded channel case.

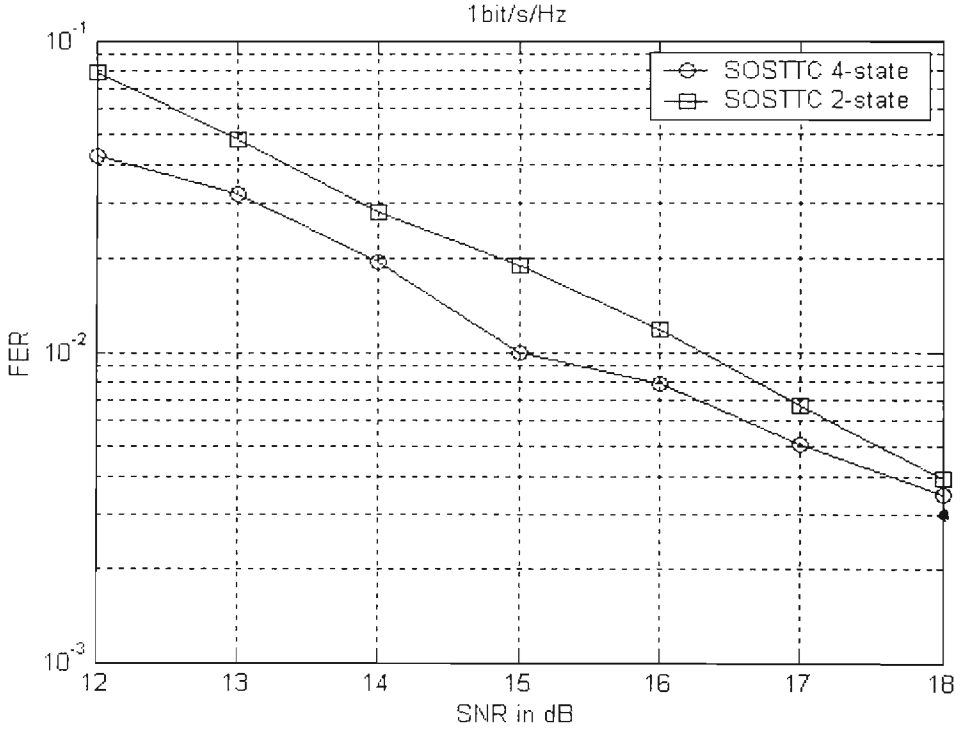

Fig. 4.10: FER for SOSTTC ($N_T = 2$, $N_R = 1$, $r = 1b/s/Hz$) (BPSK) in rapid fading.

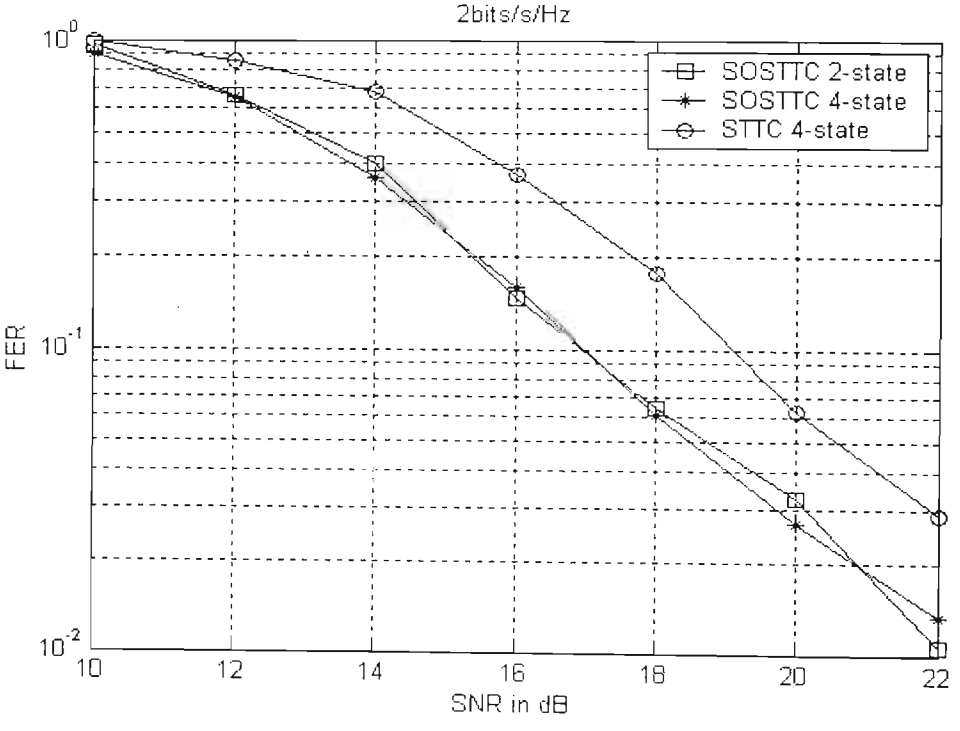

Fig. 4.11: FER for SOSTTC ($N_T = 2$, $N_R = 1$, $r = 2b/s/Hz$) (QPSK) in rapid fading.

Fig. 4.12 shows the frame error rate results versus SNR at rate $r = 1b/s/Hz$ for the 4-state code given in [89] denoted by '4-state new'. Comparisons of this code with other SOSTTC 2-state and 4-state BPSK codes are also provided. Since the '4-state new' code from [89] is designed according to rapid fading channel criteria, it outperforms the reference SOSTTC codes [21] approximately by 2dB at FER of 10^{-2}.

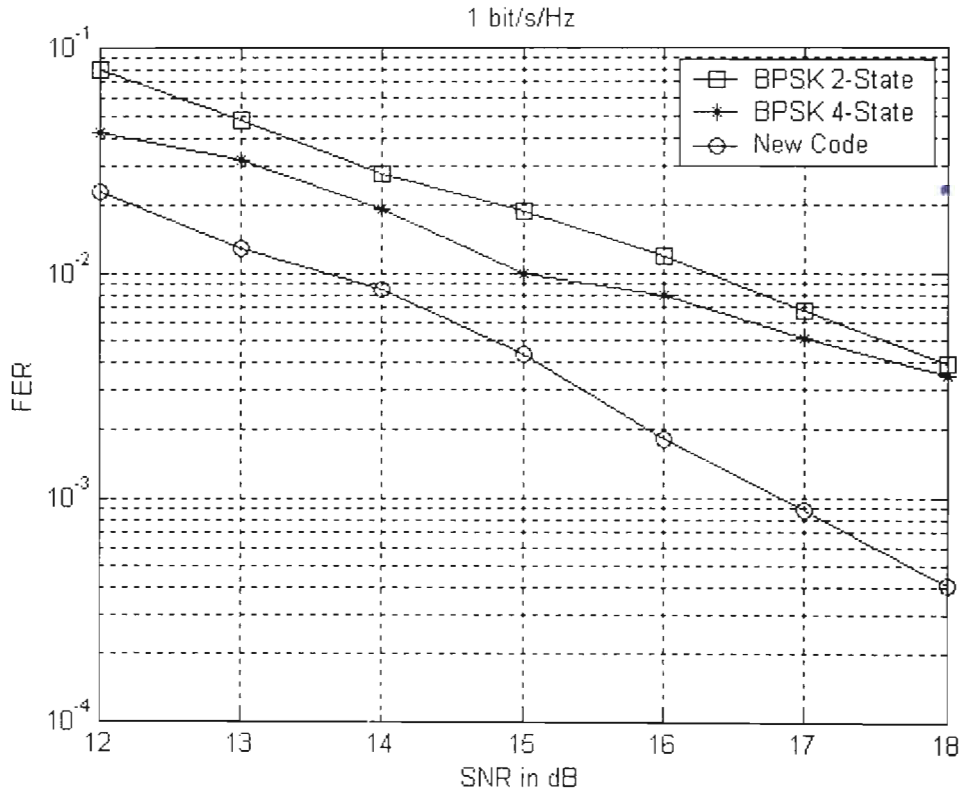

Fig. 4.12: Comparison of FER for SOSTTC ($N_T = 2$, $N_R = 1$, $r = 1b/s/Hz$) (BPSK) in rapid fading.

Fig. 4.13 shows the PWEP versus SNR for a 2-state SOSTTC code using BPSK constellation set and having single receive antenna. The PWEP for the error event path of length 1 $(N = 1)$ is the same for both rapid and quasi-static channels and is obtained by using (4.65). The PWEP is also plotted for the error event path of length 2 $(N = 2)$ using (4.68) and (4.70). The error event path of length 2 is the worst case for quasi-static fading, whereas the worst case for the rapid fading channel is the error event path of length one.

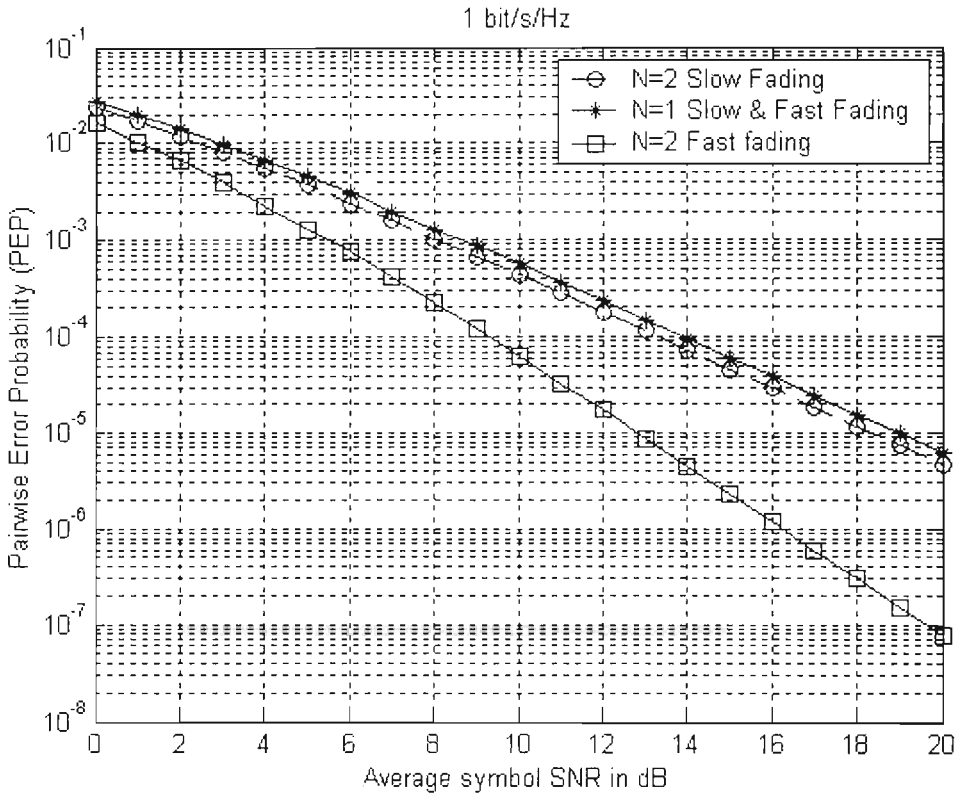

Fig. 4.13: PEP performance of $N_T = 2$, $N_R = 1$, $r = 1b/s/Hz$, 2-state (BPSK) SOSTTC over quasi-static and rapid fading Rayleigh channels.

Fig. 4.14 and Fig. 4.15 show the average bit-error probability (BEP) of the code for rapid fading channel and quasi-static channels respectively. It is seen that while considering error events up to length K=2 is sufficient for calculating the average BEP over a rapid fading channel and error events with longer lengths are needed to estimate the average BEP over quasi-static channels. The slower convergence of the PWEP to the average BEP as a function of the path lengths considered for quasi-static fading relative to rapid fading is consistent with a similar observation made by [92] for orthogonal STTCs. We provide simulation results to show the relative performance with the analytical method.

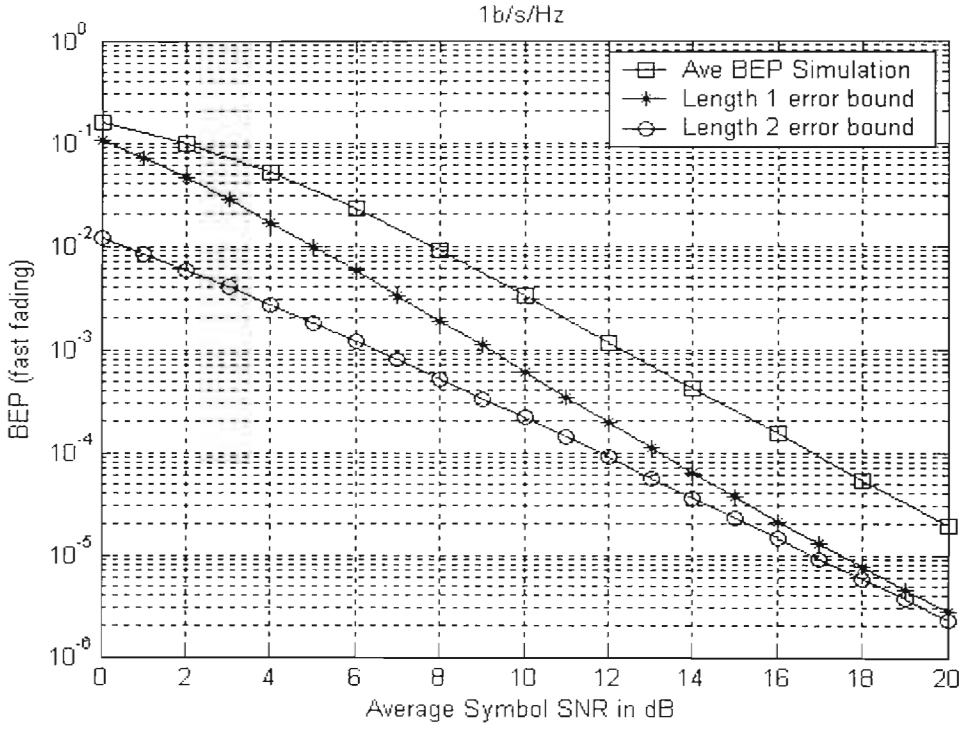

Fig. 4.14: Average Bit error probability performance of $N_T = 2$, $N_R = 1$, $r = 1b/s/Hz$ 2-state SOSTTC over rapid fading channels.

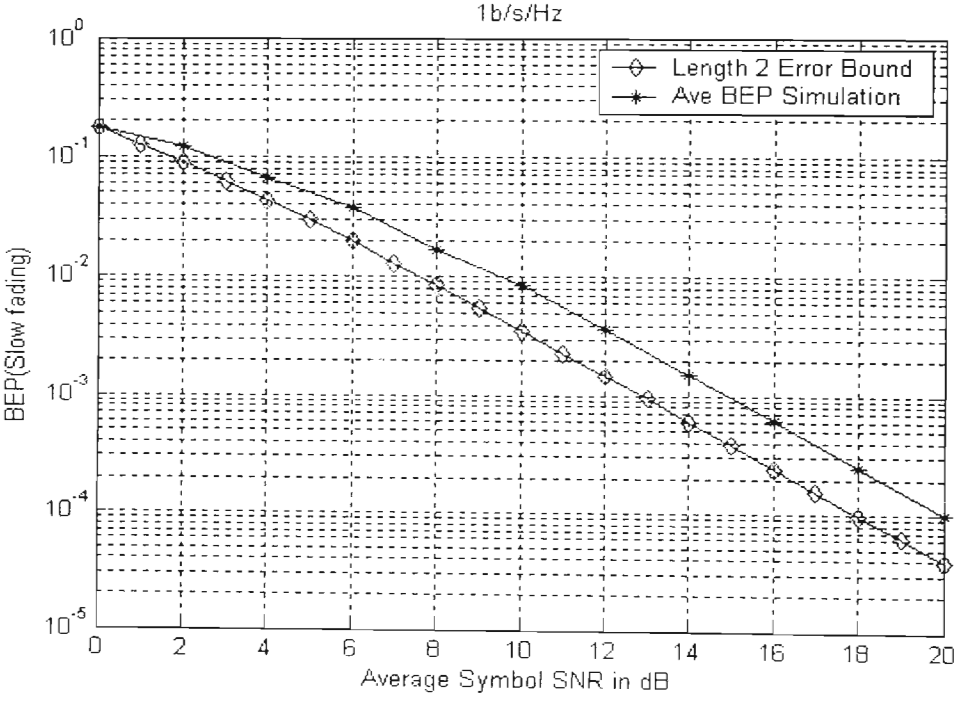

Fig. 4.15: Average Bit error probability performance of $N_T = 2$, $N_R = 1$, $r = 1b/s/Hz$ 2-state SOSTTC over quasi-static fading channels.

4.6 Conclusion

The system design and code structure for Super-orthogonal space-time trellis codes was presented. These codes provide full diversity, full rate and the code structure allows for an increase in the coding gain. It outperforms the space-time trellis codes in the literature and also provides for a systematic code design method for designing STTC at different rates and for different trellises. Simulation results for these codes are provided for both quasi-static and rapid fading Rayleigh channel conditions. A design scheme which shows superior performance in rapid fading channels is provided. Performance analysis on these codes by the coding gain distance and moment generating function methods are provided. Thus, it is seen that super-orthogonal space-time trellis codes provide a superior tradeoff between rate and coding gain while achieving full diversity.

CHAPTER 5

SUPER-ORTHOGONAL SPACE-TIME TURBO CODES

5.1 Introduction

The idea of using concatenated codes first proposed by Forney [12] proved to be a boon to the efforts of designing codes capable of achieving lower decoding complexity with equivalent error rate performance. As mentioned earlier in section 2.4, in the decoding of this concatenated code, there was an absence of the use of feedback mechanisms, between the constituent decoder components. Turbo codes with iterative decoding are known to provide larger performance gains over conventional concatenated systems and approach Shannon capacity with large interleaver size [94]. Recently, a new form of space-time coding technique called Super-orthogonal space-time trellis codes which makes use of set-partitioning and subset mapping of orthogonal space-time block codes have shown to achieve improvement in coding gains over other types of STTC schemes.

The research fraternity, over the recent couple of years, has shown that combining the principles of turbo coding and space-time trellis coding is a natural way of improving the error performance of space-time codes in MIMO fading channels. This method of combining these fields can be further justified by the fact that although in quasi-static fading channels employing short frames, turbo code structure offers little advantage over

the highly structured block and trellis design, they do so when turbo codes are designed for multiple antenna systems. The reason can be attributed to the fact that the performance in quasi-static channel is dominated by the case when all the channels in the multiple antenna transmission schemes are in a deep fade. However, when the frame size is increased the interleavers provide interleaving gain and additional amounts of memory into turbo codes. As a result, turbo codes can take much better advantage of time diversity when it is available than trellis codes.

In a bid to further improve the coding gain performance of Super-orthogonal space-time trellis codes in MIMO fading channels we propose a class of codes which are concatenations built from constituent SOSTTCs and convolutional codes. These codes are decoded using an iterative (turbo) decoding procedure and, hence, we call this family of concatenated codes as Super-orthogonal space-time turbo codes (SOSTTuC).

Firstly, an overview of the existing concatenated space-time coded structures is reviewed in the next section. Next the various decoding algorithms generally employed and the various performance parameters that affect the performance of these codes are discussed. The system models for the proposed Super-orthogonal space-time turbo codes are presented in section 5.3, where the encoding and decoding procedures are explained. A brief explanation of the bitwise additive SISO algorithm is also presented, which is used to decode the individual constituent codes. The performance of the system under channel estimation errors is studied in section 5.4. Finally, the systems' performance is evaluated by simulation in section 5.5 for quasi-static and rapid Rayleigh fading channels.

5.2 Concatenated Space-Time Trellis Codes

Several research groups have proposed different versions of concatenated space time coding structures in the literature over the last few years. This section presents a brief overview of the recent work done in this field. Full rate is achieved when the number of overall output information bits (all antennas) equals the output bits per constituent space-

time code at one time slot. For example, BPSK, QPSK and 8-PSK achieve bandwidth efficiencies of 1, 2 and 3 b/s/Hz respectively. Full spatial diversity in quasi-static channels is achieved when the rank of the codeword difference matrix (CDCM) is equal to the number of transmit antennas.

5.2.1 Current Literature

In [17] a serial concatenation of a space-time trellis code with a RS-outer code was proposed to exploit spatial and temporal variations and was named as smart greedy codes. However, there was a rate loss associated with the use of the outer code. A concatenation of a turbo trellis coded modulation (TTCM) with a STBC was proposed in [95]. The idea here is that the STBC provides the spatial diversity and the outer turbo trellis coded modulation provides the coding gain. This scheme has a rather high complexity due to the TTCM outer code. In [96] parallel concatenated turbo code was proposed which achieved maximum diversity gain and full rate of 1b/s/Hz for multiple transmit antenna systems. These codes showed large gains in rapid fading channels.

In [97] the outputs of a turbo code are bit-interleaved, mapped to QPSK symbols and transmitted using multiple antennas. Full rate is achieved but the code is not guaranteed to achieve full space diversity. Parallel concatenated space-time coding based on punctured turbo TCM have also been proposed by Liu and Fitz [98]. Here they used QPSK modulation for the space-time turbo code which achieved maximum diversity gain and full rate. The codes provided superior performance in rapid faded channels and similar to that of a 64-state STTC in quasi-static fading channels. In [99], Lin and Blum proposed the serial concatenation of an outer space-time code with a rate-1 differential encoder as the inner code on each transmit antenna separately.

In [100] [101], STTC are first modified to be recursive. Then, two encoder structures are proposed. The serially concatenated encoder uses a convolutional code as an outer code and recursive STTC as the inner code. The parallel concatenated case is in fact a self concatenated recursive STTC [102]. The structures of codes in [95], [100] guarantee full

space-diversity but full rate can not be achieved. In [103], they propose a class of full space-diversity full rate space-time turbo codes. They design both parallel and serial concatenated codes. They use a rank criterion to investigate the full diversity of various codes. They also look at the effects of space-time correlated fading channels on both their proposed systems.

In [104], [105] a parallel concatenation of two recursive STTCs as well as a serial concatenation of a recursive systematic convolutional code (RSC) and a recursive STTC were proposed. Both the systems achieved maximum diversity gain using QPSK modulation. They achieved bandwidth efficiencies of 1 b/s/Hz for serial concatenation and 2b/s/Hz for their parallel concatenated codes. They also inferred that the use of recursive STTCs in concatenated systems result in larger performance gains. In [96], the authors construct full diversity space-time turbo codes for two and three antenna cases. They derive non-binary soft decoding algorithms suitable for decoding space-time turbo codes. They also investigate the performance of these codes without perfect CSI.

In [106] the authors studied the use of turbo-coded modulation for multi-antenna systems over block Rayleigh fading channels. They investigate a large number of practical issues such as the case of large number of antennas, effects of estimated channel state information, correlation among sub-channels between different antenna pairs. Later in [71], they derive performance bounds for turbo coded systems with transmitter and receiver diversity. They derive bounds by limiting the conditional union bound before averaging over the fading process, which provide tighter upper bounds.

A very thorough review of various types of concatenated space-time codes with a range of channel codes such as convolutional, BCH, block based turbo codes are provided in [61]. In [94] new space-time turbo codes for two, three and four antennas are proposed using feedforward coefficients to maximize the minimum squared euclidean distance and minimize the iterative decoding threshold using the feedback coefficients. They compare the performance of their code with other codes, and further also investigate the impact of antenna correlation and imperfect channel estimation on the code performance.

5.2.2 Algorithms Employed in Decoding

All concatenated codes make use of the use of maximum likelihood decoding algorithms based on the iterative use of a-posteriori probability (APP) applied to the entire code trellis. A method of realizing the decoding of concatenated codes with a reasonable complexity is by the use of suboptimal, yet powerful iterative algorithms whereby the constituent codes are decoded separately and soft information is exchanged between the decoder.

The two main decoding algorithms that have been employed for the iterative turbo decoding of turbo codes are the Viterbi algorithm [28] or the maximum a-posteriori (MAP) [10] algorithm. The SOVA was proposed in [107] and was derived as an improved version of the Viterbi algorithm. A further improvement was designed in [108] which computed the reliability estimate of each bit which can be improved using the improved SOVA algorithm.

The use of the MAP or BCJR algorithm in turbo codes [13] showed the astonishing capabilities that can be achieved with these sub-optimal techniques. Unfortunately the algorithm is computationally intensive and sensitive to round-off errors which restrict its suitability in many implementation scenarios. These shortfalls can be overcome to an extent with the introduction of the log-MAP and the max-log-MAP algorithms which work in the log domain.

Previously mentioned algorithms were only suitable for decoding of turbo codes or multiple turbo codes as they only provided improved estimates of the uncoded bits. In the case of serial concatenated convolutional codes (SCCC) and hybrid codes, improved estimates of both coded and uncoded bits are required. It was with the introduction of soft-input soft-output (SISO) module proposed in [31], [11] that provided both the required estimates. The SISO module consists of four ports, where the input LLRs of the coded and uncoded bits are accepted and an update of these LLRs are calculated based on the code constraints. Also most of the proposed algorithms, not even the BCJR algorithm

[10] could cope with a trellis having parallel edges. In our concatenated scheme, the inner code is a SOSTTC code whose trellis consists of transitions between states having parallel transitions. The SISO algorithm can be implemented in two forms, namely multiplicative SISO which is an extension of the MAP algorithm and the additive SISO which is an extension of the log-MAP algorithm. The latter is explained in more detail in section 5.3.2.

5.2.3 Performance Parameters

In this section a brief discussion of the various parameters, some of which are interlinked, which affect the performance of concatenated codes is given. A more detailed comparison of these parameters is presented in [37] for the case of turbo codes and in [23] for the case of turbo codes and SCCCs.

5.2.3.1 Constituent Decoding Algorithm

The choice of decoding algorithm to be employed for a particular code would be purely based on a trade-off requirement in terms of complexity over performance. A complexity comparison between the MAP, SOVA, Log-MAP, and Max-Log-MAP in order of complexity from the most complex to the least complex is the MAP followed by the Log-MAP, then the Max-Log-MAP and lastly the SOVA. In terms of the performance advantage of these algorithms in concatenated systems, the Log-MAP's performance is slightly inferior to the MAP. The Max-Log-MAP performs worse than the Log-MAP, but maintains significant improvement over the SOVA algorithm. In selecting an algorithm which provides an overall good trade-off, the Log-MAP is a suitable choice [23].

5.2.3.2 Interleavers

It is well known that the interleaver's role in the concatenated code has a vital influence on the performance of the code. The interleaver generates a long block code from small memory convolutional codes and is capable of spreading low-weight input sequences so that the resulting codeword has high weight.

The size and structure of the interleaver used plays an important role in the performance of the code. The size of the interleaver determines the performance of the code at low SNRs and at high SNRs both size and structure are factors on the performance. A well designed interleaver will map low weight input sequences from the first encoder to high weight input sequences in the second encoder. The error floor regions decrease rapidly with increasing interleaver length. A number of interleaving structures are discussed in [23] which are block, convolutional, random, circular shifting, semi-random and odd-even interleavers to name a few.

5.2.3.3 Constituent Codes

The constraint length and generator polynomial used in the component codes are important parameters. Often in turbo codes the generator polynomials which lead to the largest minimum free distance for ordinary convolutional codes are used, although when the effect of interleaving is considered these generator polynomials do not necessarily lead to the best minimum free distance for turbo codes. The use of recursive codes over their non-recursive counterparts have shown improvement in interleaving gains translating to improved performance. Hence, the design of concatenated codes requires the selection of good interleavers in conjunction with proper selection of constituent codes.

5.2.3.4 Trellis Termination

The concatenated codes performance can be improved if the initial and final states are the same. Trellis termination involves driving the encoder to the all-zero state with the help of some additional tail bits at the end of the frame. Hence, the design of concatenated codes requires the selection of good interleavers in conjunction with proper selection of constituent codes.

5.2.3.5 Effect of Number of Iterations

The selection of a suitable number of iterations is very vital in determining the performance of the code with respect to the appropriate complexity constraints. The error rate goes down considerably when the number of iterations is increased from one to six; and much less when the number of iterations is increased from six to ten. It is almost insensitive to an increase in the number of iterations above ten, for short interleaver lengths. This number of iterations at which the error rate saturates is larger for higher interleaver sizes.

5.3 System Model for SOST-CC and SOST-SC

Super-orthogonal space-time trellis codes have shown improved performance over conventional space time trellis codes for both quasi-static and rapid fading channels. From the previous discussion in section 5.2.1, the concatenation of STTCs through simple, double and hybrid means have shown improved coding gains over conventional STTCs. Keeping these two factors in mind we propose two concatenated SOSTTC schemes in a bid to further improve the coding gain of SOSTTCs.

Any of the concatenated STTC schemes discussed in section 5.2 could be modified in order to incorporate a SOSTTC code. In selecting a concatenated code to modify, it would be ideal to choose the system with the best performance. However, no results

directly comparing the performance of these systems can be found in the literature. The serially concatenated structure of [109] [76] was simple and modified to incorporate a SOSTTC encoder. The double concatenated structure proposed in [76] was also modified to incorporate the SOSTTC encoder.

In this section, firstly an outer convolutional code is concatenated with an inner SOSTTC code to give SOST-CC and secondly two outer serially concatenated convolutional codes with an inner SOSTTC to give SOST-SC, with the aim of increasing the overall coding gain performance of the code. These codes are decoded using an iterative (turbo) decoding procedure and, hence, we call this family of concatenated codes as Super-orthogonal space-time turbo codes (SOSTTuC). These two systems can be individually referred to as SOST-CC and SOST-SC respectively. In this section, the encoding and decoding of the proposed SOST-CC and SOST-SC systems is explained. The bitwise additive SISO algorithm used to decode the constituent SOSTTCs and CCs is also described. In all cases the systems have a bandwidth efficiency of 1b/s/Hz.

5.3.1 SOST-CC and SOST-SC Transmitter

The communication systems under consideration have N_T transmit and N_R receive antennas. These antennas are sufficiently separated to ensure spatially independent or uncorrelated fading. The system architecture of the SOSTTC code and channel conditions is identical to that laid out in chapter 4 and 3 respectively.

The transmitter models for the SOST-CC and SOST-SC systems are shown in Fig. 5.1 and Fig. 5.2 respectively and are built on corresponding modifications on [28]. In both systems the input frame $\underline{u}$ of the information bits is encoded by the outer code, which is either convolutional or serial concatenated convolutional code, then interleaved and sent to the SOSTTC encoder. The SOSTTC encoder provides a vector $\underline{c_l}$ of N_T output symbols

and transmitted according to the SOSTTC transmission matrix which is then simultaneously transmitted over the N_T transmit antennas.

We use pseudo-random bit interleavers throughout. The convolutional codes employed RSC or non-recursive convolutional (NRC) codes. Since the SOSTTC encoder does not have a recursive structure, we will employ it in its normal form as the inner code in both the concatenated schemes.

5.3.1.1 Encoding of SOST-CC

The SOST-CC system is shown in Fig. 5.1 [117]. Here the outer code is a convolutional code which is concatenated to the inner SOSTTC code through an interleaver. The input bits $\underline{u}$ are encoded by C_1 and interleaved by π. These interleaved bits are then encoded by the SOSTTC encoder. It is ensured that all the constituent encoders are terminated.

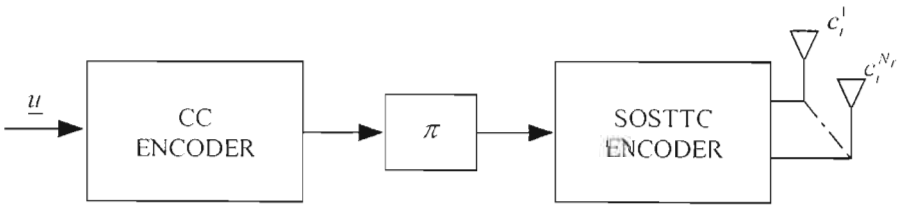

Fig. 5.1: Block diagram for the SOST-CC encoder.

5.3.1.2 Encoding of SOST-SC

The SOST-SC system is shown in Fig. 5.2. Here the outer code consists of a serial concatenation of two convolutional codes. This combination is then concatenated to the inner SOSTTC through an interleaver. The input bits $\underline{u}$ are encoded by C_1 and interleaved by π_1. These interleaved bits are then encoded by C_2 and interleaved by π_2 and lastly SOST encoded. Once again all encoders are ensured to be terminated.

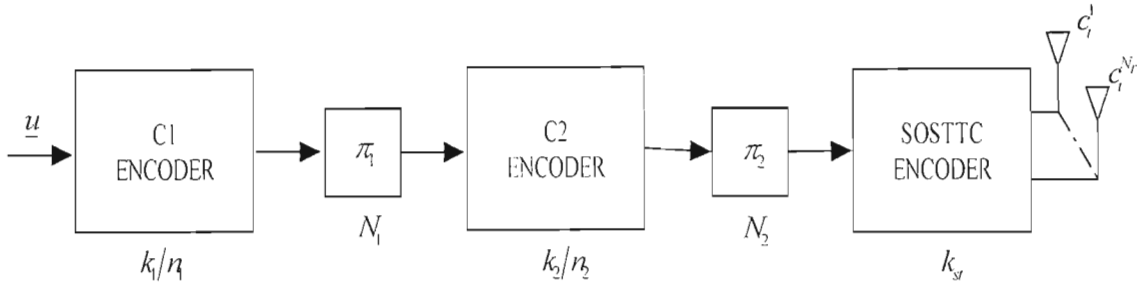

Fig. 5.2: Block diagram for the SOST-SC encoder

5.3.1.3 Puncturing

In order to compare the systems discussed in this section under identical bandwidth efficiencies, puncturing of the output symbol vectors $\underline{c}_t$ is necessary to maintain an overall bandwidth efficiency of 1 b/s/Hz. For simplicity the puncturing block is not shown in the encoder and decoder diagrams. At the transmitter the punctured symbol vectors $\underline{c}_t$ are not transmitted and at the receiver the LLRs are set to zero.

Although this may limit the diversity gain of the system in quasi-static fading, based on results shown in [76] and simulation results in section 5.5 indicate this effect is negligible.

5.3.2 SOST-CC and SOST-SC Receiver

In this section we first describe the bitwise additive SISO algorithm which is used to decode each constituent code. The decoding process of the proposed SOST-CC and SOST-SC systems is then explained.

5.3.2.1 The Bitwise Additive SISO Algorithm

All concatenated coding schemes admit a suboptimum decoding scheme based on the iterative use of a-posteriori probability algorithms [29] applied to each constituent code.

In this dissertation a description of the soft-input soft-output (SISO) module is discussed. The SISO algorithm is implemented in its bitwise additive form [110] where soft information is exchanged between decoders in the form of bit logarithmic likelihood ratios (LLRs). Hence, it eases the process of interleaving and de-interleaving as it does not require for conversions between LLRs and symbol LLRs. Previously proposed algorithms were not in a form suitable to work with a general trellis code. Most of them assumed binary input symbols, some assumed also systematic codes and none (not even the original BCJR algorithm [10]) could cope with a trellis having parallel edges. The SISO algorithm works on the trellis edges, rather than on pairs of states, and this makes the algorithm completely general and capable of coping with parallel edges and also encoders with rates greater than one, like those encountered in some concatenated schemes. Hence as we employ SOSTTC codes which have transitions it is more suitable to use the SISO module for their decoding.

Consider a general trellis encoder with m memory elements, L input symbols u and L output symbols c. The input symbols can be obtained from the set of $n_u = 2^k$ symbols each consisting of k bits where $u = \{u^1, \cdots u^k\}$ and k is the number of encoder input bits at each time instance. In the case of convolutional codes (CCs) the output symbols are drawn from the set of $n_c = 2^n$ symbols, each consisting of n bits where $c = \{c^1, \cdots c^n\}$ and n is the number of encoder output bits at each time instance. For SOSTTCs the output symbols which are to be transmitted according to the transmission matrix are drawn from a set of $n_c = M^{N_T}$ symbols each consisting of N_T M-PSK symbols where $c = \{c^1, \cdots c^{N_T}\}$.

The SISO module is a four port device that accepts the input LLRs of the coded bits $\lambda_t(c^i, I)$ and uncoded bits $\lambda_t(u^i, I)$, and outputs an update of these LLRs, $\lambda_t(c^i, O)$ and $\lambda_t(u^i, O)$, based upon the knowledge of code constraints like its inputs and trellis section.

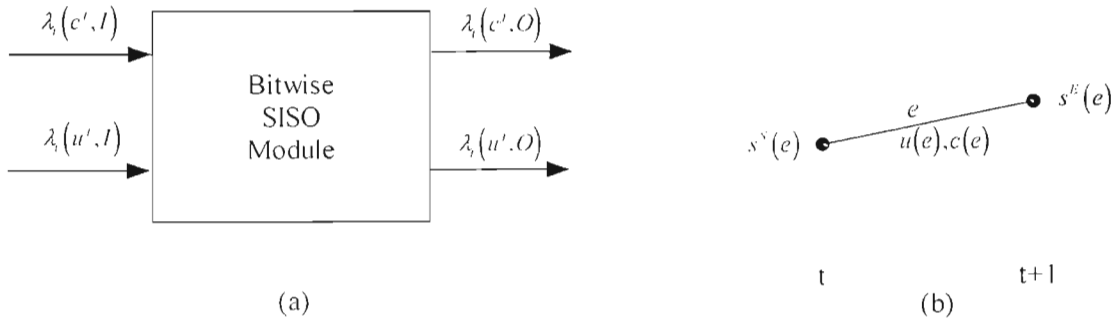

Fig. 5.3: (a) SISO module. (b) Trellis section for edge e.

The dynamics of any particular trellis code can be completely specified by a single trellis section, which describes the transitions (edges) between the states of the trellis at time instants t and $t+1$. Each trellis section is characterized by a state of the trellis at time t as $S_t = s$, and a set of $n_e = n_u \cdot n_s$ edges connecting these states, an illustration of a single trellis section for a particular edge e can be found in Fig. 5.3. Any edge (e) can be defined as the transition from an initial state $s^S(e)$ to a final state $s^E(e)$, having the corresponding input symbol $u(e)$ and output symbol $c(e)$.

For a frame length of L symbols which correspond to an input frame size of Lk bits, the input output relationships are modified from [76], for $t = \{1, \ldots L\}$,

$$\begin{aligned}\lambda_t(c^j, O) = &\max_{c:c^j(e)=1}^{*}\left\{\alpha_{t-1}(s^S(e)) + \lambda_t(u(e), I) + \sum_{i=1, i\neq j}^{n} c^i(e)\lambda_t(c^i(e), I) + \beta_t(s^E(e))\right\} \\ &- \max_{c:c^j(e)=0}^{*}\left\{\alpha_{t-1}(s^S(e)) + \lambda_t(u(e), I) + \sum_{i=1, i\neq j}^{n} c^i(e)\lambda_t(c^i(e), I) + \beta_t(s^E(e))\right\},\end{aligned} \tag{5.1}$$

and

$$\begin{aligned}\lambda_t(u^j, O) = &\max_{c:u^j(e)=1}^{*}\left\{\alpha_{t-1}(s^S(e)) + \lambda_t(c(e), I) + \sum_{i=1, i\neq j}^{n} u^i(e)\lambda_t(u^i(e), I) + \beta_t(s^E(e))\right\} \\ &- \max_{c:u^j(e)=0}^{*}\left\{\alpha_{t-1}(s^S(e)) + \lambda_t(u(e), I) + \sum_{i=1, i\neq j}^{n} u^i(e)\lambda_t(u^i(e), I) + \beta_t(s^E(e))\right\}.\end{aligned} \tag{5.2}$$

Here, the output LLRs does not depend on their corresponding simultaneous input. Thus the LLRs $\lambda_t(c',O)$ and $\lambda_t(u',O)$ are an update of the input LLRs $\lambda_t(c',I)$ and $\lambda_t(u',I)$.

The forward and backward metrics, $\alpha_t(\cdot)$ and $\beta_t(\cdot)$ are calculated in (5.3) and (5.4) below.

$$\alpha_t(s) = \max_{e:s^S(e)=s}{}^{*}\left\{\alpha_{t-1}\left(s^S(e)\right) + \lambda_t\left(u(e),I\right) + \lambda_t\left(c(e),I\right)\right\}, \text{ and} \tag{5.3}$$

$$\beta_t(s) = \max_{e:s^S(e)=s}{}^{*}\left\{\beta_{t+1}\left(s^S(e)\right) + \lambda_{t-1}\left(u(e),I\right) + \lambda_{t-1}\left(c(e),I\right)\right\}. \tag{5.4}$$

The metrics have to be initialized at the start of the decoding which is as follows:

$$\alpha_0(s) = \begin{cases} 0 & \text{if } s = S_0 \\ -\infty & \text{otherwise} \end{cases}$$

$$\beta_l(s) = \begin{cases} 0 & \text{if terminated and } s = S_0 \\ 1/n_s & \text{if non-terminated} \\ -\infty & \text{otherwise} \end{cases}.$$

The max* operator is calculated recursively and performs addition in the log domain. In order to calculate $\max_j^*(a_j)$, we evaluate (5.5) recursively where δ_1 is initialized to a_1 and $\max(\cdot)$ takes the larger of the two values considered. For $j = \{2,\cdots,J\}$,

$$\delta_j = \max\left(\delta_j,\delta_{j-1}\right) + \ln\left[1 + \exp\left(\left|\delta_j - \delta_{j-1}\right|\right)\right]. \tag{5.5}$$

On the final iteration J,

$$\max_j{}^{*}(a_j) = \delta_J. \tag{5.6}$$

The input symbol LLRs of the uncoded bits $\lambda_t(u,I)$ for both the CCs and SOSTTCs are calculated in (5.7) where $l = \{1,\cdots n_u\}$.

$$\lambda_t\left(u = u_l, I\right) = \sum_{i=1}^{k} u_l^i \lambda_t\left(u^i, I\right). \tag{5.7}$$

The input LLRs of the coded bits for the CCs are modules and not from the demodulator and can be calculated as shown below where;

$$\lambda_t\left(c=c_l,I\right)=\sum_{j=1}^{n}c_l^j\lambda_t\left(c^j,I\right). \tag{5.8}$$

For the input LLRs of the coded L-PSK symbols in the case of SOSTTCs, which are only received from the soft outputs of the demodulator and can be calculated as shown below in (5.9). The received signal r_t^j at time t on receive antenna j after matched filtering is given by (3.1). Let $\underline{g}_l$ be one of the possible output symbol vectors of the SOSTTC encoder where $l=\{1\cdots n_c\}$. Let $\underline{g}_1$ be the reference symbol vector, then

$$\begin{aligned}&\lambda_t\left(c=\underline{g}_l,I\right)=\hat{\lambda}_t\left(c=\underline{g}_l,I\right)-\hat{\lambda}_t\left(c=\underline{g}_1,I\right),\ \text{and}\\&\hat{\lambda}_t\left(c=\underline{g}_l,I\right)=-\frac{1}{2\sigma_r^2}\sum_{j=1}^{N_R}\left|r_t^j-\sum_{i=1}^{N_T}\alpha_{ij}^t g_l^j\right|^2.\end{aligned} \tag{5.9}$$

5.3.2.2 Decoding of SOST-CC

The block diagram of the SOST-CC decoder is shown in Fig. 5.4 in its simplified form [117]. We make certain modifications in representation to the various terms involved for simplification purposes for both the systems. The subscript t of λ, and the superscript j, of c and u will be dropped. The subscript of c or u will specify the decoder where *sost* is used for the SOST encoder, *cc* for the convolutional code, in the SOST-CC system.

On the first iteration $\lambda\left(u_{sost},I\right)$ is set to zero as no a-priori information is available initially. As we are under the assumption that the source symbols transmitted are equally likely, the input $\lambda\left(u_{cc},I\right)$ is always set to zero. The input LLRs to the SOST SISO module is $\lambda\left(c_{sost},I\right)$ and is calculated using equation (5.9).

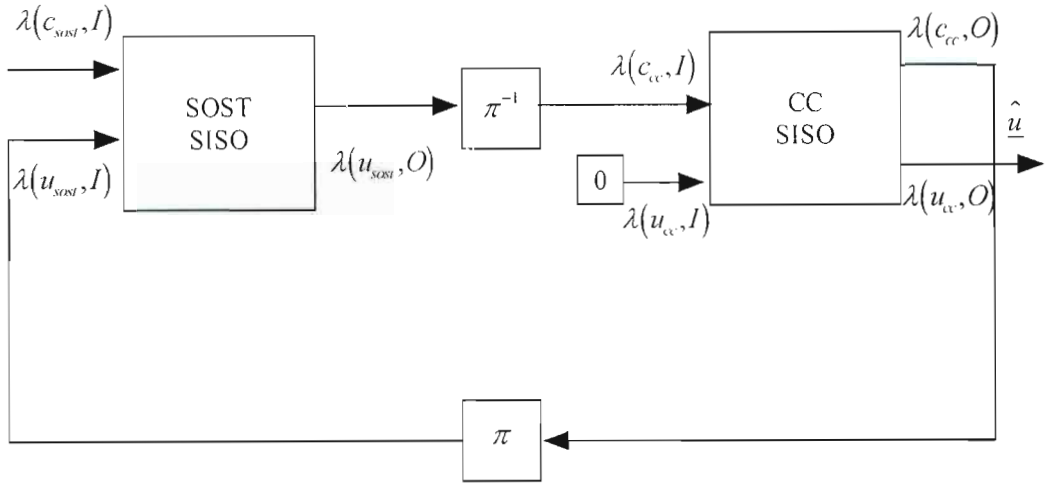

Fig. 5.4: Block diagram for the SOST-CC decoder.

The SOST SISO module determines the outputs $\lambda(u_{sost}, O)$ and this information is passed through the inverse interleaver π^{-1} to obtain $\lambda(c_{cc}, I)$. These input LLRs $\lambda(u_{cc}, I)$ are passed through the SISO module of CC and the output LLRs of CC of which the coded part is $\lambda(c_{cc}, O)$ and the uncoded part $\lambda(u_{cc}, O)$ is obtained.

In the feedback loop the output LLRs $\lambda(c_{cc}, O)$ obtained from the CC SISO module are then interleaved through π to become the a-priori information $\lambda(u_{sost}, I)$ on the next iteration. The above process is then iterated several times. On the final iteration the outputs $\lambda(u_{cc}, O)$ is used to directly to obtain the estimate of the original bit stream $\hat{\underline{u}}$.

5.3.2.3 Decoding of SOST-SC

The block diagram of the SOST-SC decoder is shown in Fig. 5.5 in its simplified form. The subscript of the c or u specifies the decoder as mentioned earlier for the case of the SOST code, *sost* is used for the SOST encoder, 1 for the convolutional encoder C1 and 2 for the convolutional encoder C2.

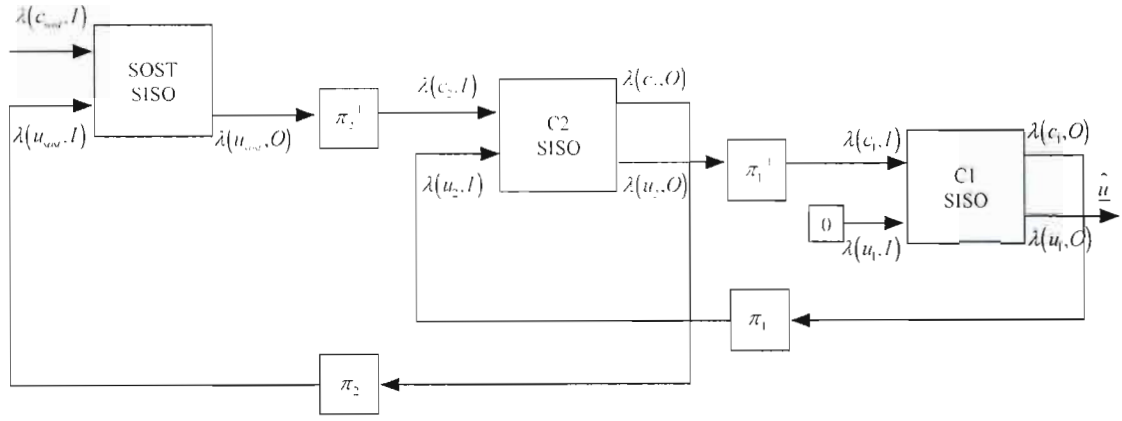

Fig. 5.5: Biock diagram for the SOST-SC decoder.

On the first iteration $\lambda(u_{sost}, I)$ and $\lambda(u_2, I)$ are set to zero as no a-priori information is available. As we are under the assumption that the source symbols transmitted are equally likely, the input $\lambda(u_1, I)$ is always set to zero. The input LLRs to the SOST SISO module is $\lambda(c_{sost}, I)$ and is calculated using equation (5.9).

The SOST SISO module determines the outputs $\lambda(u_{sost}, O)$ and this information is passed through the inverse interleaver π_2^{-1} to obtain $\lambda(c_2, I)$. The output LLRs of the SISO module of C_2 which are $\lambda(c_2, O)$ for the coded bits and $\lambda(u_2, O)$ for the uncoded bits is calculated. Next $\lambda(u_2, O)$ is passed through the inverse interleaver π_1^{-1} to obtain $\lambda(c_1, I)$. This input is used by the SISO module of C_1 to obtain the output LLRs $\lambda(c_1, O)$ for the coded bits and $\lambda(u_1, O)$ for the uncoded bits.

For the feedback loops the output LLRs $\lambda(c_1, O)$ obtained from the C_1 SISO module are then passed through interleaver π_1 to become $\lambda(u_2, I)$ on the next iteration. Also the output $\lambda(c_2, O)$ is passed through the interleaver π_2 to become $\lambda(u_{sost}, I)$ on the next iteration. On the final iteration the estimate of the original bit stream $\hat{\underline{u}}$ can be directly obtained from $\lambda(u_1, O)$.

5.4 Estimation of Channel State Information

As diversity remains to be an important factor determining the performance of wireless systems, the combination of space-time coding techniques and estimation techniques remains attractive for research. In this section we consider the effects of imperfect channel state information on the performance of the concatenated SOSTTC systems proposed in section 5.3.

In a practical scenario, there will be errors in the channel state information available to the receiver. The function of a channel estimator is to extract from the received signal approximation to the fade coefficients during each data frame. There are two general methods of generation of pilot tones, the first method of channel estimation is to turn off all transmit antennas apart from antenna i at some time instant and to send a pilot signal using antenna i. The fade coefficients $\alpha_{i,j}$ are then estimated for $1 \le j \le m$ and for $1 \le j \le n$, n and m being the number of transmit and receive antennas respectively, until all coefficients $i = 1,2,\cdots n \quad j = 1,2\cdots m$ are estimated. A second method of estimation is to send orthogonal sequences of signals for pilot signals, one from each transmit antenna, which is the method we follow. Regardless of the method used for estimation, the channel estimator provides estimates $\beta_{i,j}$ for $\alpha_{i,j}$. It is assumed that $\beta_{i,j}$ is a zero-mean complex Gaussian random variable only dependant on $\alpha_{i,j}$ and a correlation coefficient. The correlation μ has a simple expression in terms of the variance of channel estimation error. In general, we assume

$$\beta_{i,j} = \alpha_{i,j} + \varepsilon_{i,j}, \tag{5.10}$$

where, the variance $\varepsilon_{i,j}$ represents the channel estimation error.

In order to estimate the channel state information, we follow the approach of [17], which was also used by [106], and make use of a training sequence of length k. We can denote the pilot symbols to be used for training by $W_1, W_2, \cdots W_n$, where

$$W_i = \left[W_{1,i}, W_{2,i}, \cdots, W_{k,i}\right], \tag{5.11}$$

and $W_{t,i}$ are elements of the signal constellation used for $1 \le j \le n$ and $1 \le t \le k$. We need the training symbols $W_{1,i}, W_{2,i}, \cdots, W_{k,i}$ to be orthogonal sequences, i.e. $W_p \cdot W_q = 0$ whenever $p \ne q$. For the period of training $\left(\mathbf{r}' = \left[r_1', r_2', \ldots r_k'\right]\right)$, the received signal is denoted by,

$$r_{t,j} = \sum_{i=1}^{n} \alpha_{i,j} W_{t,i} + \eta_{t,j}, \tag{5.12}$$

where $1 \le i \le n$, $1 \le j \le m$, $1 \le t \le k$. The main aim here is to make use of the received signal to estimate $\alpha_{i,j}$, where $i = 1, 2, \cdots n$ and $j = 1, 2 \cdots m$. Since the training sequences are orthogonal, we have

$$r_j \cdot W_i = \alpha_{i,j}\left(W_i \cdot W_i\right) + \eta_j \cdot W_i, \tag{5.13}$$

Thus

$$\alpha_{i,j} = \frac{r_j \cdot W_i}{W_i \cdot W_i} - \frac{\eta_j \cdot W_i}{W_i \cdot W_i}. \tag{5.14}$$

Hence, the estimated path gain $\beta_{i,j}$ from the transmit antenna i to the receive antenna j, is

$$\beta_{i,j} = \alpha_{i,j} + \frac{\eta_j \cdot W_i}{W_i \cdot W_i}. \tag{5.15}$$

Now it is possible to use the estimated channel state information [17], to obtain the log-likelihoods of the received bits and proceed with the iterative decoding algorithm.

5.5 Simulation Results

In this section, the performance of the proposed SOST-CC and SOST-SC systems is evaluated by simulation in both quasi-static and rapid fading Rayleigh channels. The

results obtained can be used to asses the system performance for low to medium SNRs. The results obtained are also compared with some of the codes proposed in [76].

The application of Monte-Carlo methods are used to generate the simulation results where (5.9) is used to first determine the received signal which is then decoded as described in section 5.3.2. The number of frame errors generated for the simulations are then recorded.

The results obtained are shown with FER versus (E_b / N_0) as discussed in section (3.6.2) takes into account the code rate and hence allows for systems with different code rates. For all simulation results obtained, two input frame sizes are used, the first being a length of $N = 130$ bits and then 1300 bits. We consider this method of comparison as performed in [76] as it categorizes the two types into short and long frame lengths. The short frame is more suited to voice transmission as it has short delay, while the longer frame is more suited to data transmission as it generally results in lower FERs. For all the systems considered, two transmit and a single receive antenna is used and the number of iterations is set to six.

A 4-PSK, 4-state SOSTTC is considered from [21] having eight parallel paths per transition from each state to the other. A RSC rate $1/2$, 4-state convolutional code and RSC and NRC rate $2/3$, 4-state convolutional codes are considered. When used in the SOST-CC system, the convolutional codes used are both either RSC or both NRC codes. In all cases the overall bandwidth efficiency of the system is $1 b/s/Hz$ where puncturing is performed in every ninth transmission for the SOST-SC system.

The figures from 5.6 to 5.9, presents simulation results for SOST-CC and SOST-SC systems, comparing various combinations of constituent encoders. Fig. 5.6 shows the results obtained for the SOST-CC system in quasi-static fading channels [117]. Its performance is also compared with their identical STTC combination ST-CC from [76]. In all cases it is seen that there is no interleaving gain obtained in terms of FER achieved by increasing the input frame size. It is seen that the SOST-CC system maintains a similar performance to their ST-CC counterparts in quasi-static fading channels.

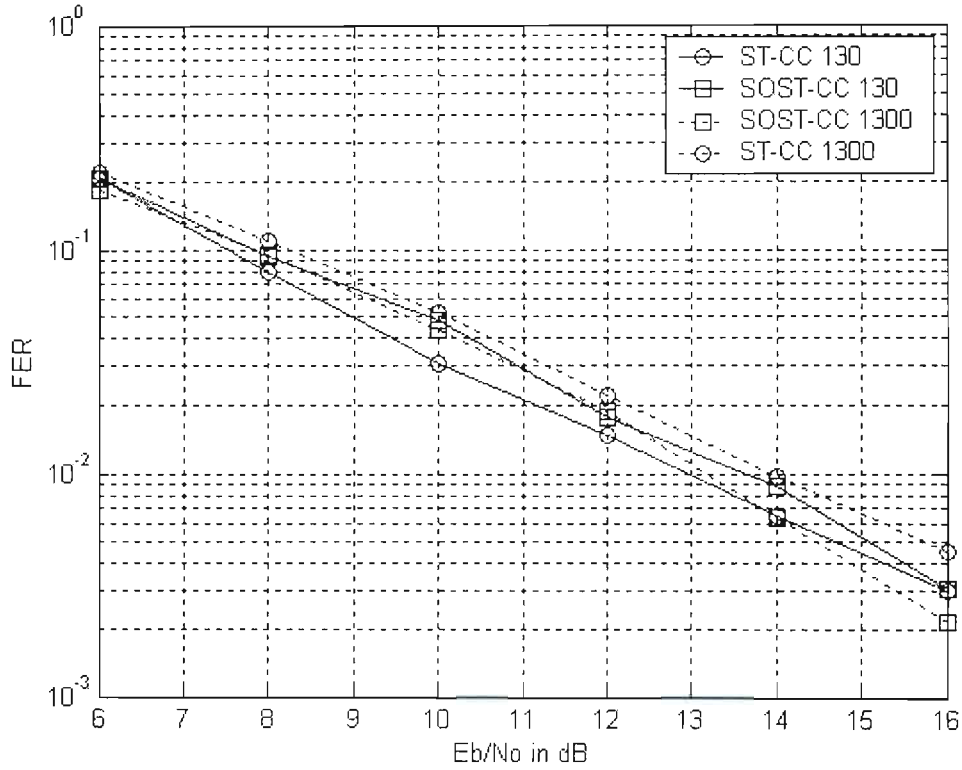

Fig. 5.6: Performance of SOST-CC system in quasi-static fading.

Simulation results for the SOST-CC system in rapid fading channels is shown in Fig. 5.7. It is seen that there is significant improvement in performance due to interleaving gains by increase of the input frame size. It is also seen the SOST-CC system outperforms the corresponding ST-CC system for both frame sizes in rapid fading channels.

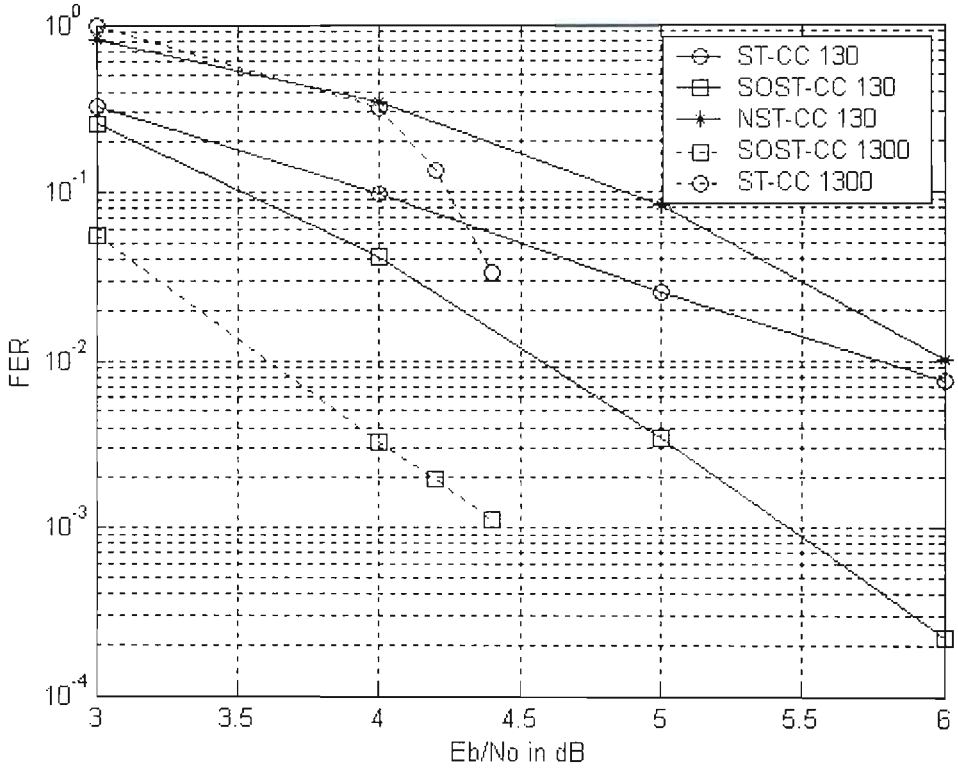

Fig. 5.7: Performance of SOST-CC system in rapid fading.

In Fig. 5.8 simulation results for the SOST-SC system are shown for the case of quasi-static fading channels. It is seen that the SOST-SC combination has degradation in performance in comparison to its corresponding STTC counterpart, the ST-SC system. The SOST-SC system however shows improvement over the ST codes using non-recursive NRC outer SCCC codes which are the ST-NSC codes. A non-recursive outer code version for the SOSTTC case is also provided, the SOST-NSC case. As can be seen from Fig. 5.8, no significant interleaving gain can be obtained for these systems in quasi-static fading case.

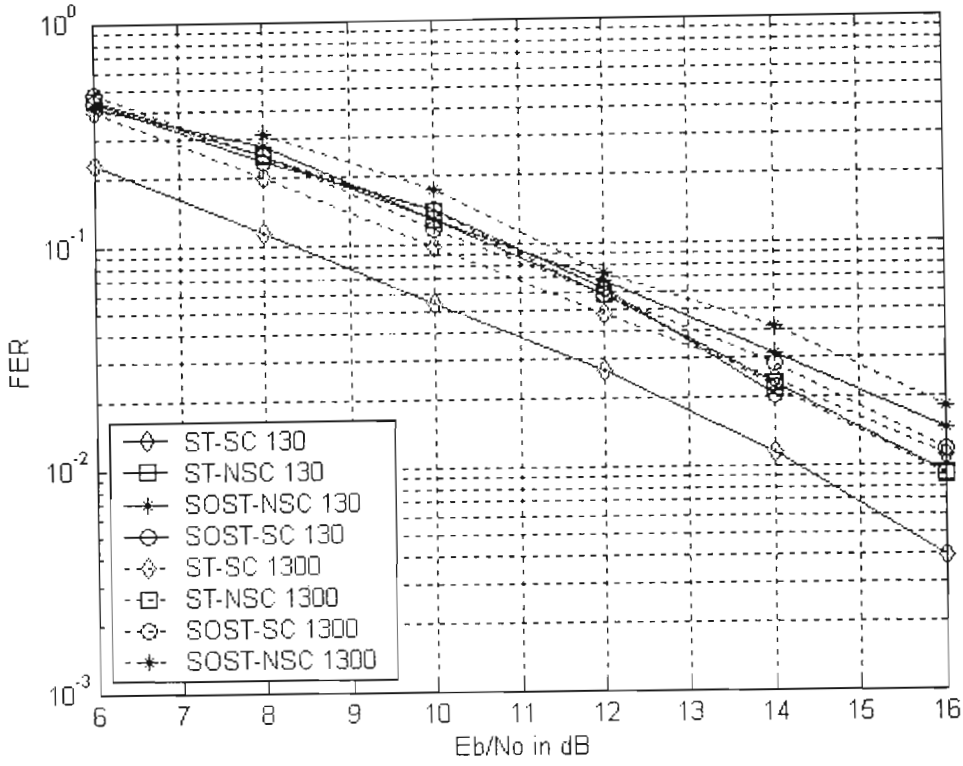

Fig. 5.8: Performance of SOST-SC system in quasi-static fading.

Fig. 5.9 shows results for the SOST-SC system in rapid fading channel. Here the system having both RSC convolutional outer SCCC codes and NRC convolutional codes are compared. It is seen that the SOST-SC system using RSC CCs perform better than their NRC CCs counterparts. The results are also compared with the corresponding STTC combinations namely ST-SC and ST-NRC systems. It is seen that the SOST-SC codes maintain a good performance with their corresponding ST-SC counterparts for both short and long frame sizes. It can be clearly seen that there is significant coding gain achievable for these types of codes in the rapid fading case, as it is able to make use of the available interleaving gains.

It has been shown from the literature that the performance of iterative decoding schemes have been shown to converge to Shannon's limit in AWGN channels. However, in the case of Rayleigh fading channels the performance has shown to be degraded for these systems [111] [23] [112]. This phenomenon is also observed in the results shown in this

chapter. Also we can say that due to the presence of temporal diversity in rapid fading channels the systems are able to make use of this advantage and perform better in rapid fading conditions than in quasi-static fading channels.

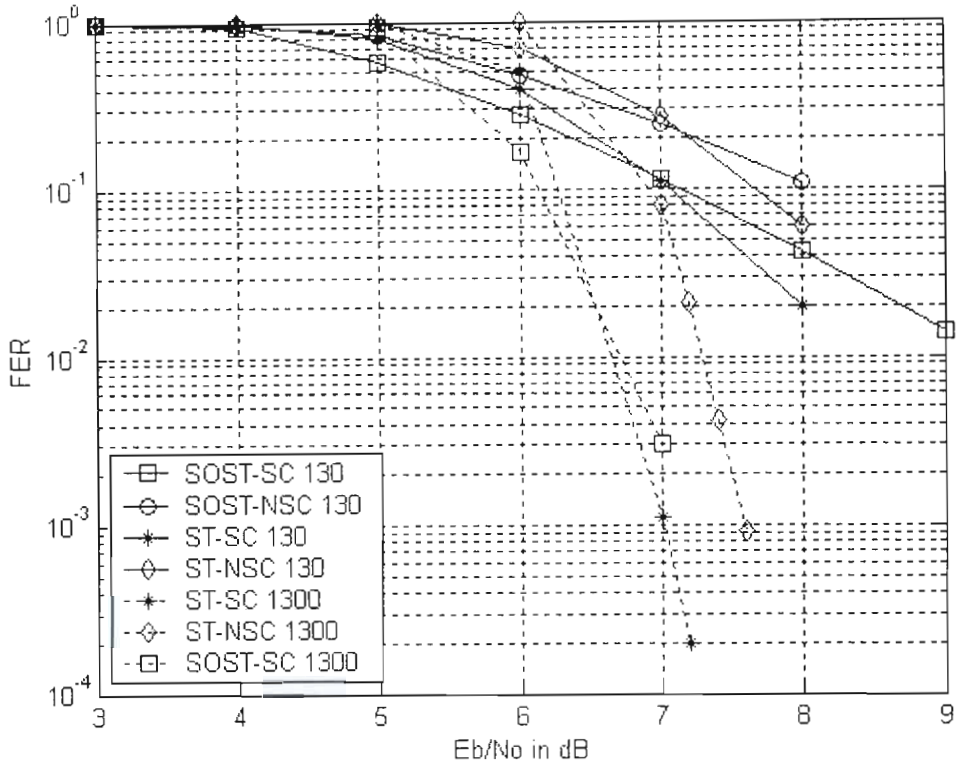

Fig. 5.9: Performance of SOST-SC system in rapid fading.

In Fig. 5.10 simulation results for the schemes using perfect channel state information and estimated channel state information with the help of the pilot aided channel estimation method is shown for quasi-static fading channels. We consider the SOST-CC system in this case. Here for the simulation $k = 8$ and N is 260 bits as considered in [17]. It is seen that there is a loss in performance due to estimation of the channel state information and it is around 3dB. Yet the result is useful to determine the performance of such a system in a more realistic scenario. Similar performance for space-time block codes using channel estimation can be found in [113], and there is also a degradation of about 3dB in performance evident in their scheme.

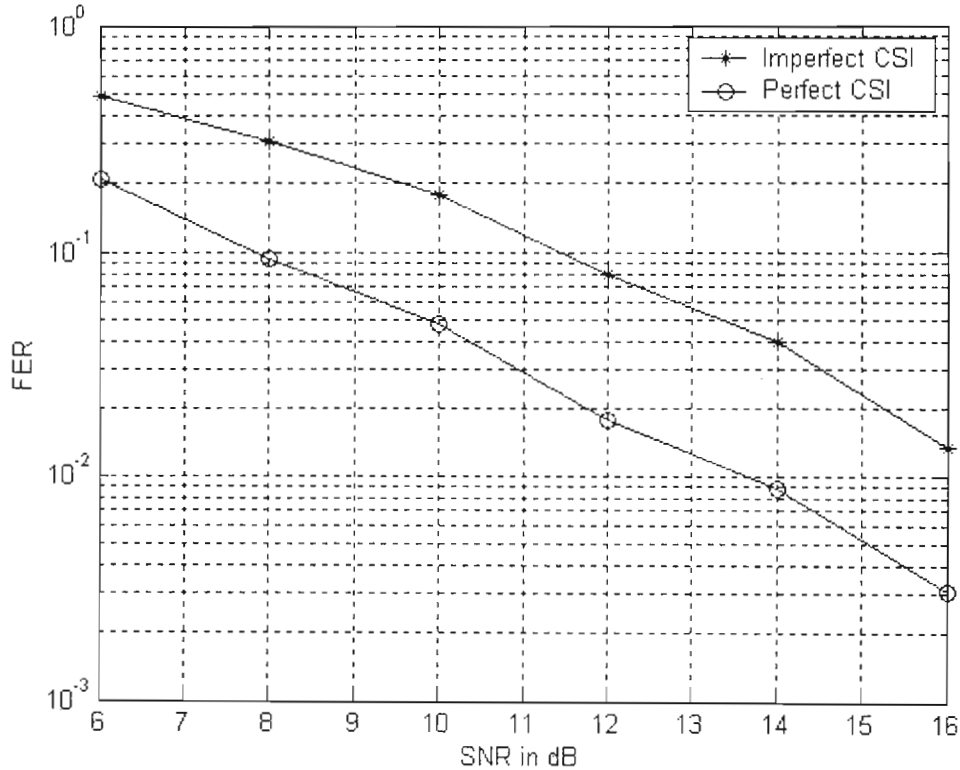

Fig. 5.10: Performance comparison of SOST-CC with perfect CSI and estimated CSI.

5.6 Conclusion

In this chapter a brief overview of existing concatenated space-time trellis codes was reviewed. Two concatenated super-orthogonal space-time trellis coded systems were proposed. The SOST-CC system consists of an outer convolutional code and an inner SOSTTC code, while the SOST-SC system consisted of a serially concatenated convolutional outer code and an inner SOSTTC code. The system model for the two proposed schemes was presented and the encoding and decoding of each were discussed. The decoding of the constituent codes using the additive bitwise SISO algorithm was also

discussed. The effect of imperfect channel state information on the performance of the system in quasi-static channels was also investigated.

Simulation results were presented for the cases of quasi-static and rapid Rayleigh fading 130 bit and 1300 bit input frame sizes as well as recursive and non-recursive CCs and compared with the results of concatenated STTCs. Interleaving gains in terms of FERs was achieved for rapid fading channels but not for quasi-static fading channels. It is seen that the SOST-CC system has significant gain in performance especially in rapid fading channels. The SOST-SC system maintained some performance improvement over codes using NRC codes, and showed slightly inferior performance over their ST-SC counterparts.

CHAPTER 6

CONCLUSIONS AND FUTURE WORK

6.1 Conclusions

This dissertation has focused on the use of coded transmit antenna diversity to improve the performance and capacity of single user wireless MIMO communication systems without sacrificing system power or bandwidth. The results presented in chapters 2 through 5, were generated using custom built software simulation environments.

The introductory chapter of the dissertation gave the reasoning for the recent renaissance in the field of wireless communications. The necessity for and demands of current and future generation wireless standards is highlighted. It was established that the ability of future wireless systems to satisfy the increasing demand for high data rates and provide high quality cost effective power and bandwidth efficient services is paramount to their future progress and development. A basic communication system model was described and methods to improve system performance, through error correcting codes and diversity were discussed. Antenna diversity was shown to improve system reliability without sacrificing system power or bandwidth. Transmit diversity was shown to be a feasible solution for improving the performance and capacity of systems where receive diversity was shown to be less effective. SOSTTC codes which are an advanced form of STTCs that merge channel coding with antenna diversity were discussed. Motivation for the research done and original contributions of this dissertation were presented.

Chapter 2 was a review on error correcting coding techniques using the use of turbo codes. A brief discussion on convolutional codes and the different types of CCs were discussed. The encoding and decoding procedure for turbo codes based on the system model was discussed. We also describe the MAP decoding algorithm and presented the iterative decoding procedure. The performance of these codes using union bounds were also shown and compared with its simulation results.

In chapter 3 a generalized system model employing multiple transmit and receive antennas is first presented. Next a literature survey on multi-antenna transmission systems employing error control coding is provided. The importance of channel capacities attainable and theoretical results of MIMO systems and also effects of channel correlation were investigated. Various types of coding for multi-antenna systems were briefly described. Current trends in research in space-time coded systems were also discussed briefly. STTCs have shown to provide good trade-off in terms of complexity and performance. AWSTTCs were also investigated and show improved performance over STTCs, but owing to their closed nature are not feasible for implementation on concatenated platforms. The PWEP bounds and the application of the union bound to the analysis of coded systems and methods to simplify the complexity of the calculation using error events were discussed. Transfer bounding approach for the quasi-static fading channel was also presented. The bounds obtained from the different methods were compared with simulation results in both quasi-static fading channels and rapid fading scenarios. The results obtained indicated that STTCs achieve maximum diversity gain yet not maximum coding gain. An investigation into the complexity issues related to the implementation of turbo codes, space-time trellis codes and their possible concatenation on hardware was also investigated.

In chapter 4 the system design and code structure for a relatively new form of space-time trellis coding, super-orthogonal space-time trellis codes is presented. These codes provide full diversity, full rate, and has improved performance in terms of coding gain over the STTC scheme. A design scheme which shows superior performance in rapid fading Rayleigh channels is provided. Performance analysis of these codes using coding gain

distance method and moment generating function methods are provided. Simulation results for these codes are provided for 2-state and 4-state codes for both quasi-static fading and rapid fading channels. The results obtained highlighted the fact that these codes achieve maximum diversity gain and there is still room for improving coding gain. This highlights the need for concatenation of SOSTTCs to further improve the performance of these systems.

In chapter 5, a brief overview of existing concatenated space-time trellis codes was reviewed. We introduce the class of super-orthogonal space-time turbo codes by proposing two concatenated SOSTTC schemes. The SOST-CC system used an outer convolutional code and an inner SOSTTC code, while the SOST-SC system consisted of a SCCC outer code and an inner SOSTTC code. The system models for the proposed two schemes were presented and their encoding and decoding procedures were discussed. The decoding of the constituent codes using the bitwise additive SISO algorithm was also discussed. Results were obtained for both short and long frame lengths in both fading channels. The results obtained were compared with corresponding similar concatenated STTCs to investigate the relative performance of the codes. Simulation results showed that the concatenated system performs well in rapid fading channels and only marginal improvement in performance is observed in quasi-static fading channels in comparison with concatenated STTCs. The effect of imperfect channel state information on the performance of the system in quasi-static fading channel was also investigated.

6.2 Future Work

As the topic of super-orthogonal space-time trellis codes is a relatively new topic and has shown significant improvement over its predecessor space-time trellis codes, this specific area of research has a while to go before reaching maturity.

Initially the study of a proper analytical model for the performance of SOSTTC codes with higher number of states and larger constellation sizes would play an important role in determining the achievable performance of these codes for higher date rates. An

analytical model for the code proposed in [23] would also be of interest. This would also further shed light on the feasibility of actually implementing such codes in hardware in a more cost effective manner.

Future work would also entail incorporation of the family of super-orthogonal space-time turbo codes in WCDMA systems to evaluate the performance of these systems in multi-user detection schemes and evaluate its performance in combating frequency selectivity in channels. An option of implementing two SOSTTC codes in a parallel concatenation, or the concatenation of a classical turbo code and SOSSTC code, can also be investigated in order see if there is any further improvement in the codes performance.

With an ultimate goal of deployment of these codes in next generation networks, the possibility of using SOSTTuCs in a differential scheme, using decoding at the receiver side employing the SOVA algorithm to reduce complexity, also promises good capabilities, as although differential schemes normally have a 3dB penalty in terms of performance, the improved performance of SOSTTC schemes still enable improvement over existing schemes.

Technology advancements would enable the use of employing SOSTTuC schemes in a CDMA system, with additional channel estimation techniques to further improve the performance of the system as whole and combat varying types of channel environments.

Another interesting option would be to change the outer codes with LDPC codes or Reed-Solomon codes to investigate the performance of these new concatenated SOSTTC structures and evaluate their performance using EXIT charts.

Appendix A

Constituent Codes

A.1 Space-Time Codes

A.1.1 Space-Time Trellis Codes

In this section the relevant trellis diagrams for the constituent STTCs used in this dissertation are given. For all the codes the number of input bits $k = 2$, the constellation size $M = 4$ and the number of transmit antennas $N_T = 2$. A few examples of the trellis diagrams are shown, whereby the encoder states are numbered along the right hand side of the trellis. The input/output relationships $u_t^2 u_t^1 / c_t^1 c_t^2$ are given on the left side of the trellis where the transitions in the trellis diagram from top to bottom correspond to the entries from left to right.

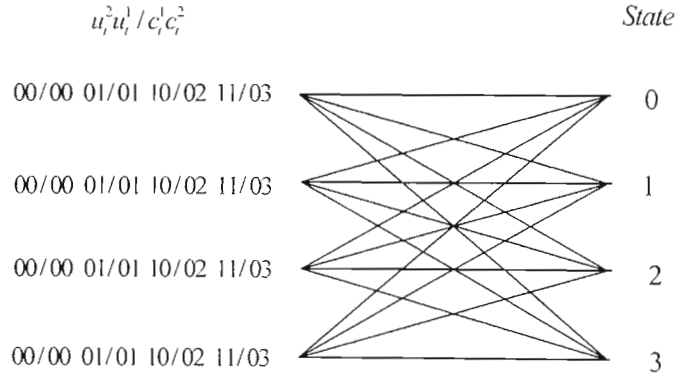

Fig. A.1: Tarokh 4-state; $k = 2,\ m = 2,\ N_T = 2,\ M = 4$

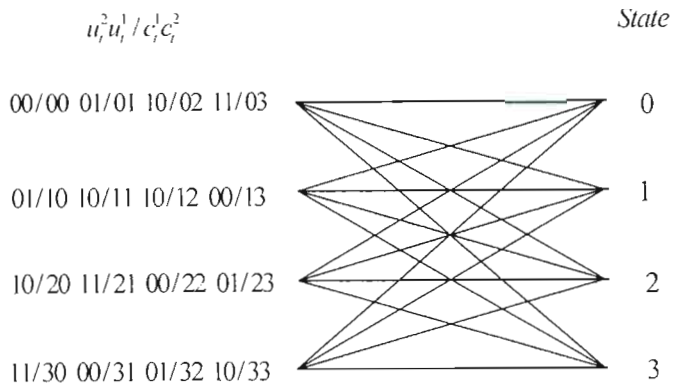

Fig. A.2: Recursive 4-state: $k = 2$, $m = 2$, $N_T = 2$, $M = 4$

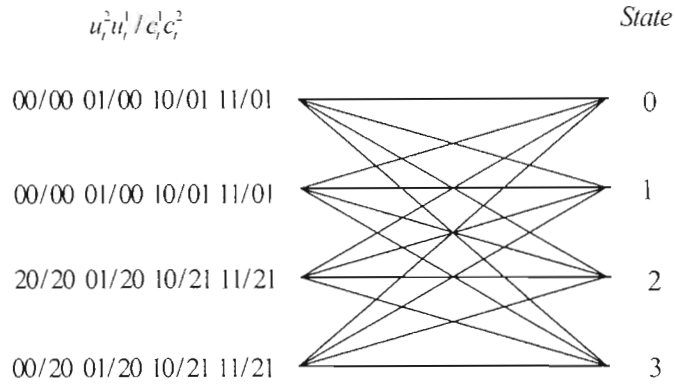

Fig. A.3: AWSTTC Trellis: $k = 2$, $m = 2$, $N_T = 2$

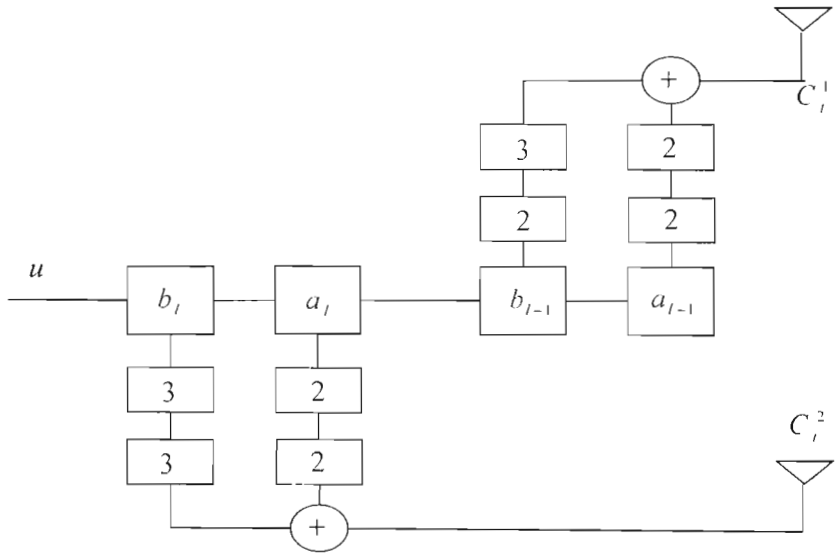

Fig. A.4: Encoder structure for AWSTTC system.

A.1.2 Super-Orthogonal Space-Time Trellis Codes

In this section the relevant trellis diagrams for the constituent STTCs used in this dissertation are given. For all the codes the number of input symbols $k = 2$, the constellation size $M = 2$ *or* 4 and the number of transmit antennas $N_T = 2$. The trellis diagrams for the various SOSTTC systems used are shown below,

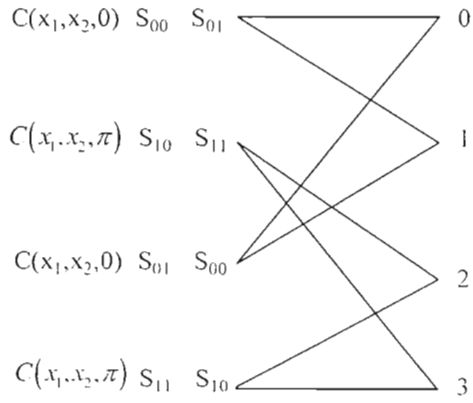

Fig. A.5: A four-state SOSTTC code $r = 1b/s/Hz$ using BPSK or $r = 2b/s/Hz$ using QPSK

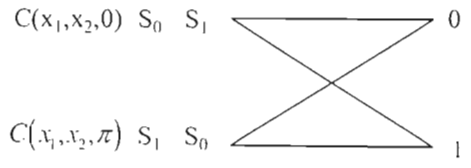

Fig. A.6: A two-state code SOSTTC $r = 1b/s/Hz$ using BPSK or $r = 2b/s/Hz$ using QPSK

The transmission matrices for a 2-state BPSK SOSTTCs are shown as an example below,

For $\theta = 0$,

$$\begin{pmatrix} 1 & 1 \\ -1 & 1 \end{pmatrix}, \begin{pmatrix} -1 & -1 \\ 1 & -1 \end{pmatrix}, \begin{pmatrix} -1 & 1 \\ -1 & -1 \end{pmatrix}, \begin{pmatrix} 1 & -1 \\ 1 & 1 \end{pmatrix}$$

and for $\theta=\pi$

$$\begin{pmatrix} -1 & 1 \\ 1 & 1 \end{pmatrix}, \begin{pmatrix} 1 & -1 \\ -1 & -1 \end{pmatrix}, \begin{pmatrix} 1 & 1 \\ 1 & -1 \end{pmatrix}, \begin{pmatrix} -1 & -1 \\ -1 & 1 \end{pmatrix}$$

The trellis diagram for the new SOSTTC code using BPSK constellation in [15 of CH4] is shown below,

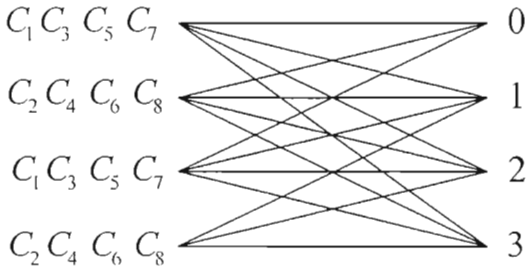

Fig. A.7: Trellis for new SOSTTC system.

The corresponding values for the transmission matrices for $C_1 \cdots C_8$ are shown below,

$$C_1 = \begin{pmatrix} 1 & 1 \\ -1 & 1 \end{pmatrix}, \quad C_2 = \begin{pmatrix} -1 & -1 \\ 1 & -1 \end{pmatrix}, \quad C_3 = \begin{pmatrix} -1 & 1 \\ -1 & -1 \end{pmatrix},$$

$$C_4 = \begin{pmatrix} 1 & -1 \\ 1 & 1 \end{pmatrix}, \quad C_5 = \begin{pmatrix} -1 & 1 \\ 1 & 1 \end{pmatrix}, \quad C_6 = \begin{pmatrix} 1 & -1 \\ -1 & -1 \end{pmatrix},$$

$$C_7 = \begin{pmatrix} 1 & 1 \\ 1 & -1 \end{pmatrix}, \quad C_8 = \begin{pmatrix} -1 & -1 \\ -1 & 1 \end{pmatrix}$$

A.2 Convolutional Codes

In this section the generating matrices for the constituent convolutional codes used in this dissertation are presented.

$$G(D) = \left[1, \frac{1+D^2}{1+D+D^2} \right]$$

Recursive systematic, rate ½, 4-state

$$G(D) = \begin{bmatrix} 1, & 0, & \frac{1+D^2}{1+D+D^2} \\ 0, & 1, & \frac{1+D}{1+D+D^2} \end{bmatrix}$$

Recursive systematic, rate $2/3$, 4-state

$$G(D) = \begin{bmatrix} 1+D, & D, & 1 \\ 1+D, & 1, & 1+D \end{bmatrix}$$

Non-recursive, rate $2/3$, 4-state

REFERENCES

[1] C.Shannon, "A Mathematical Theory of Communcation," *Bell Syst.Tech. Journal*, pp. 379-423 and 623-656, July and October 1948.

[2] J. Korhonen, "Introduction to 3G Mobile Communications," Artech House mobile communications series: 2nd Edition, 2003.

[3] J. G. Proakis, *Digital Communications.* McGraw-Hill Companies, Inc., fourth edition, 2001.

[4] C. Thomas *et al.*, "Integrated circuits for channel coding in 3G cellular mobile wireless systems," *IEEE Communications Magazine,* vol. 41, No.8, pp.150-159, Aug 2003.

[5] I. S. Reed and G. Solomon, "Polynomial codes over certain finite fields," *SIAM Journal on Applied Mathematics,* vol. 8, pp. 300-304, 1960.

[6] T. Richardson, M. Shokrollahi and R. Urbanke, "Design of capacity-approaching irregular low-density parity check codes," *IEEE Transactions on Information Theory*, vol. 47, pp. 1168-1175, July 2001.

[7] I. S. Reed, "A class of multiple-error-correcting codes and the decoding scheme," *IRE Transactions on Information Theory,* vol. IT-4, pp. 38-49, Sept. 1954.

[8] V. Ponnampalam and B. Vucetic, "Soft decision decoding of Reed-Solomon codes", *IEEE Transactions on Communications,* vol. 50, pp. 1758-1768, Nov. 2002.

[9] P. Elias, "Coding for noisy channels," *IRE Conv. Record*, vol. 4, pp. 37-47, 1955.

[10] L. R. Bahl, J. Cocke, F. Jelinek and J. Raviv, "Optimal Decoding of Linear Decoding for Minimizing Symbol Error Rate," *IEEE Transactions on Information Theory*, vol.IT-20, pp. 284-287, March 1974.

[11] S. Benedetto, D. Divsalar, G. Montorsi, and F. Pollara, "A soft-input soft-output maximum a posteriori (MAP) module to decode parallel and serial concatenated codes," *JPL TDA Progress report 42-127,* Nov. 15 1996.

[12] G.D. Forney, "Concatenated Codes," Cambridge MA: MIT Press, 1966.

[13] C. Berrou and A. Glavieux, "Near optimum Error Correcting and Decoding: Turbo-Codes," *IEEE Trans. Commun*, COM-44: 1261-71, October 1996.

[14] C.Berrou, A.Glavieux and P.Thitimajshima, "Near Shannon Limit Error Correcting Coding and Decoding: Turbo Codes," *Proc. IEEE Intl.Conf.Comm (ICC 93),* pp.1064-70, Geneva, Switzerland, May 1993.

[15] B.Vucetic and J. Yuan, *Space-Time Coding.* John Wiley & Sons Ltd, 2003.

[16] G. J. Foschini and M. J. Gans, "On limits of wireless communications in a fading environment when using multiple antennas," *Wireless Personal Communications,* vol.6, No. 3, pp. 311-355, Mar 1998.

[17] V. Tarokh, N. Seshadri, and A. R. Calderbank, "Space-Time Codes for High Data Rate Wireless Communication: Performance Criterion and Code Construction," *IEEE Transactions on Information Theory,* vol. 44, pp.744-765, Mar 1998.

[18] G. J. Foschini, "Layered space-time architecture for wireless communication in a fading environment when using multi-element antennas," *Bell Labs Technical Journal,* pp. 41-59, Autumn 1996.

[19] G. D. Golden, G. J. Foschini, R. A. Valenzuelz and P. W. Wolniansky, "Detection algorithm and initial laboratory results using the V-BLAST space-time communications architecture," *Electronic Letters,* vol.35, pp. 14-15, Jan 1999.

[20] V. Tarokh, N. Seshadri, and A. R. Calderbank, "Space-time block coding for wireless communications: Performance results," *IEEE Journal on Selected Areas in Communications*, vol.16, No.8, pp. 1451-1458, Oct 1998.

[21] H. Jafarkhani and N. Seshadri, "Super-orthogonal space-time trellis codes," *IEEE Transactions on Information Theory,* vol. 49, No. 4, pp.937-950, April 2003.

[22] A. F. Naquib, N. Seshadri and a. R. Calderbank, "Increasing data rate over wireless channels," *IEEE Signal Processing Magazine,* vol.17, pp.76-92, May 2000.

[23] B. Vucetic and J. Yuan, *Turbo Codes: Principles and Applications*, Kluwer Academic, 2000

[24] S. Lin and D. J. Costello, *Error Control Coding*, Second Edition, Prentice Hall, International Edition, 2004, ISBN 0-13-017973-6.

[25] R. W. Hamming, "Error detecting and correcting codes," *Bell Sys. Tech. Jour.,* vol.29, pp147-160, 1950.

[26] J. M. Wozencraft and B. Reiffen, *Sequential Decoding,* MIT Press, Cambridge, 1961.

[27] J. L. Massey, *Threshold Decoding*, MIT Press Cambridge 1963.

[28] A. J. Viterbi, "Error bounds for convolutional codes and an asymptotically Optimum Decoding Algorithm", *IEEE Transactions on Communications*, vol.IT-13, pp. 260-269, April 1967.

[29] J. D. Anderson, "The turbo coding scheme," presented at *IEEE Int. Symp. Info .Theory (ISIT 1994)*, Trondheim, Norway, June 1994.

[30] S. Benedetto and G. Montorsi, "Unveiling turbo codes: Some results on concatenated coding schemes," *IEEE Trans on Info Theory*, vol.42, No.2. pp. 409-428, March 1996.

[31] S. Benedetto, D. Divsalar, G. Montorsi, and F. Pollara, "Serial concatenation of interleaved codes: Performance analysis, design and iterative decoding," *IEEE Trans.Info.Theory*, IT-44:pp.909-926, May 1998.

[32] J. Hagenauer, "The turbo principle: Tutorial introduction and state of the art," *Proc.1st Intl. Symp. Turbo Codes*, ppl-11, Brest, France, September 1997.

[33] W.E.Ryan, "A turbo code tutorial," New Mexico State University, Las Cruces, wryan@nmsu.edu.

[34] D.Divsalar, and F.Pollara, "Serial and hybrid concatenated codes with applications," *Proc.1st Intl. Symp. on Turbo Codes*, ppl-11, Brest, France, September 1997.

[35] D. Divsalar, S. Dolinar, and F. Pollara, "Transfer function bounds on the performance of turbo codes", *JPL TDA Progress report 42-122,* pp. 44-55, 15 Aug. 1995.

[36] D.Divsalar, F.Pollara, "On the Design of Turbo Codes," *TDA Progress report 42-123*, Jet Propulsion Labs, Pasadena, California, Nov. 1995.

[37] J. P. Woodard and L. Hanzo, "Comparative study of turbo decoding techniques: An overview," *IEEE Transactions on Vehicular technology,* vol. 49, pp.2208-2232, Nov 2000.

[38] B.Sklar, "A primer on turbo codes," *IEEE Communications, Magazine,* pp.94-101, Dec. 1997.

[39] P. Robertson, "Illuminating the structure of parallel concatenated recursive systematic (turbo) codes," in *Proc. IEEE GLOBECOM'94,* San Francisco, CA, pp. 1298-1303, 1994.

[40] T. M. Ngatched, "Performance of turbo-coded DS-CDMA systems in fading and burst channels," *MSc Eng Dissertation*, University of Natal, 2001.

[41] S. Benedetto and G. Montorsi, "Performance evaluation of turbo codes," *IEEE Electronic Letters,* vol.31, pp.163-165, Feb 1995.

[42] A. J Viterbi, "Convolutional codes and their performance in communication systems," *IEEE Transactions on Communications,* vol.19, pp.751-772, Oct. 1971.

[43] D. N. Rowitch, "Convolutional and turbo coded multicarrier direct sequence CDMA and applications of turbo codes to hybrid ARQ communication systems," *PhD dissertation,* University of California, San Diego.

[44] Hsuan-Jung and E. Geraniotis, "Space-time turbo codes with full antenna diversity," *IEEE Transactions on Communications,* vol.49, No.1, pp.47-57, Jan 2001.

[45] S. M. Alamouti, "A simple transmit diversity technique for wireless communications," *IEEE Journal on Selected Areas in Communications,* vol.16, No.8, pp.1451-1458, Oct. 1998.

[46] V. Tarokh, H. Jafarkhani, and A. R. Calderbank, "Space-time block codes from orthogonal designs," *IEEE Transactions on Information Theory,* vol.45, No.5, pp.1456-1467, July 1999.

[47] E. Biglieri, G. Caire and G. Taricco, "Recent results on coding for multiple-antenna transmission systems," in *Proc. IEEE ISSTA 2000,* New Jersey, USA, pp. 117-121, September 2000.

[48] "Space-time signal processing and MIMO systems," *White Paper Report,* Working Group 8, Space-time signal processing, Research focus Mobikom BMBF, version 1.1-20, Feb. 2004.

[49] I. E. Teletar, "Capacity of multiple–antenna Gaussian channels," Tech Report#BL0112170-950615-07TM, AT&T Bell Laboratories, 1995.

[50] T. L. Marzetta and M. Hochwald, "Capacity of mobile multiple-anteanna communication link in Rayleigh flat fading ," *IEEE Transaction on Information Theory,* vol.45, No.1, pp. 139-157.

[51] A. Wittenben, "A new bandwidth efficient transmit antenna modulation diversity scheme for linear digital modulation," in *Proceedings of IEEE International Conference on Communications/ICC'93,* pp.1630-1634, 1993.

[52] G. Bauch, A. Naquib and N. Seshadri, "MAP equalization of space-time coded signals over frequency selective channels," in *Proc. Wireless Communications and Networking Conf.,* New Orleans, LA, Sept. 1999.

[53] G. Bauch, and N. Al-Dhahir, "Reduced complexity turbo equalization with multiple transmit and receive antennas over multipath fading channels," in *Proc. Information Sciences and Systems,* Princeton, NJ, pp. WP3v13-18, Mar. 2000.

[54] D. Agarwal *et al.*, "Space-time coded OFDM for high data-rate wireless communication wireless communication over wide-band channels," in *Proc. IEEE Vehicular Technology Conf.*, Ottawa, Canada, pp. 2232-2236, May 1998.

[55] M. P. Fitz and J. V. Krogmeier, "Further results on space-time codes for Rayleigh fading," in *Proc. Allerton,* pp. 391-400, Sept. 1998.

[56] H. El Gamal and A. R. Hammons, "The layered space-time architecture: a new perspective," *IEEE Transactions on Information Theory,* vol.47, pp.2312-2334, Sept. 2001.

[57] S. Baro, G. Bauch and A. Hansmann, "Improved codes for space-time trellis coded modulation," *IEEE Communication Letters,* No.4, pp.20-22, 2000.

[58] Z. Chen, J. Yuan and B. Vucetic, "Improved space-time trellis coded modulation scheme on slow Rayleigh fading channels," *IEEE Electronic Letters,* 37, (7), pp.440-441.

[59] Q. Yan and R. S. Blum, "Optimum space-time convolutional codes for quasi-static slow fading channels," in *Proc. Wireless Communications and Networking Conf.*, (WCNC), pp. 1351-1355, Sept. 2000.

[60] D. Gesbert *et al.*, "From theory to practice: An overview of MIMO space-time coded wireless systems," *IEEE Journal on Selected Areas in Communications,* vol. 21, No.3, pp. 281-300, April 2003.

[61] T. H. Liew and L. Hanzo, "Space-time codes and concatenated channel codes for wireless communications," in *Proceedings of IEEE,* vol. 90, No.2, pp. 187-219, Feb. 2002.

[62] Z. Chen, B. S. Vucetic, J. Yuan, and K. L. Lo, "Space-time trellis codes for 4-PSK for three and four transmit antennas in quasi-static flat fading channels," *IEEE Comm. Letters,* vol.6, pp.67-69, Feb. 2002.

[63] Z. Chen, B. S. Vucetic, J. Yuan, and K. L. Lo, "Space-time trellis codes for 8-PSK for two, three and four transmit antennas in quasi-static flat fading channels," *IEEE Electron. Letters,* vol.38, pp.462-464, May 2002.

[64] W. Firmanto, B. S. Vucetic and J. Yuan, "Space-time TCM with improved performance on fast fading channels," *IEEE Comm. Letters,* vol.5, pp.154-156, Apr. 2001.

[65] S. L. Miller and H. Bouzekri, "Space-time code performance analysis for quasi-static fading channels," in *Proceedings of IEEE International Symposium Information Theory,* pp.83, June 2001.

[66] A. Stefanov and T. M. Duman, "Performance bounds for turbo coded multiple antenna systems," in *Proceedings IEEE International Symposium on Information Theory,* Lausanne, Switzerland, pp.302, July 2002.

[67] E. Malkamaki and H. Lieb, "Evaluating the performance of convolutional codes over block fading channels," *IEEE Transactions on Information Theory,* vol.45, pp.1643-1646, July 1999.

[68] A. P. des Rosiers and P. H. Siegel, "On performance bounds for space-time coded modulation on fading channels," in *Proc. International Symposium on Information Theory and Its Applications,* Honolulu, Hawaii, USA, Nov. 5-8, 2000.

[69] D. Aktas and M. P. Fitz, "Computing the distance spectrum of space-time trellis codes," in *Proceedings of WCNC 2000,* Chicago IL, Sep. 2000.

[70] R. Gozali and B. D. Woerner, "Upper bounds on the bit-error probability of space-time trellis codes using generating function techniques," in *Proceedings of IEEE VTC 2001,* Rhodes, Greece, May 6-9, 2001.

[71] A. Stefanov and T. M. Duman, "Performance bounds for turbo-coded multiple antenna systems," *IEEE Journal on Selected Areas in Communications,* vol.21, No.3, pp.374-381, April 2003.

[72] E. G. Larson and P. Stoica, *Space-time block coding for wireless communications,* Cambridge University Press 2003.

[73] D. Bevan and R, Tanner, "Performance comparison of space-time coding techniques," *IEEE Electron Letters,* vol. 45, pp.1707-1708, Oct. 1998.

[74] E. Visotsky and U. Madhow, "Space-time transmit precoding with imperfect feedback," in *Proceedings of ISIT 2000.*

[75] Y. Li, B. Vucetic, A. Santoso and Z. Chen, "Space-time trellis codes with adaptive weighting," *IEEE Electronics Letters,* vol.4, pp.20-22, Apr. 2000.

[76] G. J. Byers, Concatenated space-time codes in Rayleigh fading channels, Thesis, University of Natal, Mar. 2002.

[77] M. P. Fitz, J. Grimm and S. Siwamogastham, "A new view of performance analysis techniques in correlated Rayleigh fading," in *Proceedings of IEEE WCNC'99,* New Orleans, LA, Sep. 21-24, 1999.

[78] Murat Uysal course notes at http://bbcr.uwaterloo.ca/~muysal/

[79] J. P. Woodard and L. Hanzo, "Comparative study of turbo decoding techniques: An overview," *IEEE Transactions on Vehicular Technology,* vol.49, No.6, Nov. 2000.

[80] J. N. Popovic, "Implementing a MAP decoder for CDMA2000 turbo codes on a TMS320C62xx DSP device," *Application Report SPRA629* Texas Instruments, May 2000.

[81] H. Yiu, "Implementing Viterbi Decoding on the TMS320C62xx DSP," *Application Report SPRA444,* Texas Instruments, Apr. 1998.

[82] J. N. Pillai and S. H. Mneney, "A review on issues related to the implementation of Turbo codes and space-time trellis codes," *Proceedings of IEEE Africon 2004,* Gaborone, Botswana, Sep. 2004.

[83] M. K. Simon and H. Jaferkhani, "Performance evaluation of super-orthogonal space-time trellis codes using moment generating function-based approach," *IEEE Transactions on Signal Processing,* vol. 51, No.11, pp.2739-2751, Nov 2003.

[84]] J. Grimm, M. P. Fitz and J. V. Krogmeier, "Further Results on Space-Time Codes for Rayleigh Fading Channels," *in Proc. 36th Annual Allerton Conference,* pp.391-400, September 1998.

[85] S. M. Alamouti, V. Tarokh, and P.Poon, "Trellis Coded Modulation and Transmit Diversity: Design Criteria and Performance Evaluation," *in Proc. IEEE Int. Conf. Universal Personal Communications (ICUPC-98),* vol.2, pp.917-920, 1998

[86] S. Siwamogsatham and M. P. Fitz, "Robust Space-Time Coding for Correlated Rayleigh Fading Channels," *IEEE Transactions on Signal Processing,* vol. 50, pp.2408-2416, Oct 2002.

[87] G. Ungerboeck, "Channel Coding for multilevel/phase Signals," *IEEE Transactions on Information Theory,* vol. IT- 28, pp.56-67, Jan 1982.

[88] D. Divsalar and M. K. Simon, "Multiple Trellis Coded Modulation (MTCM)," *IEEE Transactions on Communications,* vol.36, pp.410-419, Apr 1998.

[89] A. Birol, U. Aygolu and M. Yucel, "Super-Orthogonal Space-Time Trellis Codes for Fast Fading Channels," Yidiz Technical University, Yildiz, Istanbul Turkey April 2005.

[90] M. K. Simon and M. S. Alouini, "Digital Communication Over Fading Channels: A uniform approach to Performance Evaluation," New York: Wiley, Aug 2000.

[91] G. L. Turin, "The characteristic function of Hermitian quadratic forms in complex normal random variables," *Biometrika,* pp.199-201, June 1960.

[92] M. K. Simon, "Evaluation of average bit error probability for space-time coding based on a simpler exact evaluation of pairwise error probability," *Int. J. Commun. Networks,* vol.3, No.3, pp.257-264, Sept. 2001.

[93] M. J. Borran, M. Memarzadeh, and B. Aazhang, "Design of Coded Modulation Schemes for Orthogonal Transmit Diversity," *in Proc. IEEE Int. Symp. Information Theory (ISIT).* Washington, DC, pp.339, June 2001.

[94] Yi Hong *et al*, "Space-time turbo trellis codes for two, three, and four transmit antennas," *IEEE Transactions on Vehicular Technologies,* vol.53, No.2, pp.318-328, March 2004.

[95] G. Bauch, "Concatenation of space-time block codes and turbo-TCM," *in Proc. IEEE Int. Conf. Communications,* vol. 2, pp.1202-1206 June 1999.

[96] H. Su, E. Geraniotis, "Space-time turbo codes with full antenna diversity", *IEEE Transactions on communications*, vol. 49, pp. 47-57, Jan 2001.

[97] A. Stefanov and T.M. Duman, "Turbo coded modulation for wireless communications with antenna diversity," *in Proc. IEEE Vehicular Technologies Conf.,* vol. 3, pp.1565-1569, Sept. 1999.

[98] Y. Liu and M. P. Fitz, "Space-time turbo codes", *in Proc. 37th Annual Allerton Conf. on Commun.,Control and Comp.,* Monticello, Illinois, USA, Sept. 1999.

[99] X. Lin and R. S. Blum, "Improved space-time codes using serial concatenation," *IEEE Communication Letters*, vol. 4, pp. 221-223, July 2000.

[100] K. R. Narayanan, "Turbo decoding of concatenated space-time codes," *in Proc. 37th Annual Allerton Conf. on Commun.,Control and Comp.,* Monticello, Illinois, USA, Sept. 1999.

[101] X. Lin and R. S. Blum, "Guidelines for serially concatenated space-time code design in Rayleigh fading channels," *in Proc. IEEE 3rd Workshop Signal Processing Adv. in Wireless Communications*, pp.247-250, 2001.

[102] S. Benedetto, D. Divsalar, G. Montorsi and F. Pollara, "Self-concatenated codes with self-iterative decoding for power and bandwidth efficiency," *in Proc. IEEE Int. Symp. On Information Theory*, pp.177, 1998.

[103] Y. Liu, M. P. Fitz and Y. Takeshita, "Full rate space-time turbo codes," *IEEE Journal on Selected Areas in Communications,* vol. 19, No.5. pp. 969-979, May 2001.

[104] D. Tujkovic, "Space-time turbo coded modulation," in *Proc. Finnish Wireless Communications workshop (FWCW)*, pp. 85-89, May 2000.

[105] D. Tujkovic, "Recursive space-time trellis codes for turbo coded modulation", in *Proc. IEEE GLOBECOM '00*, San Francisco, CA, vol. 2, pp. 1010-1015, Nov. 2000.

[106] A. Stefanov and T.M. Duman, "Turbo coded modulation for systems with transmit and receive antenna diversity over block fading channels: System model, decoding approaches, and practical considerations," *IEEE Journal on Selected Areas in Communications,* vol. 19, No.5. pp. 958-968, May 2001.

[107] J. Hagenauer and P. Hoeher, "A Viterbi algorithm with soft-decision outputs and its applications," in *Proc. IEEE GLOBECOM '00*, Dallas, Texas, pp. 1680-1686, Nov. 1989.

[108] L. Papke, P. Robertson and E. Villebrun, "Improved decoding with the SOVA in a parallel concatenated (turbo-code) scheme," in *Proc. IEEE ICC '96*, Dallas, Texas, pp. 102-106, June 1996.

[109] V. Gulati and K. R. Narayanan, "Concatenated codes for fading channels based on recursive space-time trellis codes," *IEEE Transactions on Wireless Communications*, vol.2, pp.118-128, Jan 2003.

[110] Y. Wu, "Implementation of parallel and serial concatenated convolutional codes," *PhD dissertation,* Faculty of the Virginia Polytechnic Institute and State University, April 2000.

[111] M. C. Valenti, "Iterative detection and decoding for wireless communications," *PhD dissertation,* Faculty of the Virginia Polytechnic Institute and State University, July 1999.

[112] S. A. Barbelescu, "Iterative decoding or turbo codes and other concatenated codes," *PhD thesis,* University of South Australia, Feb 1996.

[113] M. Jankiraman, *Space-time codes and MIMO systems,* Artech House, Inc., 2004.

[114] R. G. Gallager, "Low density parity check codes," *IRE Transactions on Information Theory,* IT-8, pp. 21-28, Jan. 1962.

[115] J.N. Pillai and S. H. Mneney, "Adaptively weighted space-time trellis codes," *Proceedings of South African Telecommunications Networks and Applications Conference (SATNAC 2004),* Spier, Stellenbosch, South Africa, Sep. 2004.

[116] J. N. Pillai and S. H. Mneney, "Super-orthogonal space-time trellis codes for rapid Rayleigh fading channels," *Proceedings of South African Telecommunications Networks and Applications Conference (SATNAC 2005),* Central Drakensburg, Durban, South Africa, Sep. 2005.

[117] J. N. Pillai and S. H. Mneney, "Concatenated super-orthogonal space-time trellis codes in Rayleigh fading channels," *Accepted IEEE EUROCON 2005, Conference on Computer as a Tool, Belgrade, Serbia and Montenegro, Nov. 21-24 2005.*

[118] R. A. Carrasco, "Space-diversity codes for fading channels," presentation, School of Computing, Staffordshire University, United Kingdom at http://www.staff.ncl.ac.uk/r.carrasco/Space%20Time%20Presentation4.ppt

[119] S. T. Brink, "Convergence behaviour of iteratively decoded parallel concatenated codes," *IEEE Transactions on Communications*, vol.4, pp.1727-1737, Oct. 2001.

[120] D. Divsalar, S. Donlinear and F. Pollara, "Iterative turbo decoder analysis based on density evolution," *IEEE Transactions on Selected Areas in Communications*, vol.19, pp.891-907, May 2001.

[121] T. Richardson and R. Urbanke, "The capacity of low density parity check codes under message passing decoding," *IEEE Transactions on Information Theory*, vol. 47, pp.599-618, Feb. 2001.

[122] H. Chen and A. Haimovich, "EXIT charts for turbo trellis coded modulation," *IEEE Communication Letters*, vol. 8, pp. 221-223, July 2000.